Chemical and physical structure of the barrier against water transpiration of leaves: Contribution of different wax compounds

Chemischer und physikalischer Aufbau der Wassertranspirationsbarriere von Blättern: Beitrag verschiedener Wachskomponenten

Doctoral thesis for a doctoral degree
at the Graduate School of Life Sciences,
Julius-Maximilians-Universität Würzburg,
Section Integrative Biology

submitted by

Pascal Seufert

from

Ramsthal

Würzburg 2020

Submitted   on:

…………………………………………………...……………
Office stamp

Members of the *Promotionskomitee*:

Chairperson: Prof. Dr. Thomas Müller

Primary Supervisor: Prof. Dr. Markus Riederer

Supervisor (Second): Prof. Dr. Dr. Lorenz Meinel

Supervisor (Third): Dr. Adrian Friedmann

Supervisor (Fourth): Dr. Katja Arand

Date of Public Defence: 08.07.2020

Date   of   Receipt   of   Certificates:

…………………………………………….

Table of contents

I. Summary

The cuticle was one of many adaptions plants made when they colonized the land to cope with the challenges of their new environment. It covers above-ground primary plant organs like petals or leaves and fulfils various tasks. To accomplish these tasks the cuticle is constituted of the biopolymer cutin and intra- and epicuticular waxes. In some cases, it has epicuticular wax crystals, protruding from the epicuticular wax film. One of the most important tasks is protection against desiccation. Many investigations were conducted to find the transport-limiting component of the cuticle. It is evidentially confirmed that the waxes form this barrier. These waxes are multifactorial blends made of very-long-chain aliphatic (VLCA) compounds and triterpenoids (TRP). The VLCAs were proposed to constitute the transpiration barrier to water. However, experimental confirmation was lacking so far. The present study focuses on the development of a method to selectively extract TRPs from the cuticle and the impact of the removal on the transpiration barrier.

The plants deployed in this study exhibited several features. They had no epicuticular crystals on their surfaces, were astomatous, had a rather durable and possibly isolatable cuticle. A broad range of wax compositions was covered from plants with no TRP content and low wax load like *Hedera helix* and *Zamioculcas zamiifolia* to plants with high TRP content and high wax load like *Nerium oleander*. The selective extraction was conducted using a sequence of solvents. Samples were dispersed in methanol (MeOH) overnight at room temperature followed by extraction with chloroform (TCM). TRPs were extracted almost exhaustively from CMs with the first MeOH extract. Only a minor amount of shorter chained VLCAs was obtained. The remaining waxes, consisting mostly of VLCAs and some remnant TRPs, were removed with the following TCM extract. A comparison to full extracts (FE) showed good comparability to a conventionally used method (Chapter V).

After the extractions, the water permeance was investigated using transpiration chambers. Water loss through native cuticular membranes (CM), MeOH extracted (M) and dewaxed cuticular discs (MX) was measured gravimetrically. Throughout all plants, a common trend was noticeable. Compared to the water permeance of CMs, Ms showed no or only a small increase in water conductance. MXs, however, always showed strongly increased values. These results gave direct experimental proof of VLCAs to constitute the water permeance barrier of the cuticle.

The knowledge about the wax compounds constituting the transport-limiting properties is vital for different projects. For various issues, it would be favourable to have a standardized wax mixture as an initial point of research. It could be used to develop screening procedures to investigate the impact of adjuvants on cuticular waxes or the influence of wax constituents on the properties of cuticular waxes. This work concentrated on the development of an artificial wax mixture, which mimics the physical properties of a plant leaf wax sufficiently.

As target wax, the leaf wax of *Schefflera elegantissima* was chosen. The wax of this plant species consisted almost exclusively of VLCAs, had a rather simple composition regarding compound classes and chain length distribution and CMs could be isolated. Artificial binary ($C_{31}anC_{29}an$, $C_{32}olC_{30}ol$), ternary ($C_{31}anC_{29}anC_{30}ol$, $C_{31}anC_{29}anC_{32}ol$) and quaternary ($C_{31}anC_{29}anC_{32}olC_{30}ol$) waxes were investigated using differential scanning calorimetry (DSC) and X-ray diffraction (XRD) techniques. Wax blends corresponding to the conditions within the plant wax were additionally examined using Fourier-transform infrared (FTIR) spectroscopy (Chapter VI).

Phase diagrams were mapped out for a series of binary mixtures of the alkanes or alcohols, of ternary mixtures of two alkanes (with a constant ratio of $C_{31}anC_{29}an$ 2.3 - 1) and one alcohol and quaternary mixtures with two alkanes (with a constant ratio of $C_{31}anC_{29}an$ 2.3 - 1) and two alcohols (with a constant ratio of $C_{32}olC_{30}ol$ 2.3 - 1). Binary mixtures showed one solid-solid transition, assigned to the change from an orthorhombic (alkanes) or monoclinic (alcohols) to a hexagonal crystal lattice, before melting. The crystal lattice at room temperature was determined using XRD. For the binary alkane mixture $C_{31}anC_{29}an$ with the ratio 2.3 - 1, the transition was confirmed by hot stage XRD investigations. Ternary and quaternary mixtures showed up to three solid-solid transitions before melting, indicative for the presence of three phases in the mix. One phase dominated by alkanes, one dominated by alcohols and one intermixed phase. In ternary mixtures at low alcohol content, the diffractograms at room temperature exhibited an orthorhombic crystal structure. With increasing alcohol content first both, an orthorhombic and a monoclinic and finally only a monoclinic structure was revealed. Diffractograms of the quaternary mixtures exclusively exhibited orthorhombic crystallinity.

FTIR experiments were conducted using binary ($C_{31}anC_{29}an$ and $C_{32}olC_{30}ol$ with the ratio 2.3 - 1), ternary ($C_{31}anC_{29}anC_{30}ol$ and $C_{31}anC_{29}anC_{32}ol$ with the ratio 2.3 - 1 - 1.4) and a quaternary ($C_{31}anC_{29}anC_{30}olC_{32}ol$ 5.4 - 2.3 - 2.3 - 1). The blends were chosen

to represent the conditions within the wax of the adaxial CM plant wax. The experiments exhibited an increasing resemblance of the artificial wax to the plant wax with an increasing number of compounds in the artificial wax. However, differences over the progression of the melting were seen. Although qualitative values differed, the crystallinity behaviour of the quaternary mixture and adaxial CM plant wax were similar below 52 °C. Above this temperature showed the artificial wax mixture a steeper decrease than the plant wax. Differences in the FTIR experiments were assumed to occur due to differences in the composition of the artificial and plant wax. The same trend as in the melting behaviour was found for DSC thermograms. Thermograms of ternary and quaternary blends exhibited more overlapping peaks and occurred in a temperature range more similar to the range of the whole leaf plant wax. The XRD spectrum at room temperature showed good conformity with the quaternary blend. However, a comparison of the hot stage diffractograms of the quaternary and the whole leaf plant wax displayed major differences. While the artificial wax showed different stages with varying crystalline structures during its melting, the whole leaf plant wax showed only a continuous decrease of the diffractions indicating an orthorhombic crystal structure. The results of the second project were not conclusive. However, they gave a deeper view of the structure of cuticular waxes. While hot stage XRD and FTIR experiments with the leaf waxes hint at a wax structure consisting of one phase, the corresponding DSC experiments and the comparisons with the artificial wax contained hints at distinct phases of alkanes and aliphatic compounds with functional groups like alcohols.

The current work illustrates a method for selective extraction of TRPs from isolated CMs. It gives direct experimental proof of the association of the water permeance barrier with the VLCA rather than to the TRPs. Furthermore, the possibility to mimic cuticular waxes using commercially available wax compounds is investigated. The results show promising feasibility for its viability, enabling it to perform as a standardized initial point for further research (e.g. to examine the influence of different constituents on waxes), revealing valuable knowledge about the structure and the chemistry-function relationship of cuticular waxes.

II. Zusammenfassung

Die Kutikula ist eine der vielen Anpassungen, die Pflanzen entwickelten um nach der Besiedelung des Landes mit den Herausforderungen ihrer neuen Umgebung fertig zu werden. Sie überzieht überirdische Pflanzenorgane, wie Blüten oder Blätter und erfüllt verschiedene Aufgaben. Hierzu besteht sie aus dem biopolymer Kutin und intra- sowie epikutikulären Wachs. In einigen Fällen besitzt sie auch epikutikuläre Wachskristalle, welche aus dem epikutikulären Wachsfilm herauswachsen. Eine Hauptaufgabe der Kutikula ist der Schutz vor Austrocknung der Pflanze. Studien, die sich mit der Lokalisierung der transporteinschänkenden Barriere beschäftigten, zeigten, dass die Wachse sie bilden. Diese sind vielschichtige Mischungen aus langkettigen aliphatischen Verbindungen (VLCA) und pentazyklischen Verbindung wie Triterpenen (TRP). Es wird davon ausgegangen, dass VLCAs die Barriere aufbauen, ein direkter experimenteller Nachweis dafür wurde jedoch noch nicht erbracht. In dieser Arbeit wurde daher ein Verfahren zur selektiven Extraktion von TRPs aus isolierten kutikulären Membranen (CM) entwickelt und deren Auswirkung auf die Transpirationsbarriere untersucht (Kapitel V).

Die untersuchten Pflanzen wiesen keine epikutikuläre Kristalle auf, hatten keine Stomata auf der Kutikula der Blattoberseite und es war möglich ihre Kutikula zu isolieren. Die Zusammensetzung der Wachse variierte von wenig Wachs ohne TRPs (z. B. *Hedera helix*, *Zamioculcas zamiifolia*) hin zu pflanzen mit großer Wachsmenge und hohem TRP- Anteil (*Nerium oleander*). Die selektive Extraktion wurde durch die sequenzielle Nutzung zweier Lösemittel erreicht. Zunächst wurden die CMs über Nacht bei Raumtemperatur in Methanol (MeOH) eingelegt, was fast alle TRPs und geringe Mengen an kurzkettigen VLCAs extrahierte. Anschließend wurden die restlichen Wachse mit Chloroform (TCM) entfernt. In einem Vergleich der Kombination der so erhaltenen Wachse mit den üblichen Vollextrakten (FE), für die nur TCM genutzt wird, wurden für beide Verfahren ähnliche Ergebnisse erzielt.

Die gravimetrische Bestimmung der Wassertranspiration von unbehandelten, mit Methanol extrahierten (M) und entwachsten Membranen (MX) in Transpirationskammern zeigte bei allen untersuchten Pflanzenarten einen einheitlichen Trend auf. Im Vergleich zu CMs erhöhte sich die Transpirationsrate bei Ms nicht oder nur geringfügig, während bei MXs ein starker Anstieg festgestellt werden

konnte. Diese Ergebnisse stellen den ersten direkten experimentellen Nachweis der Verbindung von VLCAs zur Transpirationsbarriere kutikulärer Wachse dar.

Mit dem Wissen, sich bei der Untersuchung der Permeation durch die Kutikula sich nur auf die VLCA Fraktion beschränken zu müssen können weitere Projekte effizient angegangen werden. Ein leicht erhältliches Standartwachsgemisch könnte Ausgangspunkt für die Untersuchung des Einflusses verschiedener Pflanzenwachskomponenten auf deren physikalische Eigenschaften dienen. Eine weitere Anwendungsmöglichkeit wäre die Entwicklung von Screeningverfahren, mit denen der Einfluss von Adjuvantien auf kutikuläre Wachse untersucht werden kann. Daher wurde in dieser Arbeit die Entwicklung eines künstlichen Wachses angestrebt, welches die physikalischen Eigenschaften eines Blattwachses effizient wiederspiegelt. Als Zielwachs diente das Blattwachs von *Schefflera elegantissima*. Es bestand fast ausschließlich aus VLCAs, hatte eine recht einfache Zusammensetzung bezüglich der Stoffklassen und Kettenlängenverteilung und die Kutikula war isolierbar. Mit Hilfe von dynamische Differentialkalorimetrie (DSC) und Röntgenbeugung (XRD) wurden binäre ($C_{31}anC_{29}an$, $C_{32}olC_{30}ol$), ternäre ($C_{31}anC_{29}anC_{30}ol$, $C_{31}anC_{29}anC_{32}ol$) und quaternäre ($C_{31}anC_{29}anC_{32}olC_{30}ol$) Gemische untersucht und Phasendiagramme erstellt. Wachsgemische, die die Verhältnisse im Pflanzenwachs wiederspiegelten, wurden zusätzlich mit Fouriertransformierter Infrarot (FTIR) Spektroskopie untersucht (Kapitel VI).

Phasendiagramme wurden von einer Reihe der binären Gemische, bestehend aus Alkanen oder Alkoholen, ternären Gemischen aus zwei Alkanen und einem Alkohol ($C_{31}anC_{29}anC_{30}ol$, $C_{31}anC_{29}anC_{32}ol$, mit konstantem Verhältnis der Alkane: $C_{31}anC_{29}an$ 2.3 - 1) und quaternären Gemischen aus zwei Alkanen und zwei Alkoholen ($C_{31}anC_{29}anC_{32}olC_{30}ol$, mit konstantem Verhältnis der Alkane: $C_{31}anC_{29}an$ 2.3 - 1 bzw. Alkohole: $C_{32}olC_{30}ol$ 2.3 - 1) erstellt. Binäre Gemische wiesen einen fest-fest Übergang auf, der dem Wechsel aus dem orthorhombischen (Alkane) oder monoklinen (Alkohole) Gitter in ein hexagonales zugeordnet wurde. Die Kristallstrukturen bei Raumtemperatur wurden zusätzlich durch XRD Experimente verifiziert. Für eine binäre Alkanmischung ($C_{31}anC_{29}an$ 2.3 - 1) wurde dieser Übergang außerdem durch hot stage XRD Versuche aufgeklärt. Ternäre und quaternäre Wachse zeigten bis zu drei fest-fest Übergänge auf. Diese weisen auf das Vorhandensein dreier unterschiedlicher Phasen hin. Je eine Phase wird dabei von Alkanen oder Alkoholen dominiert, während die dritte Phase eine Mischphase darstellen könnte. Mit zunehmendem Alkoholgehalt

konnte ein Übergang von einer orthorhombischen in eine monoklinische Kristallgitterstruktur erkannt werden. Im intermediären Bereich waren dabei Gemische erkennbar, in denen beide Strukturen nebeneinander vorliegen. Diffraktogramme der quaternären Gemische wiesen ausschließlich auf orthorhombische Strukturen hin.

Infrarotspektroskopische Versuche wurden an zwei binären (C_{31}anC_{29}an und C_{32}olC_{30}ol mit dem Verhältnis 2.3 - 1), zwei ternären (C_{31}anC_{29}anC_{30}ol und C_{31}anC_{29}anC_{32}ol mit dem Verhältnis 2.3 - 1 - 1.4) und einem quaternären (C_{31}anC_{29}anC_{30}olC_{32}ol 5.4 - 2.3 - 2.3 - 1) Gemisch sowie an Wachs, welches von isolierten kutikulären Membranen extrahiert wurde, durchgeführt. Diese Gemische spiegelten die Verhältnisse der einzelnen Stoffe zueinander im Wachs der adaxialen Kutikula wider. Diese Versuche zeigten mit zunehmender Komponentenzahl eine erhöhte Ähnlichkeit der artifiziellen Wachse zum Pflanzenwachs. Jedoch wurden Unterschiede im Schmelzverlauf festgestellt. Obwohl sich die Werte der aliphatischen Kristallinität des quaternären Wachses und des Pflanzenwachses unterschieden war Ihr Verhalt unterhalb von 52 °C ähnlich konstant. Oberhalb dieser Temperatur zeigt das artifizielle Gemisch eine stärkere Abnahme als das Vergleichswachs. Die Unterschiede könnten auf die Differenzen in der Zusammensetzung liegen. Ähnlich wie beim Schmelzverhalten wurde eine stärkere Ähnlichkeit der Thermogramme der artifiziellen Gemische zum Pflanzenwachs (aus dem Extrakt ganzer Blätter) ersichtlich. Thermogramme der ternären und quaternären Gemische zeigten stark überlappende Peaks, die in einem ähnlichen Temperaturbereich lagen, wie die des Pflanzenwachses. Das Diffraktogramm des quaternären Waches stimmte auf Raumtemperatur gut mit dem des Pflanzenwachses (adaxiale isolierte Kutikula) ein. Bei den hot-stage XRD Versuchen waren jedoch starke Unterschiede erkenntlich. Während das Pflanzenwachs (aus dem Extrakt ganzer Blätter) bis zum vollständigen Schmelzen einen gleichmäßigen Verlust der orthorhombischen Kristallstruktur ohne Zwischenstufen aufwies, waren im quaternären Wachs Zwischenstufen erkennbar. Die Ergebnisse des zweiten Projekts waren nicht eindeutig, gaben jedoch Einblick in die Struktur kutikulärer Wachse. Während Hot Stage XRD und FTIR Experimente mit den Pflanzenwachsen auf das Vorhandensein einer Phase hinwiesen, deuteten die zugehörigen DSC Versuche und die Vergleiche mit artifiziellen Wachsgemischen auf das Bestehen von verschiedenen Regionen. Eine bestehend aus Alkanen und eine bestehend aus Aliphaten mit funktionellen Gruppen wie Alkoholen.

Diese Arbeit beschreibt eine Methode zur selektiven Extraktion von TRPs aus isolierten kutikulären Membranen. Sie zeigt einen direkten experimentellen Nachweis für die Assoziation der Transpirationsbarriere zu den VLCAs und nicht zu den TRPs. Zusätzlich wird die Möglichkeit kutikulare Wachse mit Hilfe von kommerziell erhältlichen Wachskomponenten nachzustellen untersucht, was vielversprechende Ergebnisse liefert. Dieses Wachs könnte daher als standardisierter Ausgangspunkt für weitere Experimente (z. B. zur Untersuchung des Einflusses verschiedener Wachskomponenten auf dessen physikalische Eigenschaften) dienen. Dies könnte wertvolle Informationen über die Struktur und die Beziehung zwischen chemischer Zusammensetzung und der Funktion kutikulärer Wachse liefern.

III. Abbreviation Index

ACL	Weighted average chain length
C_{29}an	Nonacosane
C_{30}ol	Triacosanol
C_{31}an	Hentriacontane
C_{32}ol	Dotriacosanol
CL	Cuticular layer
CM	Cuticular membrane
CP	Cuticle proper
DSC	Differential scanning calorimetry
FID	Flame ionization detector
FTIR	Fourier transform infrared
FE	Full extract
GC	Gas chromatography
HoF	Heat of Fusion
IR	Infrared
LEI	Lower secondary electron
M	Methanol extracted cuticle
MS	Mass spectroscopy
MX	Dewaxed cuticles
MeOH	Methanol
SEM	Scanning electron microscopy
TCM	Chloroform
TRP	Triterpenoid
VLCA	Very-long-chain aliphatic
XRD	X-ray diffraction

IV. Introduction

IV.1 Constitution of the cuticle

The colonialization of land posed a great challenge for plants. To cope with their new hostile environment, including temperature extremes, desiccation, gravity and increased UV radiation exposure, they developed various morphological and physiological features (Bateman et al. 1998; Waters 2003).

One of these adaptions is the cuticular membrane (CM). It forms the boundary between plants and their environment (Kenrick and Crane 1997). It consists of the cuticular layer (CL) and the cuticle proper (CP/ figure IV.1) (Sitte and Rennier 1963). The CL connects the CM to the epidermal cells, anchoring the CM to the epidermal cell wall by binding to the cell wall polysaccharides (Fich et al. 2016). In investigations on several species, a combination of pectinase and cellulase enzymes was used to isolate the cuticle, indicating a connection to pectin and cellulose (Lendzian et al. 1986; Orgell 1955). Adjacent to the CL, the CP forms the final layer, isolating the plant from its surroundings. The biopolymer cutin forms a scaffold for the CL and CP. It is a network of cross-linked hydroxyl fatty acids (Eglinton and Hamilton 1967). It is mostly composed of C_{16} or C_{18} hydroxy fatty acids or a mixture of both chain lengths. In C_{16}-based meshworks, the main components are 16-hydroxyhexadecanoic acid and 9 (or 10),16-dihydroxyhexadecanoic acid, while in networks based on C_{18} fatty acids 18-hydroxy-9, 10-epoxyoctadecanoic acid, 9, 10, 18-trihydroxydecanoic acid and their monounsaturated homologs prevail (Domínguez et al. 2011). Besides the cutin, the CP consists of imbedded (intracuticular) and overlying (epicuticular) waxes (Jeffree 2006). Some plants even possess a layer of epicuticular wax crystals, protruding from the epicuticular wax film, forming diverse aggregates (Koch and Ensikat 2008).
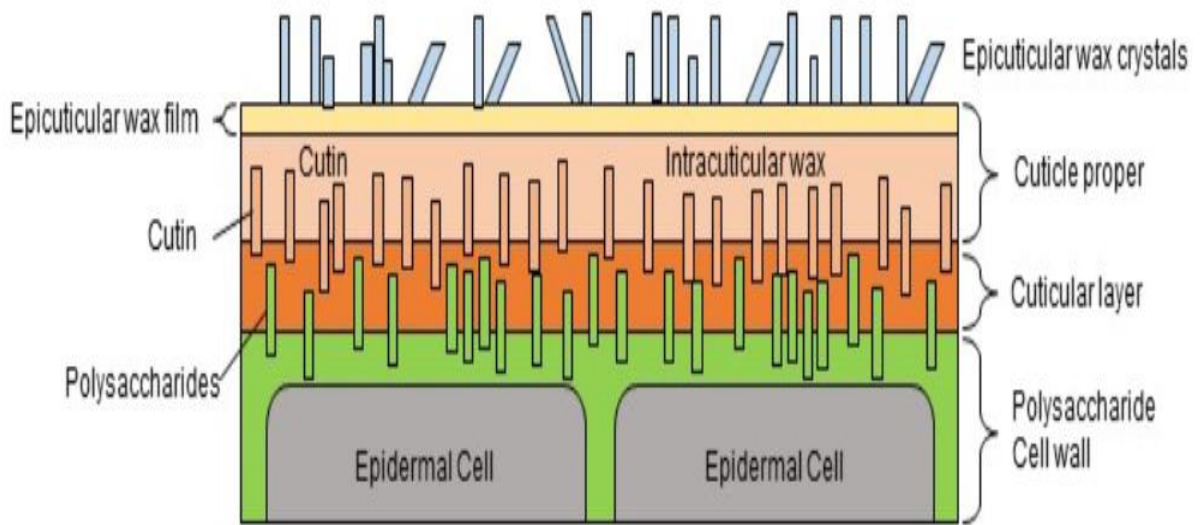
Figure IV.1: Schematic of the cuticular structure after Buchholz (2006) and Yeats and Rose (2013).

IV.2   Tasks of the cuticle

The cuticle serves as the first contact zone between plants, their environment and other organisms (Müller and Riederer 2005; Bargel et al. 2006). Bernays et al. extracted waxes from *Poa annua* and transferred it onto strips of filter paper. They found nymphs of *Locusta migratoria* L. started to bite the prepared pieces, but not the control strips without wax (Bernays et al. 1976). Cuticular waxes also play a vital role in carnivorous plants. Experiments of Scholz et al. (2010) indicate the surface structure of cuticular wax of the carnivorous pitcher plant *Nepenthes alata* Blanco to prevent insect adhesion, to help them to catch insects for nutrition. These structures can form different shapes, like tubules, crusts or platelets, and have a substantial effect on the plant surface properties including contributions to hydrophobicity, wettability or self-cleaning behaviour (Koch and Ensikat 2008). Dust and small particles on the surface of leaves can reduce the sunlight intake by shading or interfering with diffusion, thus compromising their ability of photosynthesis (Thompson et al. 1984; Naidoo and Chirkoot 2004). To address this problem, various plants developed leaves with a self-cleaning effect, better known as the lotus effect (Barthlott and Neinhuis 1997; Neinhuis and Barthlott 1997). It is named after the lotus, *Nelumbo nucifera* Gaertn., a plant species showing a pronounced self-cleaning effect on its leaves. (Barthlott and Neinhuis 1997). The surface roughness causes a high hydrophobicity and gives the cuticle anti-adhesive properties. Water is strongly repelled and form droplets. While running down a leaf, the droplets pick up dust and contaminations and clean the leaf surface (Barthlott and Neinhuis 1997). The cuticle also protects against UV radiation, either through reflection by surface waxes or absorption by cuticular pigments (Jansen et al. 1998). Holmes and Keiller (2002) showed on different leave types, surface waxes of glaucous leaves to provide sufficient UV radiation reflection. Krauss et al. (1997) showed cuticular pigments to protect the sensitive tissue beneath reasonably effectively. A nowadays crucial function of the cuticle is its function as an uptake barrier. Formulations with active ingredients for plant protection are widely used in agriculture. To take effect, many of those ingredients have to penetrate the cuticle and get into the plant. Price and Anderson (1985) investigated the uptake of 10 compounds with varying lipophilicity in different plant species. Their experiments divided the plants into three categories with variable uptake behaviour. They conclude that the assumption of high uptake of one formulation into a particular species will lead to

similar behaviour in another species is invalid and indicate the necessity of species-specific formulations to optimize compound absorption (Price and Anderson 1985). Besides its intake limiting properties, the cuticle also acts as a transpiration barrier against uncontrolled water loss from leaves, fruits and other primary parts of higher plants (Riederer and Schreiber 2001). Leaves play an essential role since they comprise the primary interface between a plant and the environment (Burghardt and Riederer 2003). For example, one square meter of meadow exhibits at least a four times greater leaf surface to the atmosphere (Barthlott et al. 2003). This circumstance makes it very important to control cuticular water loss, especially under drought conditions. Intuitively, one might assume a correlation of cuticular thickness and permeability according to Fick´s first law, but a positive relationship between water permeance and cuticle thickness was not detected (Schreiber and Riederer 1996; Riederer and Schreiber 2001). Neither was a correlation between cuticular water permeability and the amounts of cuticular waxes found, but their predominating role as the transport-limiting barrier is evident (Schreiber 2010). The ability to prevent uncontrolled water loss through the cuticle is vital for the survival of terrestrial plants. Different methods have been developed to measure cuticular transpiration.

One method utilizes radioactively labelled water in a double chamber to determine water permeability through the cuticle. Schreiber (2001) deployed this method to isolated adaxial cuticles and leaf discs of five different plant species to investigate the temperature effect on the cuticular transpiration barrier. When the temperature was increased from 10 °C to 55 °C, they found an increase in water permeability up to a factor of 264, depending on the plant species. (Schreiber 2001). Another way to describe the capability of leaves to retain water is the minimum leaf water conductance. Whole leaves were saturated with water and afterwards, their petioles were sealed with wax. The leaves were kept at low humidity in a dark place and the consecutive water loss was measured using a balance (Burghardt and Riederer 2003; Schuster et al. 2016). Schönherr and Lendzian (1981) developed a method to measure cuticular permeability using CM in transpiration chambers and found good conformity to the literature of the obtained values for *Citrus aurantium* L. leaves (Schönherr and Lendzian 1981). In a more recent study, Jetter and Riederer (2016) adapted this method and indicated the location of the transpiration barrier within the intracuticular waxes.

IV.3 Biosynthesis of cuticular wax compounds

The elemental composition of cuticular waxes is long known due to work of Chibnall et al. (1934) and others (Baker and Procopiou 1975; Croteau and Fagerson 1971; Chibnall et al. 1931). Cuticular waxes contain a wide variety of substances, which can roughly be divided into two groups. Ubiquitous compounds of a wax blend are very long chain aliphatic (VLCA) compounds like n-alkanes, primary and secondary alcohols, ketones, aldehydes, fatty acids and alkyl ester (Koch and Ensikat 2008). The latter is comprised of unbranched substances with a carbon chain length of 20 to 40 and alkyl esters made of C_{16} – C_{34} fatty acids and C_{20} – C_{36} primary alcohols (figure IV.2), with total carbon chain lengths ranging from C_{36} – C_{70} (Jetter et al. 2008; Gülz et al. 1993; Sümmchen et al. 1995). These standard compounds may contain more than 50 substances in a species-specific array (Jetter et al. 2008). Long-chain fatty acids are used as precursors to synthesize various wax components like aldehydes, primary alcohols and alkanes. The biosynthesis of VLCAs starts with the production of C_{16} or C_{18} fatty acids de novo in the stroma of plastids. From here, the acids are distributed in different pathways. They either form alkyl esters or can be elongated to very-long-chain fatty acids by joining C_2 moieties in a sequence of reactions, thus making even-numbered acids predominant (Kunst and Samuels 2003). The synthesis of alkanes includes a decarbonylation process, making odd-numbered homologs paramount (Samuels et al. 2008).

The second group, besides the earlier described ubiquitous compounds, are taxon-specific constituents of cuticular waxes, including secondary alcohols, ketones and triterpenoids (TRP) (Jetter et al. 2008). Like in alkanes, odd-numbered homologs are predominant in secondary alcohols and ketones, suggesting a link in their biosynthetic pathway (Wollrab 1969). Samuels et al. (2008) confirmed in experiments alkanes to be an intermediate product of two sets of reactions, forming secondary alcohols and ketones. While these two substance classes are VLCAs, TRPs are another category. In contrast to straight-chained VLCAs, TRPs show an incredible structural diversity (Mahato et al. 1992).
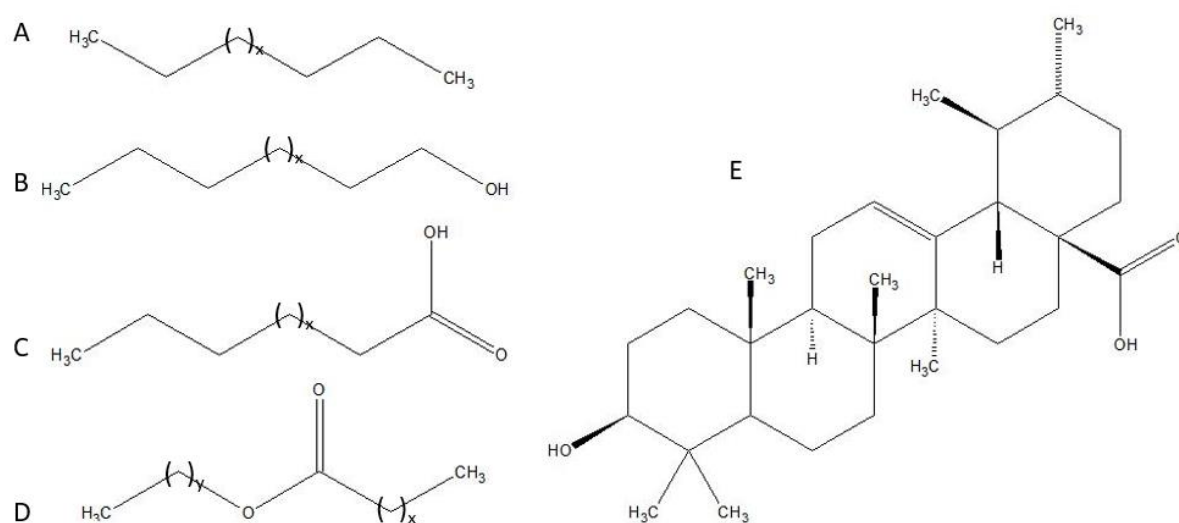
Figure IV.2: Basic structures of ubiquitously found VLCA compounds (A - C) of cuticular waxes: A alkanes, B alcohols, C fatty acids and the regularly found compounds D alkyl ester and E ursolic acid.

Depending on the enzyme, more than 200 different triterpene scaffolds can be synthesized, which are modified by tailoring enzymes in subsequent reactions (Xu et al. 2004; Thimmappa et al. 2014). Early investigations on their biosynthesis indicated squalene as a possible raw material (Eschenmoser et al. 1955). However, further studies showed TRPs to be derived from enzymatic cyclisation of 2,3-oxidosqualene after protonation, a series of intramolecular addition reactions and deprotonation (Abe et al. 1993; Kunst et al. 2008). TRPs are a numerous and versatile group of plant metabolites (Thimmappa et al. 2014). Aside from the constituents mentioned above, a significant number of taxon-specific wax components like diols, aromatic compounds, alkaloids and various further wax elements were found (Jetter et al. 2008).

IV.4 Wax sampling techniques

Cuticular wax can be segmented into three domains, defined as intracuticular wax, epicuticular wax film and epicuticular wax crystals protruding from this film, with partly drastically varying compositions (Jetter et al. 2008). A differentiated analysis of these layers frequently failed since appropriate sampling methods were hardly available. A standard extraction method is the suspensions of leaves in nonpolar solvents. Therefore, chloroform (TCM) is frequently used pure or in mixtures (Eglinton and Hamilton 1967; Fagerström et al. 2013). However, suspending the whole leaf in a solvent for extended periods results in a mix of all layers. This method gives useful quantitative information of wax compounds in the cuticle but cannot differentiate between adaxial and abaxial leaf and between intra – and epicuticular wax (crystals). To tackle the problem of lacking differentiation, several techniques have been developed over the past years.

A fast and straightforward method to distinguish between wax from the adaxial and abaxial leaf sides is to press a glass cylinder onto an intact leaf to limit the sample area and remove the waxes by agitating TCM on the surface (van Maarseveen and Jetter 2009; Buschhaus et al. 2007; Jetter et al. 2000). Buschhaus et al. (2007) placed *Rosa canina* leaves onto a flexible rubber mat, pressed a glass cylinder onto its surface and extracted cuticular waxes by agitating the solvent in the cylinder. Since the whole leaf is used for sampling, the possibility to remove substances from within the leaf is given. A more time-consuming alternative to using whole leaves is the isolation of the CM. Therefore, leaf discs are punched out of a leaf with a cork borer and are incubated in an enzyme solution containing cellulase and pectinase. After decomposition of the mesophyll tissue, the adaxial and the abaxial side of the cuticle can be harvested separately (Orgell 1955; Lendzian et al. 1986; Schönherr and Riederer 1986). From CM disks waxes can easily be extracted by dispersing them in TCM or Soxhlet extraction (Schönherr and Riederer 1986; Schuster et al. 2016). With these techniques, investigations on the different sides were conducted. Guhling et al. (2005) reported compositional differences between adaxial and abaxial leaf cuticles in *Macaranga tanarius*. In a study about the maternal or paternal inheritance of wax characters in *Rosa,* section *Caninae*, higher wax amounts on adaxial leaf surfaces and composition differences were reported (Wissemann et al. 2007). An investigation on

cherry laurel (*Prunus laurocerasus*) leaves showed a higher abundance of abaxial cuticular wax and varieties in chemical composition compared to the adaxial analogue. Besides extraction protocols in which the leaf material is treated with solvents for different durations, mechanical removal approaches were evolved (Buschhaus and Jetter 2011). During the investigation of *Macaranga* ant-plants, Markstädter et al. (2000) enriched samples with epicuticular waxes using glass wool to peel them from the leaf surfaces. This procedure gave qualitatively good results but was not fitting for quantitative analysis (Markstädter et al. 2000). Another approach is mechanical stripping using adhesives. Riedel et al. (2003) removed cuticular waxes of the cuticle of the slippery zone pitchers of *Nepenthes alata* Blanco, a carnivorous plant natively preying on ants (Scholz et al. 2010). They applied liquid water to the cuticle surface, froze it with liquid nitrogen and removed the ice together with the waxes. This procedure gave a selective view on the epicuticular wax (Riedel et al. 2003). Further approaches deployed different types of polymers to strip epicuticular wax. Haas and Rentschler (1984) used collodion, a cellulose nitrate-based polymer, to remove surface waxes from *Rubus fruticosus* (blackberry) leaves. Though it was an essential step in developing wax stripping methods, this procedure showed limitations regarding the accuracy of the obtained samples. Jetter et al. (2000) found markers for intra- and epicuticular waxes in samples collected with this method. They concluded a partial mixing of wax layers, caused by the organic solvents, in which collodion was applied, was responsible for the cross-contamination (Jetter et al. 2000). Alternatives to collodion were found in cellulose acetate and gum arabic. Zeisler and Schreiber (2016) used collodion, cellulose acetate and gum arabic to investigate the contribution of epi- and intracuticular waxes on the cuticular transpiration barrier on cherry laurel leaves. They found no increase after repeated application of collodion and gum arabic but found one for cellulose acetate. However, the latter was applied in the organic solvent acetone and they concluded the solvent to affect the barrier (Zeisler and Schreiber 2016). In several studies, gum arabic was applied using water as solvent (Jetter and Schäffer 2001; Zeisler and Schreiber 2016; Jetter and Riederer 2016; Riedel et al. 2003). Compared to the usually more lipophilic organic solvents, the polar water is an extremely bad solvent for unpolar waxes, resulting in a minimum influence on the behaviour of cuticular waxes. van Maarseveen and Jetter (2009) showed for *Kalanchoë daigremontiana* Hamet et Perr. de la Bathie ratio differences between intra-

and epicuticular waxes. With these techniques, it was possible to study intracuticular and epicuticular waxes separately. Jetter et al. (2000) found significant differences between the two layers. Epicuticular wax consisted primarily of VLCAs, while intracuticular wax was mostly made up of TRPs (Jetter et al. 2000). Haas and Rentschler (1984) found epicuticular wax of blackberry leaves to constitute about 90 % of total soluble waxes. Besides, contrary to its intracuticular waxes, it didn´t comprise any TRPs (Haas and Rentschler 1984). A similar result was found in a study on ten different plants by Zeisler-Diehl et al. (2018). They found TRPs, if existing, primarily in the intracuticular waxes and only in traces in the epicuticular waxes. Furthermore, the ratio and composition of intra- and epicuticular waxes varied widely across all plants (Zeisler-Diehl et al. 2018).

IV.5 Crystallinity of cuticular wax

Despite many efforts to correlate the composition of cuticle waxes of various plants with their respective water permeability, no such relationship has been found (Riederer and Schneider 1990; Schönherr 1976; Riederer and Schreiber 2001). Riederer and Schneider (1990) proposed a model for water permeating through the cuticular transpiration barrier analogue to technical membranes and semicrystalline olefin polymers. They suggest a structure made of two phases. The crystalline domain is inaccessible to water and reduces the water permeability by increasing the diffusional resistance and restricting the water flow through the cuticle (Riederer and Schneider 1990). These areas are encompassed with amorphous zones, enabling water to diffuse across the cuticle (Cussler et al. 1988). The amorphous pathways are formed by the chain ends of very long aliphatic compounds, while their inner sections align in regular, at room temperature orthorhombic lattices, building the crystalline zones (Riederer and Schneider 1990; Reynhardt and Riederer 1991) This is known as the brick and mortar model (figure IV.3)

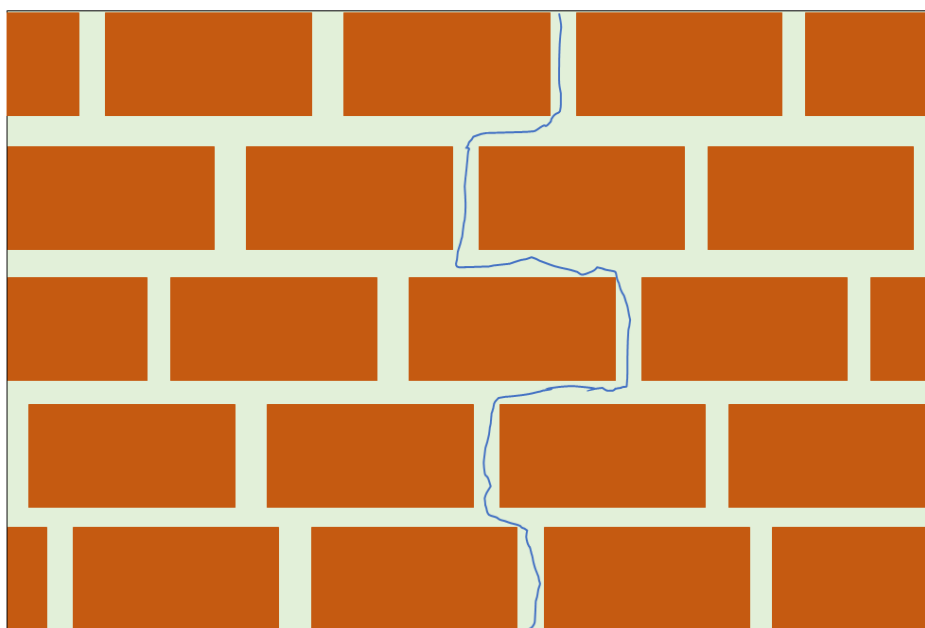Figure IV.3: Brick and mortar model according to Riederer and Schreiber (1995). Orange rectangles indicate impermeable crystalline zones. The permeable amorphous areas are depicted by green areas. The blue line indicates a possible permeation path for substances.

A viable method to investigate the structure of cuticular waxes is the infrared spectroscopy. It has been used widely to study the cuticle and its waxes (Maréchal and

Chamel 1996; Farber et al. 2019; Merk et al. 1997; Radler and Horn 1965; Barton et al. 1992; Dubis et al. 2001; Heredia-Guerrero et al. 2016). This method utilizes infrared radiation (780 nm – 1000 µm) to examine molecular vibrations (figure IV.4) of, for example, CH_2 groups of aliphatics (Günzler and Gremlich 2012).
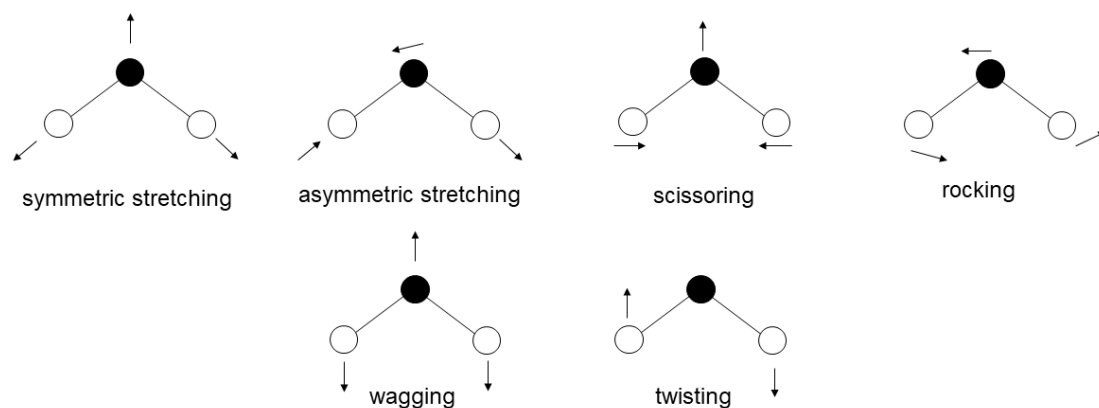
Figure IV.4: Different vibration modes of CH_2 groups modified according to Fischmeister (1975). Black circles signify carbon and white circles hydrogen atoms.

Chapman (1955) used Fourier transform infrared (FTIR) spectroscopy to investigate polymorphic transitions of a crystalline phase. At room temperature, the mid-chain CH_2 groups of cuticular waxes form an orthorhombic crystal lattice (Riederer and Schneider 1990; Reynhardt and Riederer 1991). The CH_2 units are ordered in an all-trans configuration (figure IV.5 A). They can do a transition into a hexagonal lattice. In this rotator-phase, they maintain their all-trans configuration, but they can also rotate around their longitudinal axis (Basson and Reynhardt 1991; Reynhardt and Riederer 1994; Reynhardt 1985, 1997). Hastie and Roberts (1994) showed, that upon heating the all-trans chains can turn into chains with trans-gauche, double gauche configurations and so-called "kinks" (figure IV.5 B - C).
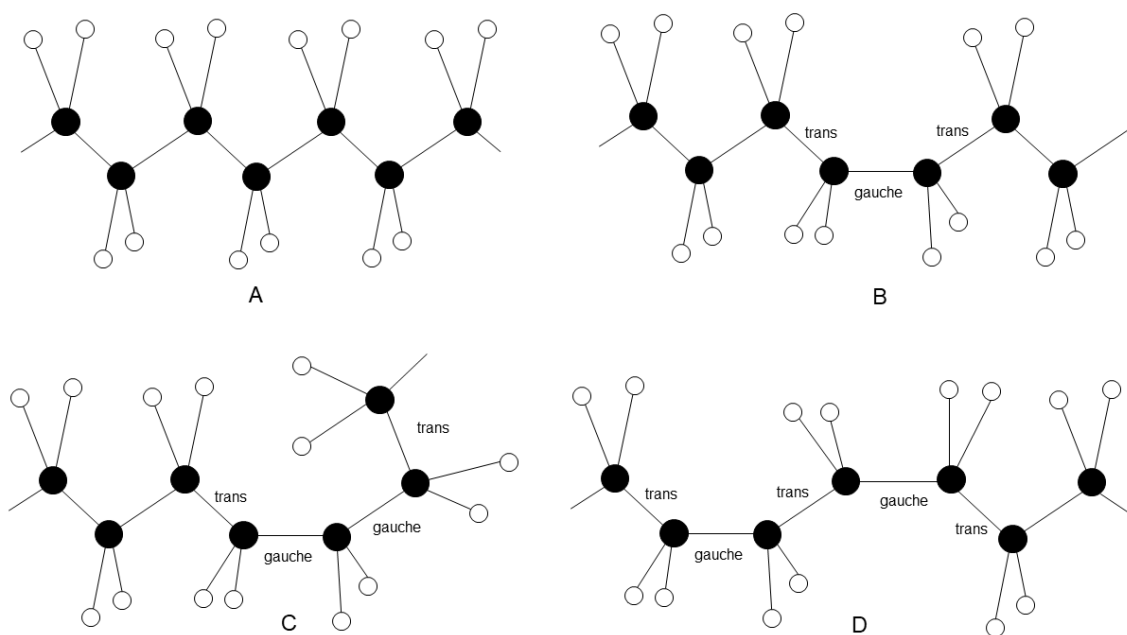
Figure IV.5: All-trans (A), trans-gauche (B), double gauche (C) and "kink" (D) conformation of polymethylene sections of very-long-chained aliphatics according to Hastie and Roberts (1994).

Chapman (1955) assigned signals in infrared (IR) spectra to distinct crystalline structures, like a split peak at a wavelength of 720 cm^{-1} to the orthorhombic lattice (Chapman 1955). Marsen (1961) matched the 720 cm^{-1} peak with absorption from amorphous and crystalline parts of the wax, whereas the 730 cm^{-1} peak only contains crystalline contributions (figure IV.6).
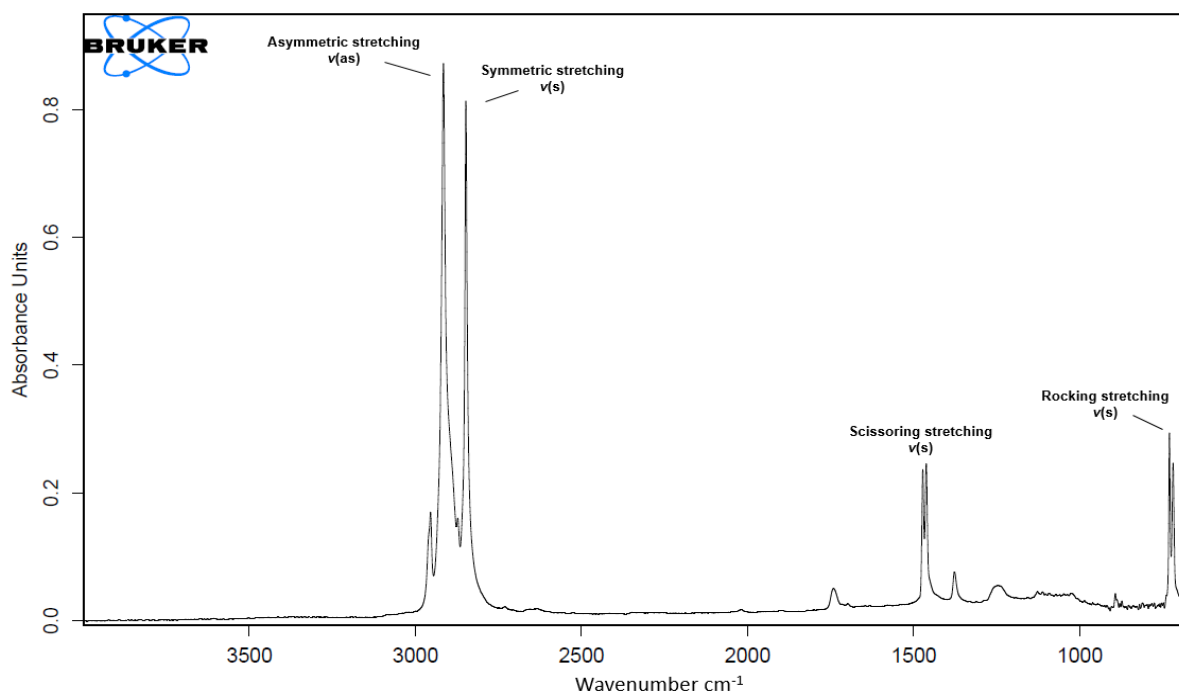
Figure IV.6: FTIR of hentriacontane. Double peak of rocking stretching (720 - 730 cm^{-1}) and scissoring stretching (1471 - 1473 cm^{-1}) indicate a crystalline structure within the substance.

Merk et al. (1997) showed a temperature-dependent decrease of one of these peaks, indicating the loss of this structure and an increase in alkyl chain disorder. Furthermore, they found no qualitative differences between reconstituted waxes, wax on intact cuticles and fresh leaves. However, this method of crystallinity determination is restricted to cuticular waxes dominated by aliphatic constituents since IR radiation interacts with CH_2 units (Merk et al. 1997). Dubis et al. (1999) conducted examinations with horizontal attenuated total reflection FTIR to investigate a rapid potential alternative to time-consuming chromatographic methods. They used derivative spectra to distinguish between bands of similar functional groups of different compounds, e.g. C=O band of alkyl esters and aldehydes. Nonetheless, a possibility to differentiate between homologues was not given (Dubis et al. 1999).

The crystallinity behaviour of waxes can also be investigated by thermal techniques. Perkins et al. (2005) used differential scanning calorimetry (DSC) and localized thermal analysis to examine the impact of surfactants on cuticular wax of *P. laurocerasus*. For DSC measurements, two crucibles, one with sample and one empty as a reference, are each placed on a temperature sensor within a temperature-controlled chamber (figure IV.7). As the temperature is changed, the heat difference in heat flow rate to the sample and reference is determined (Höhne et al. 2013).
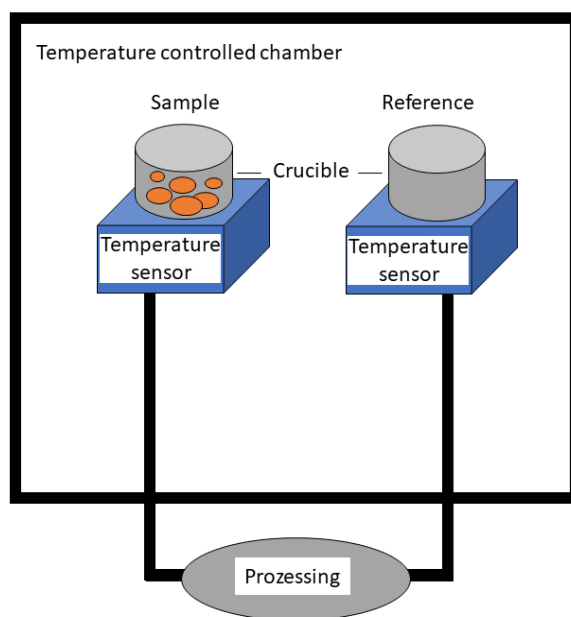
Figure IV.7: Conceptual schematic of a DSC measurement. Two crucibles are placed on Temperature sensors within a temperature-controlled chamber. One filled with a known amount of sample and one empty as reference. While the chamber is heated the heat uptake of both crucibles is measured.

This technique allows the investigation of the phase behaviour of endothermic as well as exothermic nature, heat capacity, enthalpy and transition temperatures (Höhne et al. 2013)

Perkins et al. (2005) researched *P. laurocerasus* crystalline behaviour in a temperature range between 0 to 100 °C and found two peaks. While the peak at a higher temperature could be assigned to the melting of the wax, the first one was assigned to the transition of an orthorhombic lattice to a hexagonal phase by investigations on mixtures of n-alkanes and waxes (Basson and Reynhardt 1991; Reynhardt and Riederer 1994). Perkins et al. (2005) found a shift of melting temperature and the loss of one peak in DSC thermograms after application of the surfactant Synperonic A7. The subsequent localized thermal analysis confirmed the shift to lower temperatures. In these curves, a second peak at temperatures below the melting range occurred, which was assigned to the transition to a hexagonal phase. They further found no difference in the behaviour of reconstituted and native waxes (Perkins et al. 2005). Nuclear magnetic resonance spectroscopy also showed the presence of two phases. Schreiber et al. (1997) found leads of constituents to be isotropic and rigid below the melting temperature of samples spiked with perdeuterated substances and their results

align with subsequent DSC studies. The extracts of Arabidopsis, *Thellungiella parvaula*, *Musa acuminate* and *Monstera deliciosa* were analyzed using spontaneous Raman spectroscopy and coherent anti-Stokes Raman scattering. In this study, Littlejohn et al. (2015) found wax crystallinity degrees between crystalline and amorphous.

Ensikat et al. (2006) used X-ray powder diffraction to investigate the crystal structure of cuticular waxes and found three lattice types, depending on wax composition. X-ray diffraction (XRD) is based on the scattering of X-rays "on periodic structures with geometrical variations on the length scale of the wavelength of the radiation" (Birkholz 2006). When the distance between single atoms and molecules in a crystal lattice is in the range of 0.15 – 0.40 nm, phenomena of constructive and destructive interference become observable (Birkholz 2006). Crystalline structures can occur in different types of lattices, like the orthorhombic (figure IV.8 A) or the triclinic one (figure IV.8 B).

A   B
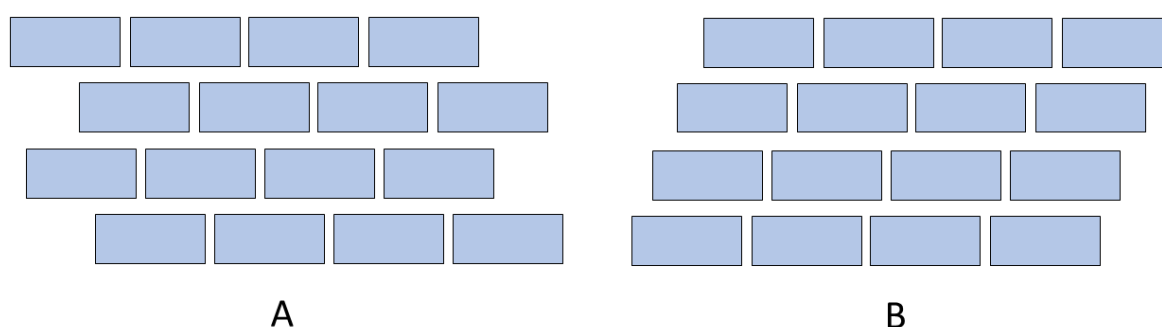
Figure IV.8: Schematic alignment of the geometrical ordering of atoms for an orthorhombic (A) and a triclinic (B) crystal lattice according to Ensikat et al. (2006)

The Bragg equation (IV.1) describes the "the position of X-ray scattering peaks in angular space" (Birkholz 2006)

$$n\,\lambda = 2d\,\sin(\theta) \qquad\qquad\qquad \text{IV.1}$$

With n signifying the diffraction order (natural number), λ the wavelength of used radiation, d the distance between the crystal layers and θ the angel of the incoming radiation to the crystal lattice (Birkholz 2006; Pope 1997). Figure IV.9 illustrates this equation.
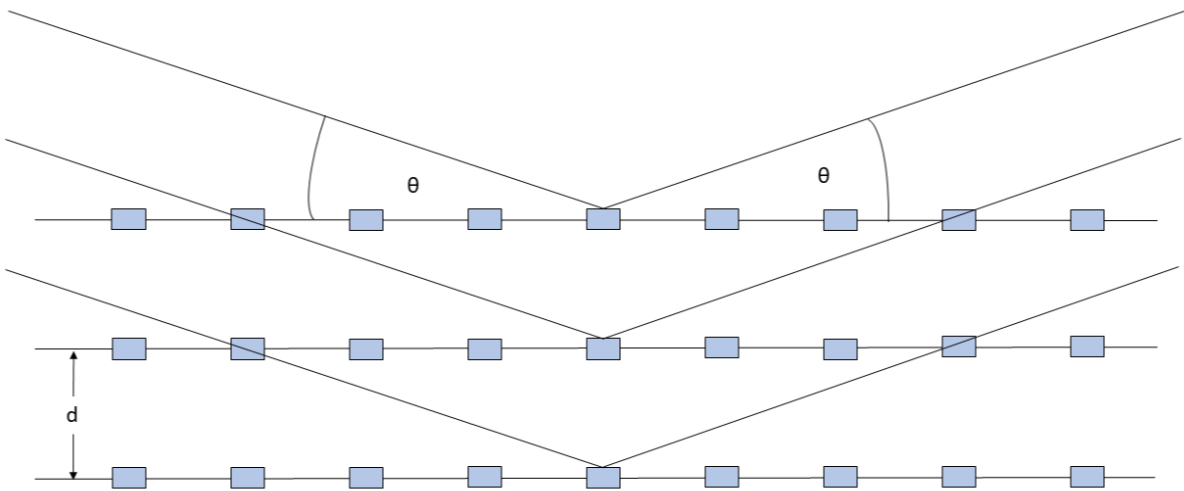
Figure IV.9: Visualization of the Bragg equation according to Birkholz (2006). Blue boxes indicate a highly ordered crystalline structure. The distance between two layers is signified by d, the angle of incidence by θ.

From the Bragg equation can be seen, that maximum constructive interference only occurs for a whole numbered phase shift of the incidental wavelength. For the measurement of powder XRD spectra, fine powdery samples are inserted into the device on a sample holder. During the analysis, the incident angle of the radiation onto the sample is changed and the resulting spectra are recorded using a detector (figure IV.10)
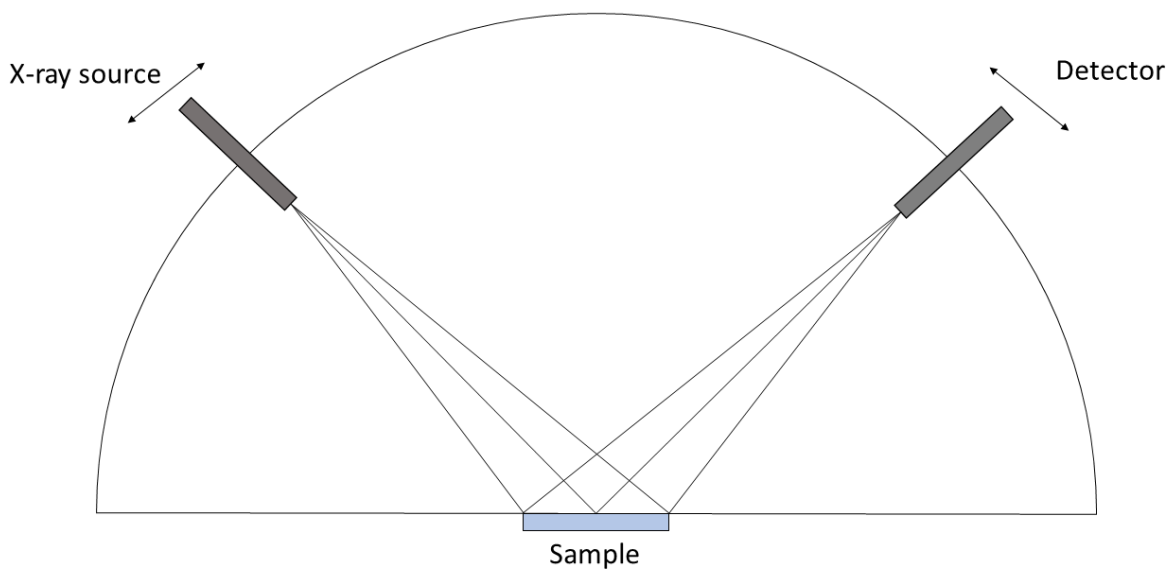
Figure IV.10: Schematic buildup of an XRD measurement. During measurement the angle of the radiation source and detector are adapted to scan an array of incident angles.

Ensikat et al. (2006) found for the majority of samples an orthorhombic order. Epicuticular wax crystals in tubular shape consisting of secondary alcohols exhibited a triclinic lattice while tubules made from ketones had a hexagonal crystal order (Ensikat et al. 2006).

Reynhardt and Riederer (1994) investigated whole leave wax of *Fagus sylvatica* L. and *Hordeum vulgare* with this technique and found both waxes to have an orthorhombic crystal lattice. They also estimated the degree of crystallinity of these to waxes to 31 ± 5 % for *Fagus* and 52 ± 5 % for *Horderum* waxes respectively (Reynhardt and Riederer 1994). Further research into the cuticular wax of *H. vulgare* L. indicated hydrogen bonding to prevent separation of short and long chain-length distributions, resulting in a comparably sizeable amorphous phase, thus lowering the crystallinity of the wax (Reynhardt 1997). In another study, adaxial cuticular wax of *Citrus aurantium L.* was also found to obtain the orthorhombic crystal structure (Reynhardt and Riederer 1991). Crystallinity estimations clocked in at a low crystallinity of roughly 20 % (Reynhardt and Riederer 1991)

IV.6 Aim of the present study

A lot of effort has been made to investigate the cuticle and its barrier function towards water transpiration. However, no connection between water permeability and cuticular properties, like its thickness, wax composition or wax coverage were found (Schreiber and Riederer 1996; Riederer and Schreiber 2001). Several studies localized the barrier within the cutin matrix and the intracuticular waxes (Zeisler and Schreiber 2016; Zeisler-Diehl et al. 2018; Jetter and Riederer 2016). Jetter and Riederer (2016) also predicted the barrier being established by the VLCAs of the intracuticular waxes. However, they lack direct experimental proof.

The first project is subjected to the localization of the cuticular transpiration barrier. Although Jetter and Riederer (2016) predicted the barrier within the VLCAs, so far, no direct experimental proof was given. In this study, a method distinguishing between aliphatic and alicyclic wax compounds was developed and its effect on the water permeability of isolated astomatous plant cuticles of several species was determined. Several techniques can be used to characterize the physical properties of cuticular wax. FTIR can be used to determine the degree of crystallinity, crystal structure, phase transitions or the melting behaviour of wax samples with changing temperature (Merk et al. 1997; Zerbi et al. 1989). DSC experiments give further inside into phase transitions and melting behaviour of waxes (Fagerström et al. 2013; Aggarwal 2001). XRD can provide detailed information about crystallinity and the crystal lattice of waxes. For methods like DSC, however, sample sizes in a milligram scale are often necessary to gain good quality results. For the development of screening methods, which could be used, for example, in agriculture, the required wax amounts of the adaxial leaf could hardly be provided with reasonable effort and purity by wax extraction from plants. Therefore, a model wax was sought.

The second chapter deals with the characterization of leaf waxes of *S. elegantissima* leaves, a plant with a reported low content of alicyclic compounds, and artificial wax mixtures comprised by commercially available standard compounds (Jetter and Riederer 2016). This project aimed to find a preferably simple mixture, made of commercially available compounds, depicting the leaf wax properties with sufficient proximity. Therefore, for characterization FTIR, DSC and XRD were used. Such a standardized plant wax proxy can be useful in various applications. It could be used as an initial point to investigate the impact of different plant wax constituents on physical

properties of cuticular wax. Another application is the development of a fast screening method to investigate the uptake behaviour of in agriculture used active ingredients or the effect of adjuvants on the wax.

V. The fractionated extraction of leaf cuticular wax compounds and their influence on the transpiration barrier

V.1 Introduction

As the outermost layer of plant leaves, the cuticle, consisting of a cutin matrix and cuticular waxes, fulfils various tasks (Koch and Ensikat 2008; Müller and Riederer 2005; Barthlott and Neinhuis 1997). One of these important tasks is its function as a barrier against uncontrolled water loss, especially under drought conditions (Riederer and Schreiber 2001).

For the establishment of the water permeability barrier, cuticular waxes play a predominant role (Schreiber 2010). Cuticular waxes are sophisticated heterogeneous mixtures varying strongly across species. However, they are typically made up by TRPs and VLCAs (Jetter and Riederer 2016). TRPs are alicyclic constituents of cuticular waxes with a wide structural diversity, which is derived from its biosynthetic pathway (Mahato et al. 1992; Thimmappa et al. 2014). This group of compounds was shown to improve the mechanical strength of the cuticle (Tsubaki et al. 2013). TRPs were also shown to have antifungal effects (Hamburger et al. 1989). In another study, Baskar et al. (2014) found friedelin to have good activity against two pests. They were also shown to be present almost exclusively in the intracuticular wax. (Buschhaus et al. 2007; Tsubaki et al. 2013). Due to their high melting points, TRPs were proposed to restrict thermal damage to the transpiration barrier (Schuster et al. 2016). However, a study on plastic membrane showed the application of the TRP oleanolic acid not to affect the water permeability of the membrane (Grncarevic and Radler 1967). Results of further experiments on this artificial system from the same study of Grncarevic and Radler (1967) indicate VLCAs to constitute the barrier against water loss possibly. VLCAs are ubiquitously found in epi- and intracuticular plant waxes. Epicuticular waxes and potential epicuticular wax crystals are the outermost layer of the cuticle and play an important role in interactions with the surrounding environment. A widely common known effect of these waxes is the self-cleaning or lotus effect, resulting from surface roughness on a microscopic level, giving the cuticle anti-adhesive properties (Barthlott and Neinhuis 1997). Jetter and Riederer (2016), Zeisler and Schreiber (2016) and Zeisler-Diehl et al. (2018) showed intracuticular waxes to have a major influence on water permeance. Jetter and Riederer (2016) indicated intracuticular VLCAs to

constitute the transpiration barrier, but lack experimental evidence. Staiger et al. (2019b) have shown VLCAs to constitute the uptake barrier against active ingredients into the plant. They used an extraction sequence to selectively remove TRPs from CMs and determined the impact of this treatment on the barrier properties of the wax against two model compounds. In this work an adapted method was used to produce TRP free cuticles, of which subsequently the water permeance was measured.

To measure the water loss, commonly two experimental setups are used. Experiments to determine the minimum water conductance were conducted measuring the mass loss of detached leaves under conditions of maximum stomatal closure (Burghardt and Riederer 2003). This technique is suitable if the leaves are not hypostomatous or the cuticle is not isolatable (Kirsch et al. 1997). Although this technique would permit the determination of the minimum water conductance of a wide variety of plant species, it wasn´t used in this work. Staiger et al. (2019b) showed methanol (MeOH) to extract alicyclic compounds effectively from isolated CMs but not from intact leaves. Therefore, an adapted method developed by Schönherr and Lendzian (1981) was used. They introduced a method to measure cuticular water permeability on isolated CMs. They mounted a cuticle on a water-filled transpiration chamber and subsequently measured the water loss gravimetrically (Schönherr and Lendzian 1981).

In this chapter of the work VLCAs as the water transpiration barrier are discussed. A method for fractioned extraction of TRPs and VLCAs to determine their influence on this barrier was tested on CMs of eight plant species. The plant species were chosen to cover a broad range of various compositions from species with low wax load and no TRPs like *Hedera helix* and *Zamioculcas zamiifolia* to plants with high wax load and high TRP content like *Nerium oleander*. The composition and the effect of wax extraction on water permeance in regards to the extracted wax fraction were evaluated.

V.2 Material and Methods

V.2.1 Plant material

All plant material was obtained from the botanical garden of Würzburg. *Camellia sinensis, Ficus elastica* and *Z. zamiifolia* were continuously kept in the greenhouse. Potted plants of *N. oleander* were kept in a greenhouse throughout winter and outside during summer. *H. helix, Ilex aquifolium, Prunus laurocerasus* and *Vinca minor* were uniformly kept outdoors. For experiments, only mature leaves were harvested. If possible, care was taken to harvest leaves of the same plant to provide a common initial point for each plant species.

Adaxial leaf CMs were prepared after an adapted method of Schönherr and Riederer (1986). Preferably nervure free discs (diameter of 1.89 cm) were punched out of fresh leaves, using a cork borer and the adaxial side was marked. The discs were incubated with an enzyme solution consisting of 1 % pectinase (Trenolin, Erbslöh, Geisenheim, Germany), 1 % cellulase (Celluclast, NCBE, University of Reading, U.K.), 1 mM citric acid monohydrate (Applichem, Darmstadt, Germany) and 1 mM sodium azide (Sigma-Aldrich, Steinheim, Germany) to prevent bacterial growth. The incubated disks were kept at room temperature until the dissolution of leaf tissue. The solution was replaced twice a week. Finally, adaxial leaf discs were picked out, washed thoroughly and stored in distilled water until use.

V.2.2 Wax extraction and analysis

Two types of wax samples have been prepared from adaxial cuticle discs. Full extracts (FE) were prepared by dispersing five CMs (two for *H. helix*) twice in 20 mL TCM (≥99,8%; Roth, Karlsruhe, Germany) for 10 min. The extracts were combined, n-tetracosane (Sigma Aldrich, Steinheim, Germany) was added as an internal standard, and the solvent was removed under a gentle N_2-stream. For gas chromatography (GC), an aliquot of the wax sample was derivatized using N, O-bis(trimethylsilyl)trifluoroacetamide (Macherey-Nagel Düren, Germany) in dry pyridine (Roth, Karlsruhe, Germany) for 45 min at 70 °C. Quantitative analysis was conducted using GC coupled with a flame ionization detector (FID). Samples were injected by an on-column injector (7890A, Agilent Technologies, Waldbronn, Germany) onto a fused silica capillary column (DB1-ms, 30 m length x 0.32 mm ID, 0.1 µm film, Agilent Technologies) using H_2 as carrier gas. The temperature program was: injection

at 50 °C and held for 2 min, raised by 40 °C min^{-1} to 200 °C and held for 2 min, raised by 3 °C min^{-1} to 320 °C and held for 30 min. Quantification was executed by comparison of the peak area of the internal standard with the peak area of the analytes. Qualitative analysis was performed using GC coupled with mass spectroscopy (MS; 5975iMSD, Agilent Technologies). The separation conditions were the same as with FID except helium was used as carrier gas.

Selective wax extraction was achieved by dispersing 5 CMs overnight at room temperature in 20 mL MeOH; (UPLC-grade; Roth, Karlsruhe, Germany). Cuticles were removed, washed with MeOH and the solvents were combined. The MeOH extracted cuticles (M) were dried under an air stream and opened out on Teflon platelets. Dewaxed cuticles (MX) were obtained by dispersing the Ms in 10 mL TCM twice for 10 min. MXs were removed, washed with TCM, put on Teflon platelets and dried under a gentle air stream. The solvents were combined, and tetracosane was added as an internal standard to both wax samples. The analysis was conducted as described above.

Average chain length was calculated according to Huang et al. (2017) with equation (V.1):

$$ACL = \frac{\sum(C_n \times n)}{\sum(C_n)} \qquad (V.1)$$

where c_n is the amount of aliphatic compounds with the same carbon chain length and n is the number of carbons in the chain.

V.2.3 Transpiration measurement

An adapted variant of the method of Schönherr and Lendzian (1981) was used to measure cuticular water permeation of CM, M and MX. The membranes were attached on stainless steel transpiration chambers using Teflon paste (Roth, Karlsruhe, Germany) and secured with a ring-like lid. The chamber was filled with deionized water and completely sealed with adhesive tape. The surface area available for transpiration amounted 1.12 cm². The chambers were placed upside down on a grid above dried silica beads (Applichem, Darmstadt, Germany) in a closable container and were incubated at 25 °C overnight. Six gravimetric measurements in irregular time intervals were done to determine water loss by transpiration. Water permeance P in m s^{-1} was achieved with equation V.2:

$$P = \frac{J}{A \times \Delta c}$$ (V.2)

with J being the loss of water in g s^{-1}, A the cuticle surface area exposed to the air in m^2 and Δc the difference of water vapour concentration of inner (C_i = 23.074 g m^{-3}) and outer (C_0 = 0 g m^{-3}) side of the cuticle.

V.2.4 Investigation of surface structures

Surfaces structure of adaxial cuticular disks were investigated using scanning electron microscopy (SEM, JEOL JSM-7500F, JEOL GmbH, Freising, Germany) with an accelerating voltage of 5.0 kV and a working distance of 7.9 mm equipped with a field emission gun and a lower secondary electron (LEI) detector. CMs, Ms and MXs were carefully mounted on aluminium holders and sputter-coated with a mixture of 80/20 gold/palladium.

V.2.5 Statistics

OriginPro 2018b (Systat Software GmbH) was used for statistical analysis. Water permeance values and their log transformations were rejected for normal distribution with Shapiro-Wilk normality test. Therefore, the median (Median; 25th - 75th percentile) and nonparametric statistics were used. Investigation of significant differences of permeances was conducted by Kruskal-Wallis test ANOVA with posthoc Dunn´s test ($p < 0.05$). For wax analysis, normal distribution was found for all species except for the VLCAs of the MeOH and TCM extracts of *V. minor* and the VLCAs of the MeOH extract of *Z. zamiifolia*. For normally distributed data, significant differences were

investigated using one-way ANOVA ($p < 0.05$). Otherwise, the Kruskal-Wallis ANOVA with posthoc Dunn´s test was used. Values are given in mean (± standard deviation).

V.3 Results

V.3.1 Analysis of fractioned and full wax extracts of adaxial leaf cuticles

Extracted leave waxes were analyzed using GC-FID and GC-MS. The cuticular wax of the investigated plants covered a wide range of wax compositions and loads. *Z zamiifolia* and *H. helix* had low total wax amounts (about 10 µg cm^{-2}), consisting almost entirely of VLCAs. *C. siensis* CMs were covered with a similar amount, but only one third consisted of VLCAs and two-thirds of TRPs. Wax samples of *F. elastica, P. laurocerasus* and *V. minor* exhibited an intermediate wax amount (about 40 – 60 µg cm^{-2}) with high proportions of TRPs and minor VLCA content. *N. oleander* and *I. aquifolium* leaves had high cuticular wax loads (about 189 µg cm^{-1}) with high ratios of TRPs and small amounts of VLCAs (detailed view in table V.1). Similar proportions of the two wax fractions were found in FE and the combined MeOH – TCM extracts. No significant differences in the total amount of TRPs and VLCAs were found between the two extraction methods in each species (figure V.1)

Table V.1 Wax load (mean ± standard deviation) of isolated adaxial leaf cuticles of triterpenoids (TRP) and very-long-chain aliphatics (VLCA) of methanol (MeOH), subsequent chloroform (TCM) and full extracts (FE) of seven plant species. n = 4 - 8

Plant species	Triterpenoid content				Very-long-chain aliphatic content			
	MeOH ($\mu g\ cm^{-2}$)	TCM ($\mu g\ cm^{-2}$)	combined ($\mu g\ cm^{-2}$)	FE ($\mu g\ cm^{-2}$)	MeOH ($\mu g\ cm^{-2}$)	TCM ($\mu g\ cm^{-2}$)	combined ($\mu g\ cm^{-2}$)	FE ($\mu g\ cm^{-2}$)
Camellia sinensis	9.74 ± 0.97	0.22 ± 0.18	9.96 ± 1.09	9.72 ± 0.79	1.34 ± 0.25	2.36 ±0.26	3.70 ±0.45	2.96 ± 0.34
Ficus elastica	45.5 ± 3.27	0.47 ± 0.45	45.9 ± 3.62	48.3 ± 8.10	2.09 ± 2.91	5.34 ± 2.47	7.42 ± 3.26	9.32 ± 3.3
Hedera helix	0.18 ± 0.06	0.02 ± 0.03	0.20 ± 0.05	0.29 ± 0.32	2.24 ± 0.54	6.77 ± 1.64	9.01 ± 1.65	11.8 ± 1.16
Ilex aquifolium	148 ± 15.1	0.37 ± 0.35	149 ±14.8	144 ± 16.3	0.50 ± 0.14	0.35 ± 0.06	0.85 ± 0.10	0.87 ± 0.12
Nerium oleander	182 ± 26.0	0.16 ± 0.04	183 ± 26.8	190 ± 52.0	4.29 ± 1.37	4.39 ± 1.43	7.88 ± 2.63	6.65 ± 1.71
Prunus laurocerasus	46.7 ± 12.4	0.25 ± 0.05	46.9 ± 12.4	47.3 ± 5.84	2.58 ± 0.50	7.73 ± 0.49	10.3 ± 0.63	9.84 ± 1.31
Vinca minor	44.5 ± 10.1	0.04 ± 0.06	44.6 ± 10.20	39.3 ± 2.75	0.32 ± 0.24	2.50 ± 0.72	2.82 ± 0.80	3.64 ± 0.46
Zamioculcas zamiifeia	0.12 ± 0.12	0.00 ± 0.00	0.12 ± 0.12	0.24 ± 0.23	1.07 ± 0.31	8.70 ± 1.51	9.77 ± 2.19	7.27 ± 0.93
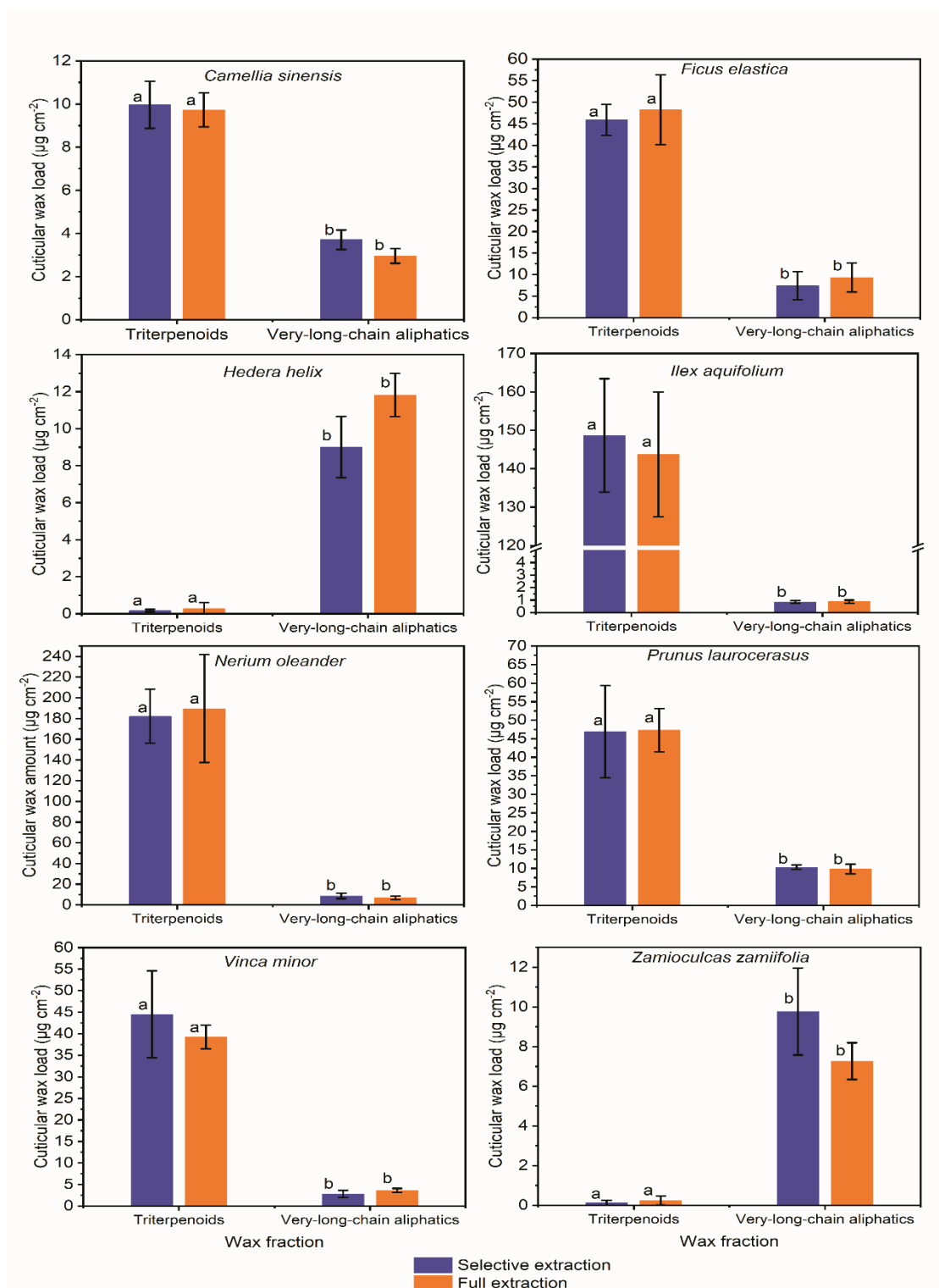
Figure V.1: Comparison of total cuticular amounts of very-long-chain aliphatics (VLCA) and triterpenoids (TRP) in selective wax extracts (purple) and full extracts (FE; orange) of seven plant species. Normal distribution was found for data of all species. Investigation of significant differences within a wax fraction was conducted using one-way ANOVA. Letters signify significant differences ($p < 0.05$) between the two extraction methods within a wax fraction. Columns show mean values and whiskers standard deviation. (n = 4 – 8)

The treatment with MeOH removed TRPS thoroughly in all species containing a cyclic fraction in their wax. In most species, rather small amounts of the total VLCAs were extracted with this treatment (between 11 % and 44 %). Only in extracts of *I. aquifolium* CMs, about 60 % of the total VLCAs were removed with MeOH. Subsequent TCM extracts exhibited almost exclusively VLCAs, beside some minor remnants of TRPs (figure V.2)
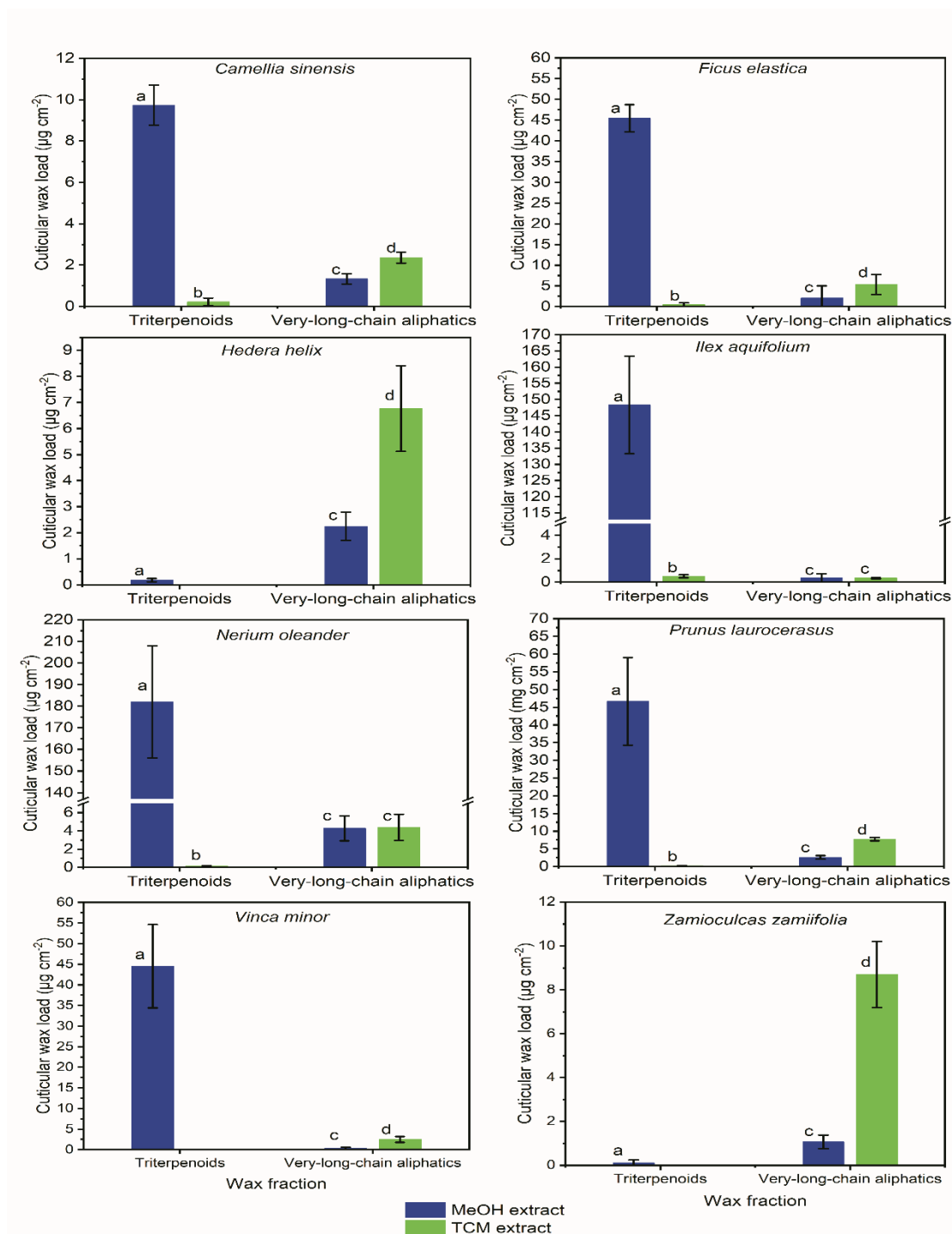
Figure V.2: Comparison of extracted waxes within the consecutive methanol (MeOH; blue) and chloroform (TCM; green) extraction steps. Normal distribution was found for data of all species except very-long-chained aliphatics (VLCA) of both steps of *V. minor* and the VLCAs of the MeOH extraction of *Z. zamiifolia*. If the normal distribution was found, was the investigation of significant differences conducted using one-way ANOVA ($p < 0.05$). Otherwise, the Kruskal-Wallis test ANOVA with posthoc Dunn´s test ($p < 0.05$) was used. Letters signify significant differences ($p < 0.05$) between the two extraction methods within a wax fraction. Columns show mean values and whiskers standard deviation. (n = 4 – 8)

The chain length distribution of aliphatics in MeOH extracts shows, that preferentially shorter chained substances were removed, while the subsequent TCM extract also contained substance with higher carbon numbers (figure V.3).

In MeOH extracts, *H. helix* showed the smallest and *I. aquifolium* the highest ACL. All values were well below 30, except for *N. oleander*. In the subsequent TCM extract, *C. sinensis* and *Z. zamiifolia* showed ACL values below 30. The remaining plants showed ACLs well above 30 with *N. oleander* having the highest. In FEs *H. helix* showed the lowest ACL. The values for extract *C. sinensis*, *H. helix* and *Z. zamiifolia* were just below 30 while the remaining plants had higher ACLS with *N. oleander* having the highest (table V.2). All plants, except *N. oleander*, showed significantly higher ACL in the TCM extract than in the previous MeOH extract ($p < 0.05$). The ACL of *N. oleander* showed no significant difference between these two extracts. The ACL of the combined MeOH and subsequent TCM extracts showed no significant difference to the ACL of FEs. ($p > 0.05$).
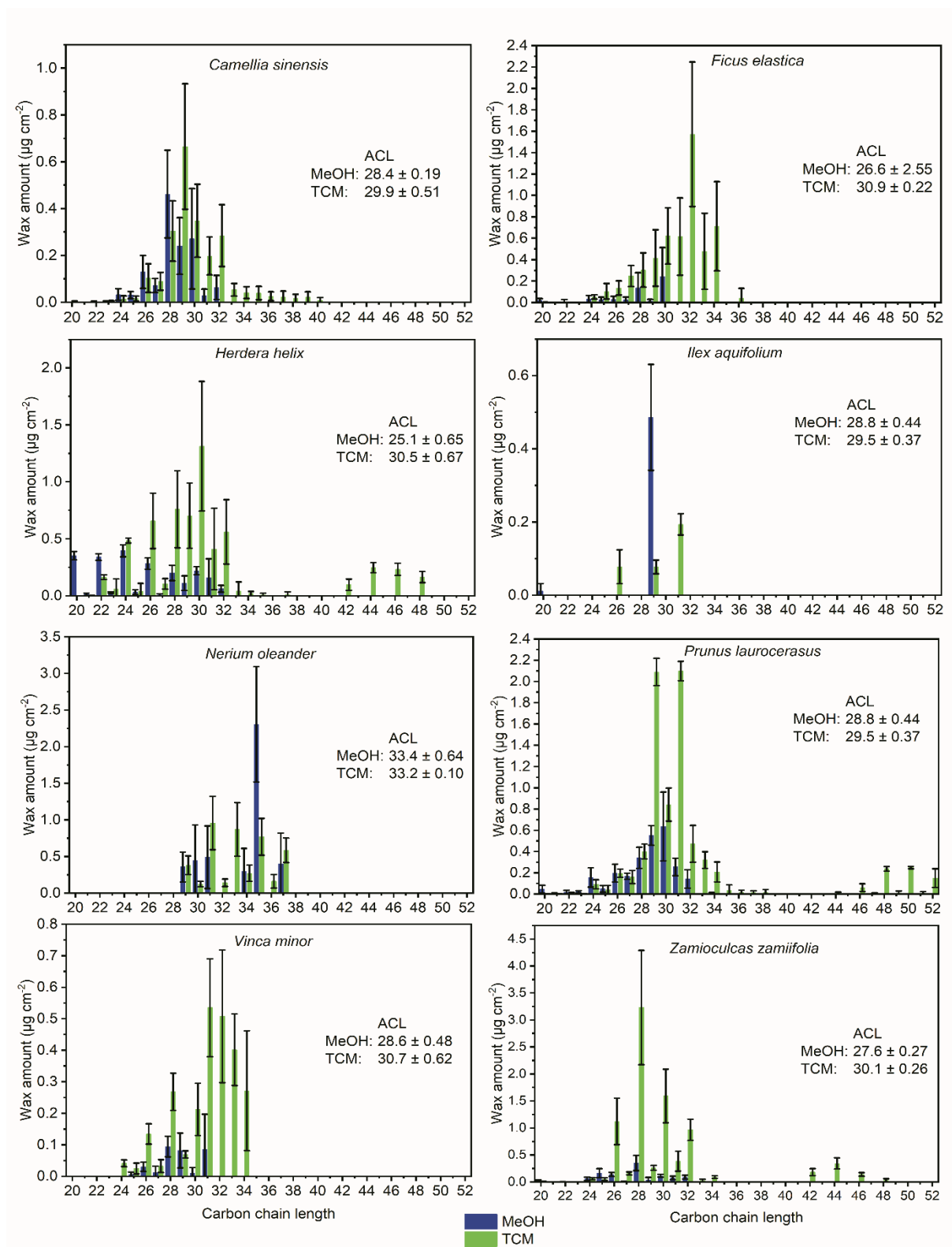
Figure V.3: Chain length distribution of very-long-chain aliphatics (VLCA) in methanol (MeOH, blue) and subsequent chloroform (TCM) extract (green) of eight plant species. Weighted average chain length (ACL) is used to compare MeOH and TCM extracts. Columns show mean values and whiskers standard deviation. (n = 4 - 8)

Table V.2: Weighted average chain length of the extraction with Methanol (MeOH), the subsequent chloroform (TCM) extract, the combined MeOH and subsequent TCM extracts and full extracts (FE) of seven investigated plant species. Values show mean ± standard deviation (n = 4 - 8)

Plant species	Weighted average chain length (number of C atoms)			
	MeOH extract	subsequent TCM extract	Combined MeOH and TCM extract	FE
Camellia sinensis	28.4 ± 0.20	29.8 ± 0.61	29.4 ± 0.38	29.7 ± 0.46
Ficus elastica	27.9 ± 1.11	30.8 ± 0.51	29.8 ± 1.16	31.0 ± 0.23
Hedera helix	27.1 ± 1.43	28.9 ± 0.27	29.7 ± 2.12	29.5 ± 0.45
Ilex aquifolium	29.0 ± 0.29	31.6 ± 0.60	30.5 ± 0.52	30.2 ± 0.24
Nerium oleander	28.9 ± 0.51	32.0 ± 0.24	31.6 ± 0.24	32.7 ± 0.18
Prunus laurocerasus	28.5 ± 0.53	31.9 ± 0.35	31.04 ± 0.42	31.2 ± 0.13
Vinca minor	27.9 ± 0.69	30.9 ± 0.56	30.5 ± 0.64	31.0 ± 0.19
Zamioculcas zamiifolia	28.6 ± 1.40	29.3 ± 0.45	29.4 ± 0.30	29.8 ± 0.26

V.3.2 Water Permeance of isolated adaxial cuticular membranes after partial and complete wax extraction

An adaption of the method of Schönherr and Lendzian (1981) was used to gravimetrically determine cuticular water loss of CMs, Ms and MXs and calculate water permeances (supplement table 2). For CMs permeances were between 3.77×10^{-6} m s^{-1} (2.77×10^{-6} - 5.52×10^{-6} m s^{-1}; *P. laurocerasus*) and 4.27×10^{-5} m s^{-1} (1.49×10^{-5} - 7.60×10^{-5} m s^{-1}; *C. sinensis)*. For Ms permeances were between 5.67×10^{-6} (1.37×10^{-6} - 2.07×10^{-5} m s^{-1}; *Z. zamiifolia*) and 9.19×10^{-5} (5.51×10^{-5} - 1.52×10^{-4} m s^{-1}; *N. oleander*) and for MXs between 1.07×10^{-5} (5.15×10^{-6} - 2.85×10^{-5} m s^{-1}; *Z. zamiifolia*) and 5.09×10^{-4} (3.70×10^{-4} - 6.50×10^{-4} m s^{-1}; *V. minor*).

Significant differences ($p < 0.05$) between CMs and Ms were found for *P. laurocerasus*, *N. oleander* and *V.* minor, but not between the five remaining plants (figure V.4). Ms of these three plants showed a minor, but significant increase in water permeance compared to the values of their CMs. Permeability values of MXs of all plant species were strongly and significantly increased compared to their CMs and Ms ($p < 0.05$).
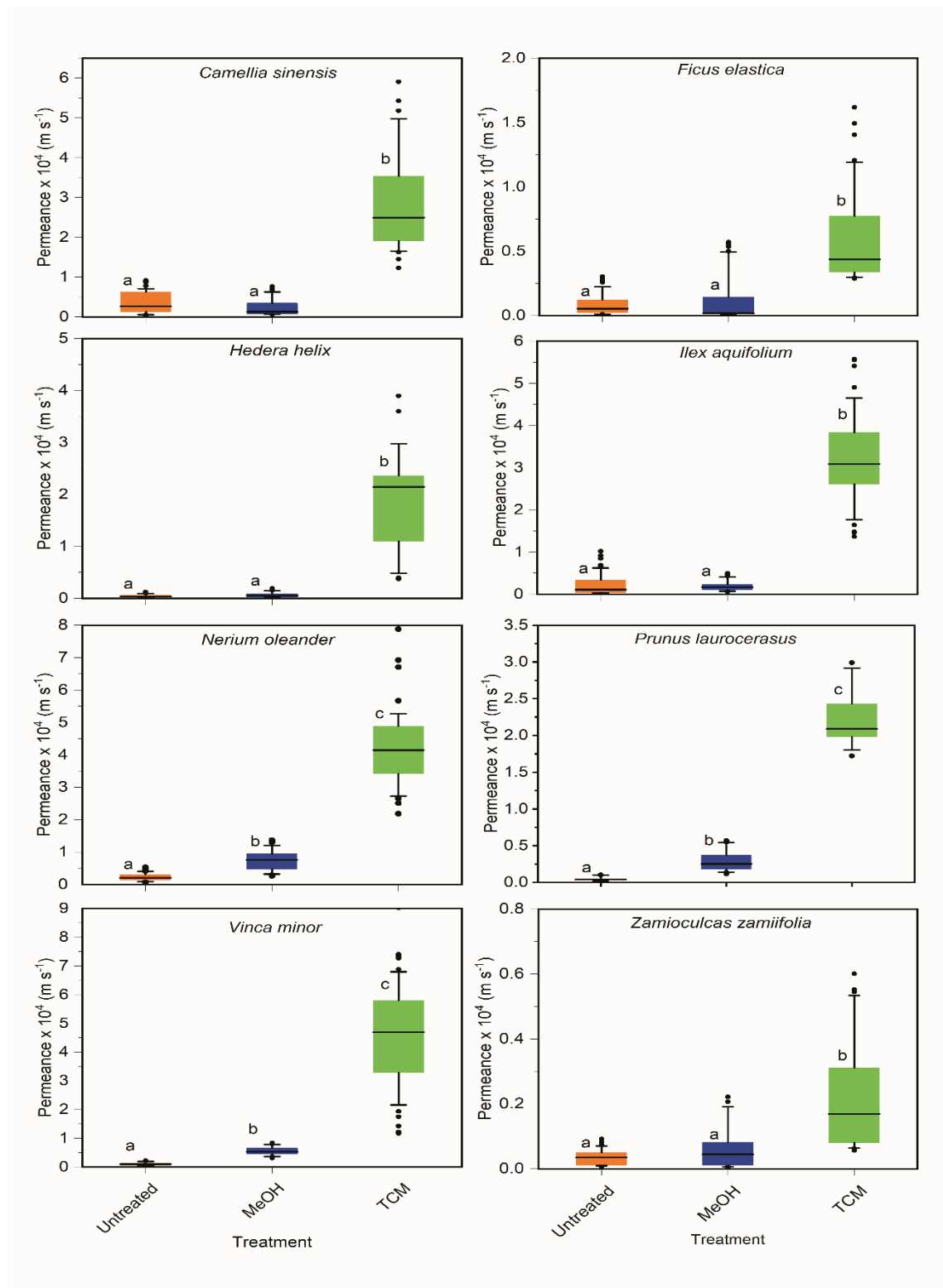
Figure V.4: Comparison of permeance of untreated (CM, orange), methanol extracted (M, Blue) and chloroform extracted (MX, green) cuticular discs of eight plant species Investigation of significant differences was conducted by Kruskal-Wallis ANOVA with posthoc Dunn´s test. Boxes interquartile ranges from 25 – 75 %, whiskers 10 – 90 % and dots signify outliers. Letters signify significant differences (p < 0.05). The black line is the median. (n > 28)

V.3.3 Investigation of surface structures

The surface of all investigated showed no continuous coverage with epicuticular wax crystals. The surface structure of *C. sinensis* exhibited tiny, scattered wax accumulations, and the surface of *F. elastica* appeared encrusted. Ms of both plant species surfaces with a small decrease in surface roughness. MXs were devoid of surface waxes, except some minor remnants (figure V.5). The surface of CMs of *H. helix and I. aquifolium* showed a smooth surface with occasional wax accumulations. The M of *I. aquifolium* showed rather small differences to the corresponding CM. The M of *H. helix* appeared slightly more granulated than its CM. Except some minor remnants on MXs of *H. helix*, no surface wax was found on MXs (figure V.6). The wax on the surface of *N. oleander* appeared smooth with occasional accumulations on CM and M. The surface of *P. laurocerasus* had a granulated appearance. The surface of MX was found devoid of wax (figure V.7). No surface wax was found on MX (figure V.7) The CM and M of *V. minor* were encrusted with wax. The surface of CMs and Ms of *Z. zamiifolia* had a partially granulated appearance with occasional small wax accumulations. On the surface of MX of both plants, no wax was found (figure V.8).

Camellia sinensis   Ficus elastica

Figure V.5: Scanning electron microscopy (SEM) images of adaxial isolated cuticular membranes (CM), methanol treated membranes (M) and chloroform treated membranes (MX) of *Camellia sinensis* (left) and *Ficus elastica* (right).

Figure V.6: Scanning electron microscopy (SEM) images of adaxial isolated cuticular membranes (CM), methanol treated membranes (M) and chloroform treated membranes (MX) of *Hedera helix* (left) and *Ilex aquifolium* (right).

Figure V.7: Scanning electron microscopy (SEM) images of adaxial isolated cuticular membranes (CM), methanol treated membranes (M) and chloroform treated membranes (MX) of *Nerium oleander* (left) and *Prunus laurocerasus* (right).

Figure V.8: Scanning electron microscopy (SEM) images of adaxial isolated cuticular membranes (CM), methanol treated membranes (M) and chloroform treated membranes (MX) of *Vinca minor* (left) and *Zamioculcas zamiifolia* (right).

V.4 Discussion

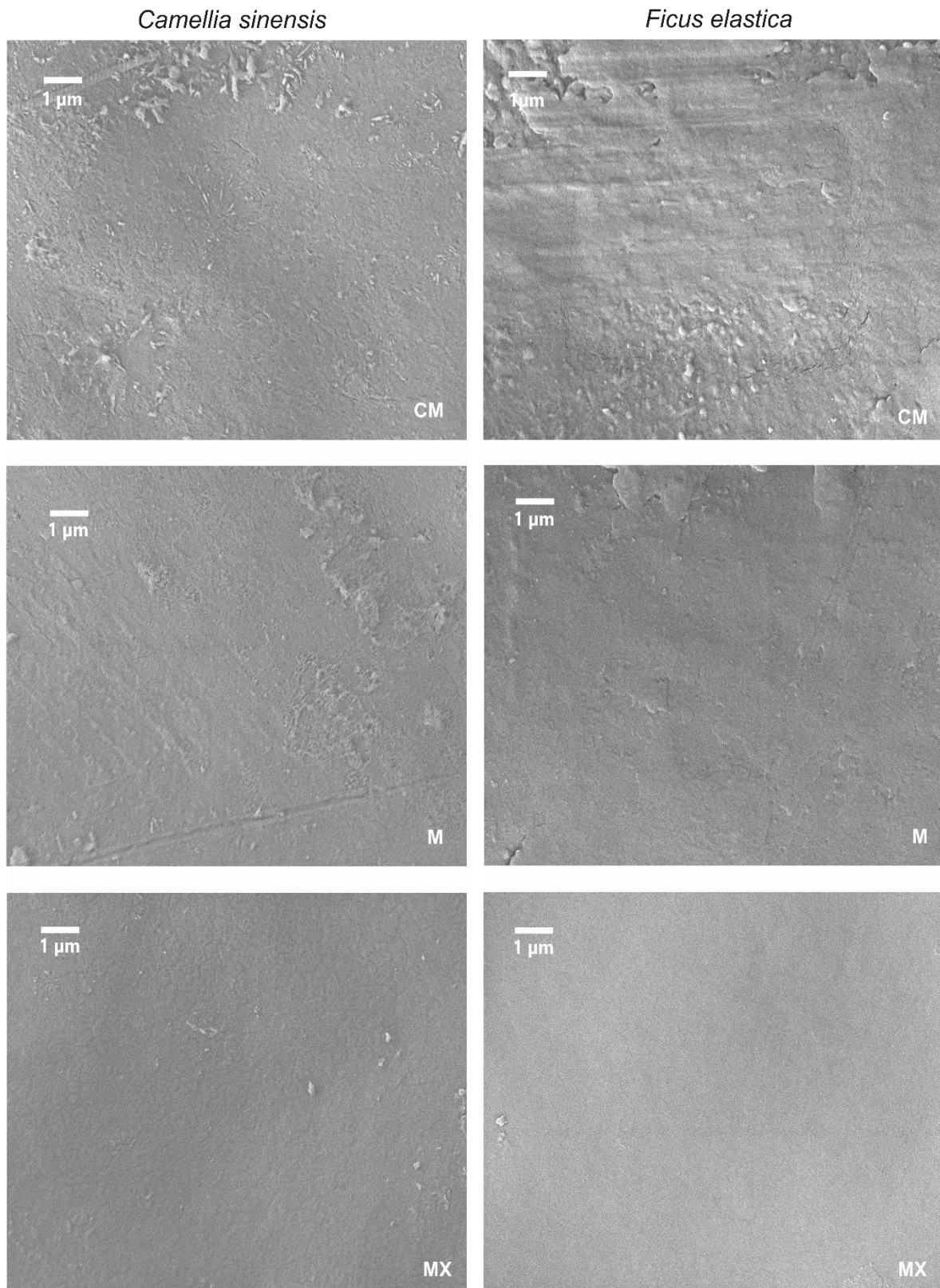This project's aim was the development of a direct method to identify the water transpiration barrier within the cuticular waxes. Therefore, a means to extract TRPs selectively was designed. In a second step, water permeance of CMs, Ms and MXs were determined using an adapted method of Schönherr and Lendzian (1981) for gravimetric determination of water loss.

The challenging task in this project was to find a solvent for selective TRP extraction, leaving VLCAs nearly untouched on the cuticles. A common trend observed in studies investigating the solubility of VLCAs is the decreased solubility with increasing carbon chain length. Although this trend was often shown on hydrocarbons with shorter chain lengths, a steady-going extension can be expected. It was shown in several solvents for even primary n-alcohols with a carbon number between 10 and 18 (Hoerr et al. 1944). Kiser et al. (1961) found similar results for hydrocarbons with a carbon chain length between five and ten in MeOH. After recalculating data from several publications, Riederer and Schneider (1989) computed the relative solubility of three substances, found in cuticular wax, in various solvents in contrast to their solubility in TCM. The latter easily constituted the best solvent for 1-octacosanol and octadecanoic acid. Beyond that, both substances exhibited only minor solubility in MeOH. In contrast, the alkane n-dotriacontane was more soluble in more unpolar solvents like benzene or cyclohexane (Riederer and Schneider 1989). The solubility of two TRP compounds found in cuticular wax, ursolic, and oleic acid was investigated in different solvents (Jin et al. 1997). They showed their solubility in MeOH to be similar to their solubility in TCM (Jin et al. 1997). Presuming equal accessibility for the solvent, the present data indicated a good solubility of TRPs in MeOH but not for VLCAs, enabling a selective wax extraction from CMs.

As assumed from literature, MeOH extracted the relatively polar TRPs (almost) quantitively, leaving only small remnants on the cuticle, which were removed by the subsequent TCM treatment (figure V.2). Regarding the extraction of VLCAs only smaller amounts, mostly with shorter carbon chain lengths were found in MeOH in most plants. They were extracted with the following TCM extract (figure V.2). Although VLCAs have poor solubility in MeOH, in two plants, *I. aquifolium* and *N. oleander*, was a major fraction of the total VLCA amount removed with this solvent. In the remaining

plants, less than 36 % were extracted with MeOH. Therefore, it can be concluded, that the developed extraction procedure removed TRPS rather exhaustively, but was not able to avoid VLCA removal completely.

The investigated plants showed a broad variety in wax load as well as varying TRP and VLCA content (figure V.1, figure V.2). Cuticular waxes reached from species with wax consisting almost only of VLCAs and a low wax load (*Z. zamiifolia* and *H. helix*), over species with minor VLCA content and considerable TRP content (*V. minor*, *P. laurocerasus, F. elastic, C. sinensis* and *I. aquifolium*) to species with high wax amounts and significant TRP and VLCA amounts (*N. oleander*). Independently from wax amount and composition, the selective extraction showed similar results for all plants species investigated, indicating good applicability regarding the selectivity of the method. Additionally, a comparison of the combined MeOH and TCM extracts with FEs showed good suitability. The minor deviation of wax load and composition can be explained by natural variation (Baker 1974). However, since no significant differences between the combined MeOH and TCM extracts and FEs were found, good applicability of this extraction method could be assumed (figure V.1).

SEM pictures of Ms showed at most minor differences compared to surfaces images of CMs. (figure V.5, figure V.6, figure V.7, figure V.8). The most noticeable, but still small changes were found in *C. sinensis, F. elastica*, *H. helix* and *P. laurocerasus* (figure V.5, figure V.6, figure V.7). For *C. sinensis, F. elastica* and *P. laurocerasus* a slight decrease of the wax accumulation or granules were apparent. The surface of Ms of *H. helix* appeared slightly more granulated. Considering the properties of epicuticular waxes and the applied solvents, a minor effect of MeOH, but a major impact of TCM onto this wax fraction could be assumed. Jetter and Riederer (2016) showed epicuticular waxes of different plants to consist predominantly (or even exclusively) of VLCAs. TRPs were found primarily in intracuticular waxes. Further studies of Zeisler and Schreiber (2016) and Zeisler-Diehl et al. (2018) supported these findings, indicating a layered structure with epicuticular waxes consisting mostly of VLCAs and intracuticular waxes consisting of VLCAs and (if existing) TRPs. This and the result of only a small fraction of VLCAs being extracted with MeOH undergirded this assumption. The surface of MXs showed a different appearance than CMs and Ms. On the surface of MXs of all plants, except *H. helix*, no wax was found. The MX of

H. helix exhibited scattered remnants of wax left on its surface (figure V.6). However, Jetter and Riederer (2016), Zeisler and Schreiber (2016) and Zeisler-Diehl et al. (2018) showed epicuticular waxes to only have a minor influence on the cuticular water permeability barrier. Therefore, the impact of remnant epicuticular waxes can be assumed to be negligible for the measurement of water transpiration through native and treated cuticles. Considering the previously discussed solubility behaviour of VLCAs and TRPs, the assumption of MeOH to not alter the surface of CMs strongly and TCM to have a major impact on the surface structure was mostly confirmed.

In most plant species, except *N. oleander*, *P. laurocerasus* and *V. minor*, water permeability showed no significant increase between Ms and CMs. However, compared to the massive amounts of waxes (primarily TRPs) extracted from the CMs of these three plants, was the increase of water permeance minimal. After VLCA extraction (in case of *N. oleander*, *P. laurocerasus* and *V. minor* only a smaller fraction of their waxes), MXs of all species showed a significant increase in water transpiration (figure V.4). Jetter and Riederer (2016) proposed intracuticular VLCAs to constitute the major part of the cuticular water transpiration barrier. However, they didn´t give direct experimental proof. The developed extraction sequence allowed for the first time the selective extraction of TRPs. Consequently, the first direct proof of VLCAs constituting the transpiration barrier was found. However, the results of the species *I. aquifolium*, *N. oleander*, *P. laurocerasus* and *V. minor* indicated a more complex relation between water permeance and the VLCAs. *I. aquifolium* showed no increase in water permeance after the MeOH treatment, although almost 60 % of its VLCAs were removed. A small, significant increase in water permeance was found for *N. oleander* after roughly half of the VLCAs were removed with MeOH. *V. minor* and *P. laurocerasus* showed a small but significant increase of water permeance, although only about 11 % and 25 % of their total VLCAs, respectively, were removed with MeOH. These results indicated that not only the composition of cuticular waxes have an important influence on the barrier properties, but also its structure.

In preliminary experiments, it was not possible to extract TRPs with MeOH through dipping whole leaves in the solvent. This result supported the picture of a layered structure of cuticular waxes, since only after isolation of CMs, when the inner side of the cuticle was accessible for MeOH, TRPs were extracted. Therefore, the proposal of

the different wax fractions to separate by their polarity seemed natural. Buschhaus and Jetter (2011) and Jetter and Riederer (2016) showed the tendency of VLCAs to accumulate on the outside, facing the environment, while TRPs were associated with the interior, facing the hydrophilic cell wall. Further experiments of Zeisler and Schreiber (2016) and Zeisler-Diehl et al. (2018) showed epicuticular waxes to consist of VLCAs, which could seal the surface against MeOH and protecting underlying intracuticular TRPs from extraction (figure V.9).
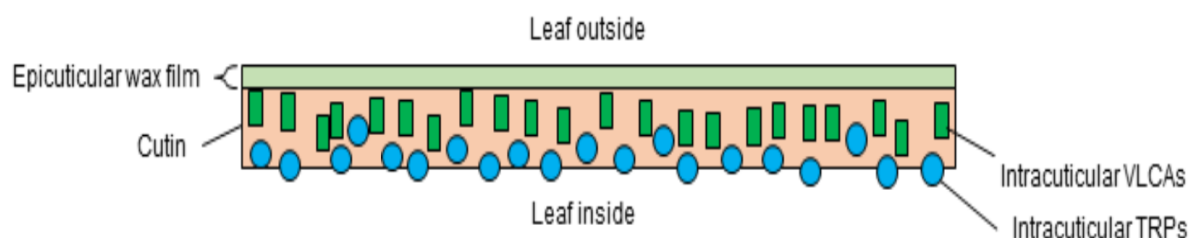
Figure V.9: Theoretical scheme of a layered structure of cuticular waxes proposed by Jetter and Riederer (2016). The outer surface is covered by an epicuticular wax film consisting of aliphatic compounds. The intracuticular wax separates into two domains. Intracuticular aliphatics are located nearer the outer surface while triterpenoid (TRP) constituents are closer to the inside, with an overlapping area in between.

Since in most plants, cuticular water permeance showed no significant increase after MeOH extraction, the assumption can be made, that the integrity of the barrier was intact. However, *N. oleander*, *P. laurocerasus* and *V. minor* showed a significant increase in water permeability after TRP removal.

This could hint at a transient in the cuticular wax, were TRPs and VLCAs partially intermix. The extraction of a massive amount of TRPs could then lead to punctual disruption of this region, leading to higher water permeability of the cuticle. Supporting this theory, Jetter and Riederer (2016) concluded TRPs to not contribute directly to the transpiration barrier, but high amounts and concentrations of TRPs to affect the barrier properties.

The effect of selective wax extraction was calculated according to equation V.3:

$$Effect = \frac{P_{M,MX}}{P_{CM}}$$
(V.3)

With P_{CM} the permeance of untreated cuticles, P_M the permeance after MeOH extraction and P_{MX} the permeance after the subsequent TCM treatment. Compared to the remaining plants, *N. oleander*, *P. laurocerasus* and *V. minor* showed a higher effect

on water permeance (table V.3). *C. sinensis* showed the lowest, *P. laurocerasus* the highest impact. After extraction with TCM, the effects on water permeances were higher. *Z. zamiifolia* showed the lowest and *P. laurocerasus* again the highest value. After a comparison of the impact of MeOH and TCM, the substantial contribution of VLCAs to the water transpiration barrier was visible. In some plants, TRPS constituted the major components of the cuticular wax. However, their removal only had comparatively small effects on the transpiration barrier. This was not only found for plant species with low (*H. helix*, *Z. zamiifolia*) or mediocre (*C. sinensis*) TRP content and low wax load, but also for plants with high TRP content and wax load (*F. elastica*, *I. aquifolium*, N*. oleander*, *P. laurocerasus*, *V. minor*). In contrast, the subsequent removal of the usually small amounts of VLCAs with TCM caused a strongly increased water transpiration and had in addition to that high effects on the permeance. These results aligned well with the literature known theory of VLCAs constituting the water permeance barrier (Huang et al. 2017; Schreiber and Riederer 1996; Jetter and Riederer 2016).

Table V.3: Effect (Median, 2.5[th] - 97.5[th] percentile) on water permeance of adaxial cuticles after methanol (M) and subsequent chloroform (MX) extraction

	Effect on permeance	
Plant species	Effect on permeance of Ms	Effect on permeance of MXs
Camellia sinensis	0.52; 0.34 - 0.80	7.46; 4.45 - 12.5
Ficus elastica	1.31; 0.78 - 2.20	7.27; 4.29 - 12.3
Hedera helix	1.31; 1.03 - 2.23	16.5; 11.4 - 23.7
Ilex aquifolium	2.02; 1.45 - 2.81	26.8; 19.0 - 37.9
Nerium oleander	4.95; 3.97 – 6.17	21.9; 17.3 - 27.6
Prunus laurocerasus	8.30 6.31 - 10.9	66.4 50.0 - 88.1
Vinca minor	6.32; 5.23 - 7.63	36.9; 30.0 - 45.4
Zamioculcas zamiifolia	1.13; 0.70 - 1.80	3.33; 2.07 - 5.38

During selective extraction of wax compounds, it could not be avoided to extract some VLCAs alongside the TRPs. To characterize VLCAs in different extraction steps, the weighted average chain length (ACL) was calculated to depict the solvents ability to extract VLCAs with varying chain lengths. Despite repeated efforts to correlate properties, like total wax amount or composition with the capability to limit cuticular water loss, was the assumption of intracuticular waxes, presumably the VLCA fraction, to constitute this barrier a rather recent development (Riederer and Schneider 1990; Horrocks 1964; Jetter and Riederer 2016; Vogg et al. 2004; Zeisler and Schreiber 2016; Zeisler-Diehl et al. 2018). However, a correlation between the amount of intracuticular waxes and the barrier capability was not confirmed (Jetter and Riederer

2016). Riederer and Schneider (1990) proposed the molecular structure of VLCAs to form the transport-limiting barrier (figure V.10).
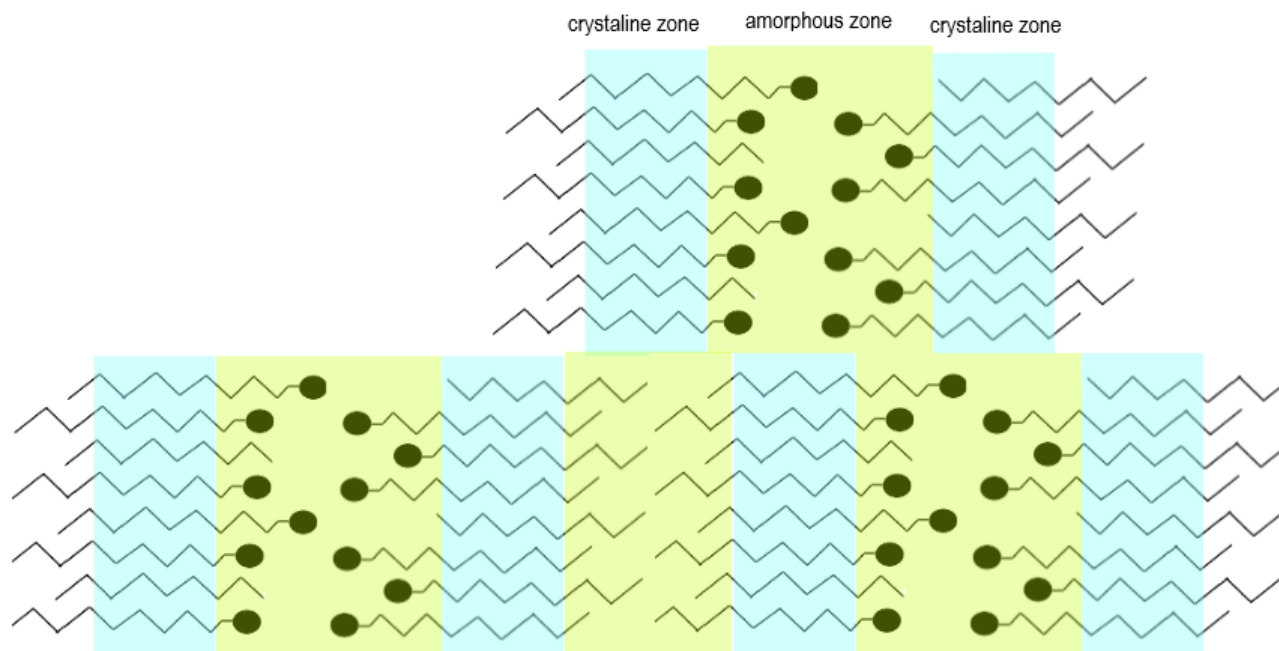
Figure V.10: Scheme after Riederer and Schneider (1990) of the water permeability barrier indicated by Hot stage XRD and FTIR experiments with wax from *Schefflera elegantissima*. Blue areas depict impermeable crystalline zones and green areas depict permeable amorphous regions. The chains indicate methylene groups and circles indicate functional groups.

It was proposed, that mid-chain sections of VLCAs form crystalline domains, impermeable for water. The end-chain methylene group, as well as possibly present functional groups, were supposed to form a less rigid amorphous zone through which water could diffuse (Riederer and Schneider 1990; Reynhardt and Riederer 1991). This model was named the 'brick and mortar modal', where bricks depicted the crystalline regions, while the mortar represented the amorphous zones. A higher ACL could, therefore, indicate more crystalline fractions, thus a more tortuous pathway for water or organic compounds to diffuse through, thus leading to a better water transpiration barrier. However, a correlation was not shown, and it was assumed, that other factors, like cutin polymer structure, or cutin wax interactions play a role in the formation of the permeability barrier of cuticles (Huang et al. 2017). In this work, ACLs were used to compare the combined results of the selective extraction to the results of conventional FEs. Overall the ACLs showed good conformity, indicating that the selective removal led to similar results (after a combination of the data of MeOH and TCM extract) than

a standard extract with TCM (table V.2). Together with the good accordance of the extracted VLCA and TRP amounts, this leads to the conclusion, that combined results are comparable to the routinely used method. In addition, facilitation of the analysis of GC data was observed in plant species containing higher amounts of TRPs. Due to the separate extraction of TRPs which could cover up peaks of VLCAs (and potentially vice versa), improved analysis of the wax composition was enabled. This was mainly observed for plant species like *F. elastica, N. oleander* and *V. minor*. This could also explain the minor differences found of the ACL of the combined MeOH and the FE found in *F. elastica* and *N. oleander.*

Altogether the developed method for selective extraction of TRPs from isolated adaxial cuticles showed good results. It enabled the investigation of the contribution of different wax fractions towards the cuticular water transpiration barrier. It was demonstrated that TRP removal had no or only a minor effect on water permeance. Only after the extraction of VLCAs using TCM the barrier was corrupted. This trend was also found for several plant species with high TRP content and amount in their cuticular waxes. In accordance with Staiger et al. (2019b) the results confirmed the exhaustive extraction of TRPs from CMs using MeOH, however, they also showed that variable amounts of VLCAs could be removed with this solvent. Subsequent transpiration measurements showed no significant increase between CMs and Ms in most cases, but always a significant increase for MXs.Plants showing an increase after MeOH treatment were highly abundant in TRPs. Besides, the impact onto transpiration was of minor magnitude compared to after TCM treatment. Therefore, the hypothesized localization of the transpiration barrier within the VLCA wax fraction was confirmed. Our results aligned well with previous work of Jetter and Riederer (2016), who presumed VLCAs to constitute the cuticular transpiration barrier

VI. Preparation and characterization of physical properties of an artificial wax mixture mimicking *S. elegantissima* adaxial leaf wax.

VI.1 Introduction

Cuticular waxes were shown to have a predominating role in the buildup of the plant cuticular transport barrier (Burghardt and Riederer 2008; Horrocks 1964). By intuition, a correlation of cuticular thickness and permeability according to Fick´s first law might be assumed. Schreiber and Riederer (1996), Riederer and Schreiber (2001) and Burghardt and Riederer (2008) found no positive correlation between water permeance and cuticular thickness. Furthermore, no correlations to traits like total wax amount, amounts of epi- and intracuticular waxes or the composition of cuticular waxes were found (Jetter and Riederer 2016; Riederer and Schneider 1990). These findings indicate other properties to have an impact on the barrier, emphasizing the necessity to characterize physical properties of cuticular waxes like their crystalline structure thoroughly. Riederer and Schneider (1990) proposed a model for cuticular permeability barriers, analogous to technical membranes and semicrystalline olefin polymers. According to the "brick and mortar" model waxes consist of two phases. The crystalline phase consists of the mid-chain methylene groups of VLCAs, forming highly ordered impermeable crystals. These crystals cannot be permeated by water, increasing the tortuosity of the wax. The amorphous phase consists of the end-chain methylene groups and functional groups of the VLCAs, allowing water to permeate through the wax (Reynhardt and Riederer 1994; Riederer and Schneider 1990). Investigations of physical properties of substances are conducted in various fields. Thereby, different methods have been developed to perform the experiments.

FTIR is a versatile tool to investigate the physical structure of compounds. In chemistry, it was often used for structural elucidation of (novel) compounds. Smith III et al. (1993) used FTIR spectroscopy to determine and compare the symmetry of fullerene. Brycki et al. (2011) applied this technique to characterize an antifungal mircrobiocide. Blume (1996) deployed this technique to investigate the structure, conformation and dynamic properties of lipids in lamellar phases. Due to the use of isotopic labelling techniques, he couldn´t only investigate the conformational behaviour, but he could distinguish different hydration sites of functional groups at the end of alkyl chains (Blume 1996). Cheng et al. (2006) used attenuated total reflectance FTIR to investigate the chemistry

of dry and annealed lotus leaves. They found their spectra to show similarities to a combination of the spectra of cellulose and carnauba wax (Cheng et al. 2006). A comparative study showed the utility of FTIR methods for compositional analysis. Dubis et al. (1999) showed horizontal attenuated total reflection FTIR to be a reliable and fast method to investigate the composition of surface waxes of leaves. Merk et al. (1997) investigated the aliphatic crystallinity of cuticular waxes using FTIR. They used different double bands, indicative for orthorhombic crystal structure, to measure aliphatic crystallinity (Merk et al. 1997). FTIR was used to investigate the melting behaviour of wax samples and compare them to the behaviour of extracted leaf wax of *Schefflera elegantissima* upon heating. This plant was chosen due to beneficial properties of its cuticle and cuticular wax. The adaxial cuticle was hypostomatous and isolatable. The waxes consisted almost exclusively of VLCAs and had a rather simple compositional pattern and chain length distribution. Also, aliphatic crystallinity of a quaternary wax blend and the plant wax was calculated after Zerbi et al. (1989)

The DSC was deployed in pharmacy to investigate the compatibility of drugs and adjuvants or their mode of action. It was also applied to study the mechanism of the penetration enhancing effects of lipophilic compounds commonly used in ointments. Therefore, isolated sheets of human *stratum corneum* were measured untreated or after pretreatment with lipophilic liquids (Leopold and Lippold 1995). In another study, DSC experiments were conducted to investigate the enhancing effect of benzyl alcohol onto the percutaneous absorption of drugs (Saitoh et al. 1995). The investigation of the mode of action of an adjuvant or its interaction with drugs is not only important in pharmacy. In agriculture, many active ingredients and adjuvants are in daily use to protect crops from weeds, fungi or pests to improve the harvest. Fagerström et al. (2014) examined the softening effect of two commercially used surfactants onto a model wax. They used DSC to characterize the effects of tebuconazole and the surfactants $C_{10}EO_7$ (hepta (ethylene glycol) mono iso-decyl ether) and $C_8G_{1.6}$ (2-ethyl hexyl glycoside) on the phase behaviour of their model wax (Fagerström et al. 2014). Another application is the investigation of the physical properties of waxes. When diesel is cooled, the formation of wax crystals takes place below certain temperatures. Gimzewski and Audley (1993) monitored this process and the melting of crystallized waxes to investigate thermodynamic reversibility of it. Fagerström et al. (2013) used

this method to investigate plant leaf intracuticular wax and two of its major constituents in different hydration states. They also tried to develop a model wax based on the wax of *Clivia Miniata* Regel leaf wax (Fagerström et al. 2013). Aggarwal (2001) examined the phase behaviour of isolated apple and capsicum cuticles and found them to undergo an endothermic transition. It was assigned to the melting of waxes, which were present in the cuticle. DSC investigations of n-alkanes and waxes showed the transition of the orthorhombic crystal lattice to a hexagonal phase prior to melting (Basson and Reynhardt 1991; Reynhardt and Riederer 1994). These researches greatly demonstrated the value of DSC experiments for the investigation of physical properties of waxes or their interaction with further compounds. In this work, the DSC was used to investigate the behaviour of artificial waxes and *S. elegantissima* leaf wax. Paraffin waxes were shown to pass through solid-solid transitions before melting (Edwards 1957). Therefore, DSC was used to map out phase diagrams to research the influence of composition and number of constituents on artificial wax blends. In addition, DSC thermograms were used to compare the behaviour of plant leaf wax samples and artificially produced waxes.

XRD is a valuable method to determine the structure of many materials. For example, it can be used to investigate the crystal structure of transfer RNA. Kim and Rich (1968) showed formyl methionyl transfer RNA to form a hexagonal lattice and found the structure to contain 88 % water. Polymers are another interesting material for XRD studies. Chung and Scott (1973) developed a practical method, suitable for routine analysis of polymers like polyethene terephthalate. Tashiro et al. (1996) investigated the phase transition of the orthorhombic to the hexagonal phase of polyethene crystals. They conducted time-resolved measurements of a sample, which was continuously heated. With increasing temperature, they found a decrease in the signals indicating orthorhombic structures until they vanished. On the opposite side, the intensity of the reflections, indicative for the hexagonal crystal lattice appeared and its intensity increased (Tashiro et al. 1996). Craig et al. (1998) investigate binary and more complex tertiary and quintenary mixtures of n-alkanes and found their samples to take the orthorhombic crystal lattice. Their thorough analysis of the diffraction patterns also revealed the presence of end-chain and interchain disorder indicating the presence of amorphous regions within the blends (Craig et al. 1998). Ensikat et al. (2006) used

XRD to show the orthorhombic crystal lattice to be most common for aliphatic compounds of their investigated plant species. In the present work, XRD techniques were used to investigate the crystalline structure of wax blends. Similarly, to the DSC experiments, the influence of composition and number of constituents on artificial wax blends was determined. Hot stage XRD experiments of few selected waxes were conducted, to investigate the behaviour of the wax crystal structure more thoroughly. The wax mixtures were chosen to depict certain conditions within the *S. elegantissima* leaf wax.

Staiger et al. (2019b) showed VLCAs to constitute the uptake barrier for organic solutes like active ingredients used in agriculture. For ecological and economic aspects, a good foliar uptake of active ingredients or its enhancement by formulation additives is necessary (Staiger et al. 2019b). However, the development of a screening sequence to determine the permeability of active ingredients through the cuticle proved challenging, since the location of the barrier within cuticular waxes was not well-founded. Besides that, several reasons slowed its development down. For permeability studies, CMs are used in double chamber experiments. For the characterization of physical properties, some methods like DSC require rather high amounts of sample to give good results. To gather these amounts, a huge number of plants had to be grown to obtain the material in sufficient amounts, making their growth time consuming and expensive. Therefore, to have an artificial wax blend that mimics cuticular wax properties sufficiently would be beneficial to develop a fast method to characterize the influence of agriculturally used adjuvants and active ingredients on the uptake barrier of the cuticle.

In this chapter, several methods (FTIR, DSC and XRD) were used to characterize various blends of commercially available VLCA compounds, wax extracts of full leaves and isolated CMs of *S. elegantissima*. The aim was to find an artificial mixture, which mimics the properties of wax of isolated cuticles of *S. elegantissima* sufficiently.

VI.2 Material and Methods

VI.2.1 Plant material

S. elegantissima plants were grown in a greenhouse in an accessible public area of the botanical garden Würzburg. Only mature, fully expanded leaves were harvested. Leaf wax was obtained by two methods. The wax from the whole leaf was gathered by dispersing the leaves in chloroform twice for 30 s. Before wax extraction, leaves were kept in water overnight in a dark place at room temperature, to ensure stomatal closure. The wax from adaxial leaf CMs was obtained after enzymatic isolation of the cuticle after an adapted method of Schönherr and Riederer (1986). Leaf discs (diameter of 1.89 cm) were punched out using a cork borer, and the adaxial side was marked. The discs were incubated with an enzyme solution consisting of 1 % pectinase (Trenolin, Erbslöh, Geisenheim, Germany), 1 % cellulase (Celluclast, NCBE, University of Reading, U.K.), one mM citric acid monohydrate (Applichem, Darmstadt, Germany) and 1 mM sodium azide (Sigma-Aldrich, Steinheim, Germany) to prevent bacterial growth. The incubated disks were kept at room temperature until the dissolution of leaf tissue. The solution was replaced twice a week. Finally, adaxial CMs were picked out, washed thoroughly and stored in distilled water until use. Adaxial leaf wax was collected by dispersing the CMs twice in TCM (Roth, Karlsruhe, Germany) for 5 min.

VI.2.2 Investigation of composition of adaxial leaf wax of *S. elegantissima* and surface structure analysis

For compositional elucidation, five CMs from *S. elegantissima* were dispersed twice in 10 mL TCM (≥99,8%; Roth, Karlsruhe, Germany) for 10 min. The extracts were combined, n-tetracosane (Sigma Aldrich, Steinheim, Germany) was added as an internal standard, and the solvent was removed under a gentle N_2-stream. The analysis of whole leaf wax was done from leaves harvested at a later point of time, due to a tight schedule. Whole leaf extracts were prepared by dispersing a leaf in TCM for 30 s twice. The extracts were combined, n-tetracosane (Sigma Aldrich, Steinheim, Germany) was added as an internal standard, and the solvent was removed under a gentle N_2-stream. For GC, an aliquot of the wax sample was derivatized using N, O-bis(trimethylsilyl)trifluoroacetamide (Macherey-Nagel Düren, Germany) in dry pyridine (Roth, Karlsruhe, Germany) for 45 min at 70 °C. Quantitative analysis was conducted using GC coupled with a FID. Samples were injected by an on-column

injector (7890A, Agilent Technologies, Waldbronn, Germany) onto a fused silica capillary column (DB1-ms, 30 m length x 0.32 mm ID, 0.1 µm film, Agilent Technologies) using H_2 as carrier gas. The temperature program was: injection at 50 °C and held for 2 min, raised by 40 °C min^{-1} to 200 °C and held for 2 min, raised by 3 °C min^{-1} to 320 °C and held for 30 min. Quantification was executed by comparison of the peak area of the internal standard with the peak area of the analytes. Qualitative analysis was performed using GC coupled with MS (5975iMSD, Agilent Technologies). The separation conditions were the same as with FID except helium was used as carrier gas. The leaf surface area was determined using the open-source program GIMP 2.0. Surfaces structure of adaxial cuticular disks were investigated using scanning electron microscopy (SEM, JEOL JSM-7500F, JEOL GmbH, Freising, Germany) with an accelerating voltage of 5.0 kV and a working distance of 7.9 mm equipped with a field emission gun and lower secondary electron (LEI) detector. CMs were carefully mounted on aluminium holders and sputter-coated with a mixture of 80/20 gold/palladium.

VI.2.3 Artificial wax

Nonacosane (C_{29}an, purity >98%), hentriacontane (C_{31}an, purity >98%) and triacontanol (C_{30}ol, purity >98%) were purchased from Sigma-Aldrich (Steinheim, Germany). Dotriacontanol (C_{32}ol, purity > 90%) was sourced from MuseChem (Fairfield, New Jersey, USA). Samples for FTIR experiments were prepared to depict the conditions of adaxial cuticular wax of *S. elegantissima* as best as possible. Therefore, a binary alkane mixture (C_{31}an/C_{29}an 2.3 - 1), a binary alcohol mixture (C_{32}ol/C_{30}ol 2.3 - 1), a ternary blend with C_{31}an/C_{29}an and either C_{32}ol or C30ol (2.3 - 1 – 1.4) and a quaternary blend (C_{31}an/C_{29}an/ C_{32}ol/C_{30}ol (5.4 – 2.3 - 2.3 - 1) was investigated. The ratios were chosen to depict the ratio of the four major compounds of the adaxial CM wax sufficiently: the ratio of the two major alkanes to each other, the ratio of the two alcohols two each other and the ratio of the binary alkane to binary alcohol mixture. For DSC and XRD experiments, two series of binary mixtures were prepared, one using C_{31}an and C_{29}an and one using C_{32}ol and C_{30}ol. Starting with an amount-of-substance fraction of 100/0 C_{31}an/C_{29}an or C_{32}ol/C_{30}ol to a fraction of 0/100 C_{31}an/C_{29}an or C_{32}ol/C_{30}ol in 10 mol% steps respectively. Ternary mixtures were prepared using an alkane mixture C_{31}an/C_{29}an with the ratio 70/30. To this mixture,

either C_{30}ol or C_{32}ol was added in 10 mol% steps. The wax was prepared with an alkane/alcohol ratio from 100/0 to 0/100. Quaternary mixtures were prepared using an alkane (C_{31}an/C_{29}an) and an alcohol (C_{32}ol/C_{30}ol) mixture with the ratio 70/30 respectively. For the quaternary blends, the alkane and alcohol mixtures were mixed in ratios (alkane/alcohol) between 100/0 and 0/100 in 10 mol% steps.

VI.2.4 Fourier transform infrared spectroscopy

FTIR spectra were obtained using a Tensor27 (Bruker, Ettlingen, Germany) with an attenuated total reflection FTIR unit with a silicon ZnSe crystal and temperature control using a K20 water bath and a DC30 heating spiral from Thermo (Waltham USA). The device was purged with purge gas from a purged gas generator K-MT3-LAB (Parker, Corsico, Italy). OPUS 7 software (Bruker Ettlingen, Germany) was used to set up experiments and collect the data.

The wax of adaxial CMs of *S. elegantissima,* binary, ternary and quaternary artificial wax blends, depicting conditions in the plant wax, were investigated. Wax samples were applied in TCM solution. The solvent was removed, and IR spectra were obtained between 20 °C and 92 °C. Between 20 °C and 44 °C, every 4 °C and between 44 °C and 92 °C every 1 °C spectra were taken after an equilibration time of one minute.

For data evaluation, OPUS 7 (Bruker Ettlingen, Germany) was used to obtain wavenumbers of symmetric (2850 cm^{-1}) and asymmetric (2920 cm^{-1}) stretching oscillation of methylene groups. Peak deconvolution app of OriginPro 2018b (Systat Software GmbH, Erkrath, Germany) was used for peak fitting and to recover the peak intensity of the double peak of the rocking (720/730 cm^{-1}) oscillation band. Crystallinity was calculated with Excel 2016 (Microsoft, Munich, Germany), according to Zerbi et al. (1989). They postulated the peak at 720 cm^{-1} to consist of two signals

$$I_{720} = I_{720}^{cr} + I_{720}^{am} \qquad\qquad (VI.1)$$

where I_{720} is the total intensity of the peak at 720 cm^{-1}, I_{720}^{cr} is the intensity of the crystalline fraction of the peak at 720 cm^{-1} and I_{720}^{am} is the intensity of the amorphous fraction of the peak at 720 cm^{-1}. The ratio of the group splitting of skeletal modes of orthorhombic polyethene was calculated after

$$\frac{I_{730}}{I_{720}^{cr}} = 1.233 \qquad\qquad (VI.2)$$

with I$_{730}$ as the intensity of the peak at 730 cm^{-1} and I$_{720}^{cr}$ is the intensity of the crystalline fraction of the peak at 720 cm^{-1} (Abbate et al. 1979; Zerbi et al. 1989). Equation (VI.1) and (VI.2) were combined to

$$I_{720}^{am} = I_{720} - \frac{I_{730}}{1.233} \tag{VI.3}$$

From here, the fraction of amorphous material was calculated

$$x_{am} = 100 \times \frac{I_{720}^{am}}{(I_{720}+I_{730})} \tag{VI.4}$$

with x_{am} being the fraction of amorphous material. The crystalline fraction x_{cr} was then calculated with

$$x_{cr} = 1 - x_{am} \tag{VI.5}$$

OriginPro 2018b (Systat Software GmbH, Erkrath, Germany) was used for plotting and statistical analysis. For normally distributed data, significant differences were investigated using one-way ANOVA ($p < 0.05$). Otherwise, the Kruskal-Wallis test ANOVA with posthoc Dunn´s test was used. Values are given in mean (± standard deviation).

VI.2.5 Differential scanning calorimetry

Wax samples were weighed into aluminium crucibles and sealed with a lid. The plant wax sample consisted of wax obtained from the whole leaf. The lid was pierced once to ensure pressure compensation. Experiments were conducted using a Mettler Toledo DSC 1 (Mettler-Toledo GmbH, Gießen, Germany). The temperature ramp started at 20°C and increased to 100 °C with 2°C min^{-1}. Two consecutive temperature cycles, each consisting of one heating and one cooling ramp were applied. The first cycle was used to form a solid mixture by melting the samples. Preliminary experiments showed identical thermal behaviour of wax samples of the second cycle and if the sample was submitted to more temperature cycles. Therefore, the results from the heating ramp of the second cycle were used for data analysis. Resulting thermograms were evaluated using STARe (Mettler-Toledo GmbH, Gießen, Germany). For evaluation purpose, onset, peak temperature and endset of the signals were determined. Graphs were plotted using OriginPro 2018b (Systat Software GmbH, Erkrath, Germany).

VI.2.6 X-ray diffraction

For XRD measurements of the artificial waxes at room temperature, the molten DSC samples were used. The wax from both, adaxial CMs of *S. elegantissima* and the whole

leaf were used for experiments at room temperature. For hot stage XRD experiments, plant wax obtained from the entire sheet was used. The DSC crucible was opened, and the wax was removed carefully. The wax was then given onto XRD sample holders and flattened with a glass slide. The sample holder was then inserted into the X-ray diffractometer (Bruker D8 pXRD, Bruker, Ettlingen, Germany). During measurement, the sample holder was rotated slowly. XRD diagrams were obtained between angles of 3.5 ° and 40 ° (coupled two Θ/Θ). Hot stage experiments were conducted using a temperature adjustable sample holder. The temperature was increased with 12°C min^{-1} until five 5 °C below the first signal and kept for six minutes. Afterwards, it was increased with 1.2 °C min$^{-1,}$ and a measurement was conducted every 1°C after an equilibrium time of six minutes. The analysis ended after the melting of the sample, which was previously determined by DSC. XRD diagrams were obtained between angles of 10 ° and 40 ° (coupled two Θ/Θ). Resulting difractograms were evaluated using Diffrac.Eva (Bruker, Ettlingen, Germany).

VI.3 Results

VI.3.1 Composition and surface structure of leaf waxes of *S. elegantissima*

The adaxial cuticular leaf wax of *S. elegantissima* consisted majorly of VLCAs (20.1 ± 1.41 µg cm^{-2}). TRPs (1.37 ± 0.67µg cm^{-2}) constituted only a minor partition of the wax (figure VI.1). The whole leaf wax of *S. elegantissima* consisted almost exclusively of VLCAs (8.73 ± 0.25 µg cm^{-2}). TRPs (0.01 ± 0.01 µg cm^{-2}) were only found in traces (figure VI.1). The VLCA and TRP amount of isolated CM was significantly higher compared to whole leaf extracts ($p < 0.05$).

Figure VI.1: Wax composition of adaxial cuticular membranes (CM; brown) and whole leaf extracts (purple) of *S. elegantissima* segmented into very long chain aliphatic (VLCA) compounds and triterpenoids (TRP). Bars show the mean and error bars show standard deviation. Letters signify statistically significant differences between wax samples of different sample types within a wax fraction. (n = 4).

A more thorough look into the VLCAs of isolated adaxial CMs (figure VI.2) showed alkanes to be the dominant substance class (10.9 ± 0.12 µg cm^{-2}), followed by alcohols (4.80 ± 0.88 µg cm^{-2}), aldehydes (2.60 ± 0.79 µg cm^{-2}) and alkyl acids

(1.61 ± 0.43 µg cm^{-2}). Besides, minor amounts of benzylic acid ester (0.21 ± 0.12 µg cm^{-2}) were found (figure VI.). Alkanes (7.78 ± 0.21 µg cm^{-2}) were also the dominant substance class in whole leaf extracts. Minor amounts of alcohols (0.21 ± 0.01 µg cm^{-2}), aldehydes (0.47 ± 0.06 µg cm^{-2}), alkyl acids (0.22 ± 0.05 µg cm^{-2}) and benzylic acid ester (0.05 ± 0.01 µg cm^{-2}) were found (figure VI.2). The amounts of alkanes, alcohols, aldehydes and alkyl acids were significantly higher ($p < 0.05$) than in the whole leaf extracts. The amounts of benzylic acid ester showed no significant difference ($p > 0.05$).
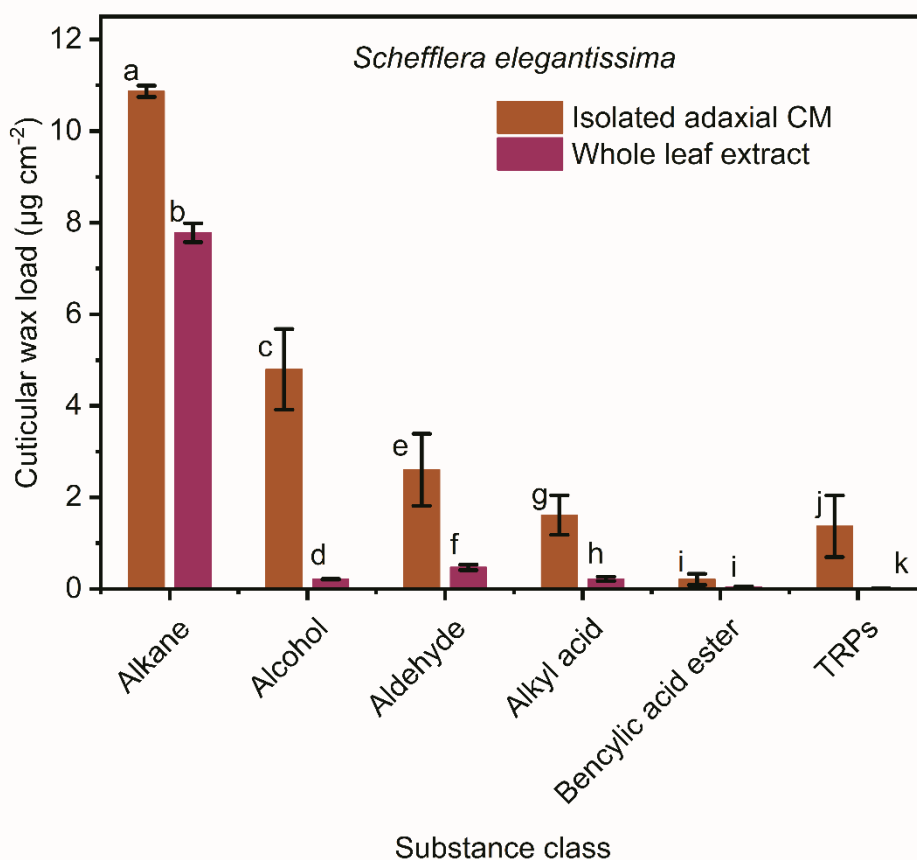
Figure VI.2: Wax substance class composition of adaxial cuticular membranes (CM; brown) and whole leaf extracts (purple) of *S. elegantissima* segmented into different substance classes. Bars show the mean and error bars show standard deviation. Letters signify statistically significant differences between wax samples of different sample types within a substance class. (n = 4).

The chain length distribution of the adaxial CM wax was dominated by four major chain lengths. VLCAs with a carbon number of 31 (7.32 ± 0.11 µg cm^{-2}) were the most abundant, followed by chains with 32 (5.50 ± 0.96 µg cm^{-2}), 29 (3.14 ± 0.06 µg cm^{-2})

and 30 (2.06 ± 0.11 µg cm^{-2}) carbon atoms (figure VI.3). Thereby, the chain lengths 31 and 29 were dominated by alkanes, and the chain lengths 32 and 30 were dominated by alcohols (table VI.1). The chain length distribution of the whole leaf extracts was dominated by four major chain lengths. VLCAs with a carbon number of 31 (4.88 ± 0.15 µg cm^{-2}) were the most abundant, followed by chains with 29 (2.62 ± 0.11 µg cm^{-2}), 30 (0.62 ± 0.05 µg cm^{-2}), and 32 (0.34 ± 0.03 µg cm^{-2}) carbon atoms (figure VI.3). Thereby, the chain lengths 31 and 29 were dominated by alkanes, and the chain lengths 32 and 30 were dominated by aldehydes (table VI.1)

.

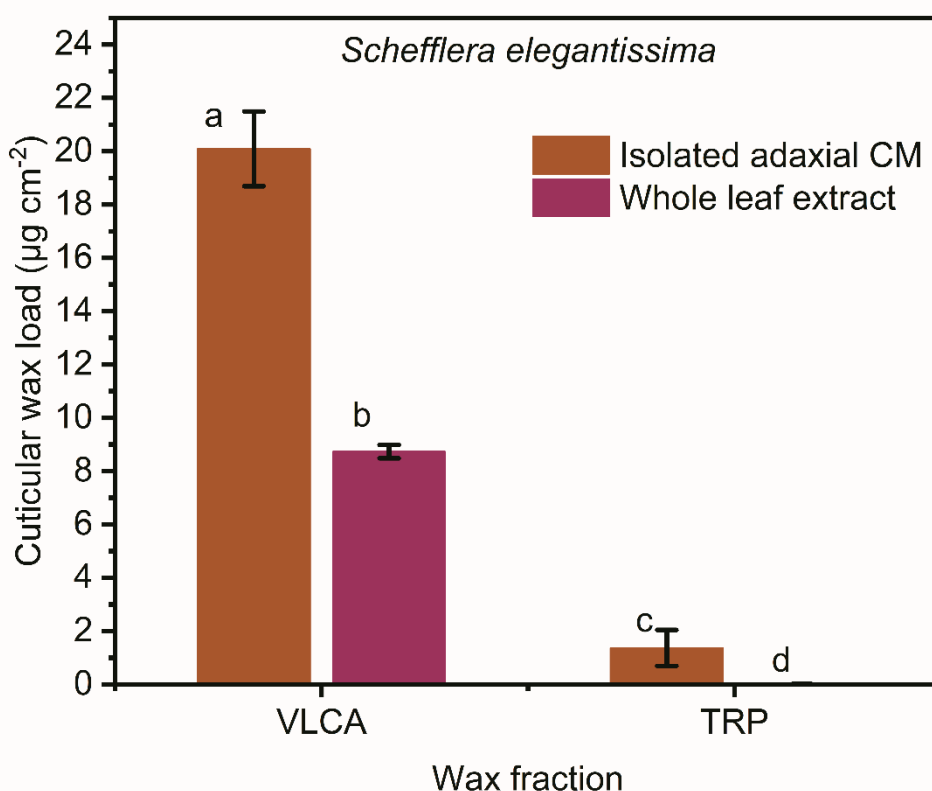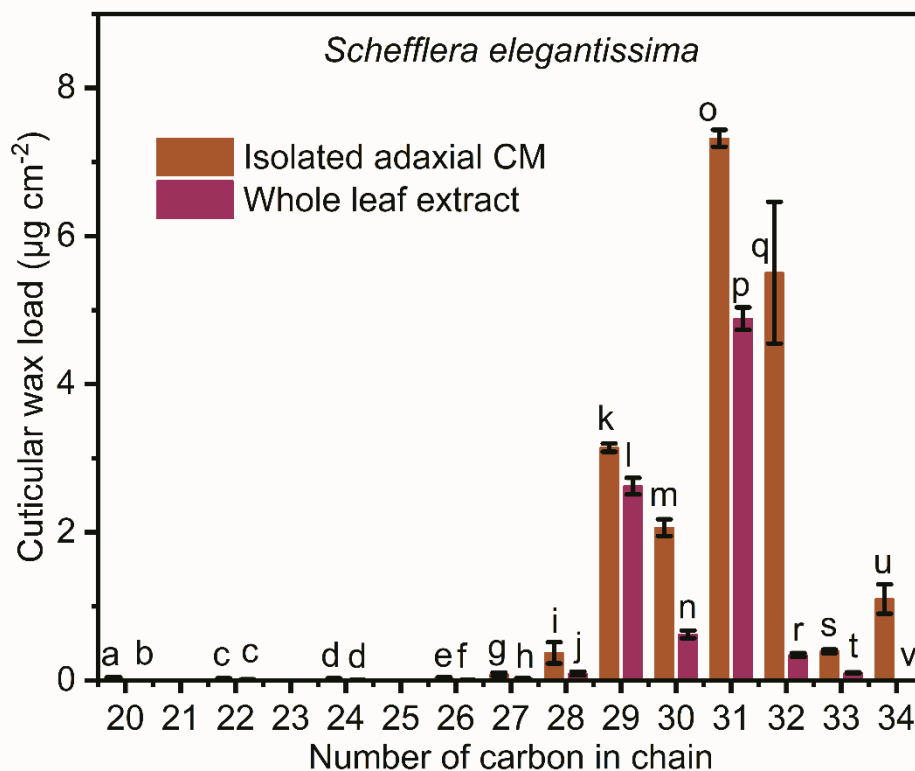Figure VI.3: Carbon chain length composition of adaxial cuticular membranes (CM; brown) and whole leaf extracts (purple) of *S. elegantissima* segmented into different substance classes. Bars show the mean and error bars show standard deviation. Letters signify statistically significant differences between wax samples of different sample types within a chain length. (n = 4).

Table VI.1: Breakdown (mean, standard deviation) of the most abundant substance classes according to their carbon chain length of wax from adaxial cuticular membranes (CM) and whole leaf extracts of *Schefflera elegantissima*. (n = 4)

Class	Carbon number	Isolated adaxial CM Amount ± Deviation ($\mu g\ cm^{-2}$)	Whole leaf Amount ± Deviation ($\mu g\ cm^{-2}$)
Alkane	29	3.06 ± 0.03	2.62 ± 0.11
Alkane	31	7.16 ± 0.08	4.88 ± 0.15
Alcohol	30	0.94 ± 0.02	0.10 ± 0.00
Alcohol	32	2.68 ± 0.77	0.09 ± 0.01
Aldehyde	30	0.39 ± 0.18	0.26 ± 0.03
Aldehyde	32	1.92 ± 0.41	0.19 ± 0.02
Alkyl acid	30	0.49 ± 0.10	0.13 ± 0.02
Alkyl acid	32	0.80 ± 0.30	0.03 ± 0.01

The SEM pictures of isolated adaxial CMs of *S. elegantissima* (figure VI.4) showed an encrusted, partially granulated surface, but no epicuticular wax crystals.

Figure VI.4 Scanning electron micrograph of the top of an isolated adaxial cuticle of *Schefflera elegantissima* using a lower secondary electron detector.

VI.3.2 Determination of melting behaviour and aliphatic crystallinity using FTIR

The melting behaviour was investigated using the shift of the wavenumber of the asymmetric and symmetric stretching oscillation of carbon-hydrogen bonds. Both oscillations showed very similar behaviour, but the range of the shift was constantly greater for the asymmetric oscillation (figure VI.5). In the graphs of all artificial samples investigated, at least one small, but sharp step was exhibited.

For the binary alkane mixture (figure VI.5 A, F), the wavenumbers of the asymmetric oscillation showed a small, but significant ($p < 0.05$) increase between 20 °C and 59 °C from 2847.8 ± 0.08 cm^{-1} to 2848.3 ± 0.07 cm^{-1} For the symmetric one, the same behaviour was found from $2913.p \pm 0.19$ cm^{-1} to 2914.6 ± 0.15 cm^{-1}. Between 59 °C and 60 °C a significant, small and sharp increase to 2849.2 ± 0.06 cm^{-1} and 2915.4 ± 0.07 cm^{-1}, respectively, was observed, followed by a small, significant increase to 2849.6 ± 0.07 cm^{-1} and 2915.8 ± 0.16 cm^{-1} until 65 °C ($p < 0.05$). Between 65 °C and 72 °C a significant, steep increase was found for both oscillations to 2853.5 ± 0.21 cm^{-1} and 2920.3 ± 0.11 cm^{-1} ($p < 0.05$). In the temperature range of 72 °C to 92°C a non-significant, minor increase to 2853.8 ± 0.11 cm^{-1} and 2920.4 ± 0.13 cm^{-1} was observed ($p > 0.05$).

For the binary alcohol mixture (figure VI.5 B, G), the wavenumbers of the asymmetric oscillation showed a small, but significant ($p < 0.05$) increase between 20 °C and 66 °C from 2848.5 ± 0.15 cm^{-1} to 2849.2 ± 0.10 cm^{-1} For the symmetric one a similar but non-significant behaviour was found from 2915.3 ± 0.40 cm^{-1} to 2915.8 ± 0.28 cm^{-1}. Between 66 °C and 71 °C a significant, small and sharp increase to 2849.9 ± 0.09 cm^{-1} and 2916.4 ± 0.21 cm^{-1}, respectively, was observed ($p < 0.05$). Between 71 °C and 89 °C a significant increase with increasing shift of wavenumbers over temperature was found for both oscillations to 2853.3 ± 0.06 cm^{-1} and 2919.7 ± 0.09 cm^{-1} ($p < 0.05$). In the temperature range of 89 °C to 92°C a non-significant, minor increase to 2853.4 ± 0.04 cm^{-1} and 2919.7 ± 0.10 cm^{-1} was observed ($p > 0.05$).

For the ternary mixture, consisting of $C_{31}an$, $C_{29}an$ and $C_{30}ol$ (figure VI.5 C, H), the wavenumbers of the asymmetric oscillation showed a small, non-significant ($p > 0.05$) increase between 20 °C and 58 °C from 2848.3 ± 0.26 cm^{-1} to 2848.7 ± 0.29 cm^{-1} For the symmetric one a similar non-significant ($p > 0.05$) behaviour was found from

2914.5 ± 1.21 cm^{-1} to 2915.0 ± 1.09 cm^{-1}. Between 58 °C and 66 °C, exhibited the asymmetric oscillation a small but significant ($p < 0.05$) increase in wavenumbers to 2849.7 ± 0.22 cm^{-1}. In the same temperature range, a small, nonsignificant ($p > 0.05$) shift to 2916.0 ± 0.80 cm^{-1} was found for the symmetric stretching. Between 66 °C and 69 °C a significant ($p < 0.05$), small increase in wavenumbers to 2852.4 ± 0.08 cm^{-1} and 2919.1 ± 0.20 cm^{-1}, respectively, was observed. Between 69 °C and 80 °C a significant increase ($p < 0.05$) with decreasing shift of wavenumbers over temperature was found for both oscillations to 2853.6 ± 0.12 cm^{-1} and 2920.3 ± 0.31 cm^{-1}. In the temperature range of 80 °C to 92°C a non-significant ($p > 0.05$), minor increase to 2853.9 ± 0.06 cm^{-1} and 2920.4 ± 0.23 cm^{-1} was observed.

For the ternary mixture, consisting of C$_{31}$an, C$_{29}$an and C$_{32}$ol (figure VI.5 D, I), the wavenumbers of the asymmetric oscillation showed a small, non-significant ($p > 0.05$) increase between 20 °C and 55 °C from 2848.1 ± 0.30 cm^{-1} to 2848.6 ± 0.36 cm^{-1} For the symmetric one a similar non-significant ($p > 0.05$) behaviour was found from 2914.2 ± 0.86 cm^{-1} to 2914.7 ± 0.84 cm^{-1}. Between 55 °C and 60 °C, exhibited both oscillations a small, rather sharp, but non-significant ($p < 0.05$) increase in wavenumbers to 2849.5 ± 0.29 cm^{-1} and 2915.5 ± 0.66 cm^{-1}, respectively. Between 60 °C and 71 °C a large, significant ($p < 0.05$) increase in wavenumbers with an increasing shift of wavenumbers over temperature to 2852.8 ± 0.21 cm^{-1} and 2919.2 ± 0.25 cm^{-1}, respectively, was observed. Between 71 °C and 80 °C a non-significant increase ($p > 0.05$) was found for both oscillations to 2853.6 ± 0.17 cm^{-1} and 2920.1 ± 0.25 cm^{-1}. In the temperature range of 80 °C to 92 °C the graphs flattened out with a non-significant ($p > 0.05$), minor increase to 2853.8 ± 0.16 cm^{-1} and 2920.3 ± 0.28 cm^{-1}.

For the quaternary mixture, consisting of C$_{31}$an, C$_{29}$an, C$_{32}$ol and C$_{30}$ol (figure VI.5 E, J, the wavenumbers of the asymmetric oscillation showed a small, significant ($p < 0.05$) increase between 20 °C and 57 °C from 2848.2 ± 0.18 cm^{-1} to 2848.7 ± 0.18 cm^{-1}. For the symmetric one a similar, but non-significant ($p > 0.05$) behaviour was found from 2914.6 ± 0.40 cm^{-1} to 2915.1 ± 0.35 cm^{-1}. Between 57 °C and 61 °C, both oscillations exhibited a small but significant ($p < 0.05$) increase in wavenumbers to 2849.5 ± 0.15 cm^{-1} and 2915.8 ± 0.32 cm^{-1}. Between 61 °C and 64 °C a non-significant ($p > 0.05$), small increase in wavenumbers to 2849.7 ± 0.13 cm^{-1} and

2915.1 + 0.31 cm^{-1}, respectively, was observed. Between 64 °C and 82 °C a significant increase ($p < 0.05$) with decreasing shift of wavenumbers over temperature to 2853.6 ± 0.14 cm^{-1} and 2920.1 ± 0.18 cm^{-1} was found for both oscillations. In the temperature range of 82 °C to 92 °C the graphs flattened out with a non-significant ($p > 0.05$), minor increase to 2853.8 ± 0.14 cm^{-1} and 2920.3 ± 0.20 cm^{-1}.
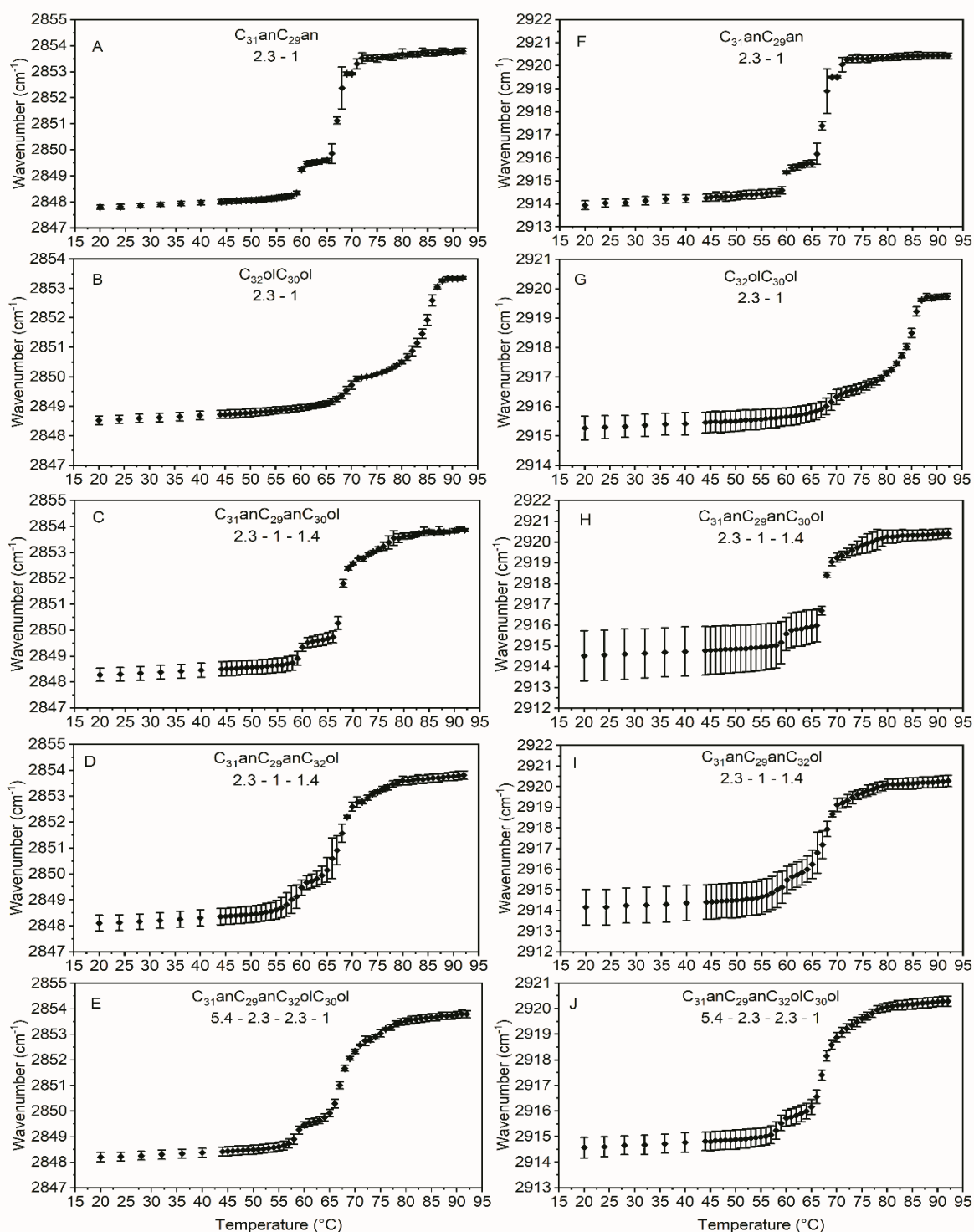
Figure VI.5: Melting behaviour determined from the wavenumber shift of the symmetric (A - E) and asymmetric (F - J) stretching oscillation of carbon-hydrogen bonds of various wax blends consisting of hentriacontane (C_{31}an), nonacosane (C_{29}an), dotriacontanol (C_{32}ol) and triacontanol (C_{30}ol). The ratios are normalized to the compound with the smallest amount. Data points show the mean and error bars show standard deviation (n = 3 - 4)

The *S. elegantissima* adaxial cuticular wax exhibited a rather fluent behaviour of the wavenumber shifts upon heating (figure VI.6 A, B). There was no step found like in the artificial wax mixtures. Between 20 °C and 88 °C the wavenumber significantly ($p < 0.05$) increased gradually magnified from 2848.9 ± 0.16 cm^{-1} and 2914.7 ± 0.70 cm^{-1} to 2853.7 ± 0.23 cm^{-1} and 2920.9 ± 0.44 cm^{-1}. Until 92 °C the wavenumber shift flattened out to 2853 ± 0.23 cm^{-1} and 2921.0 ± 0.40 cm^{-1}.
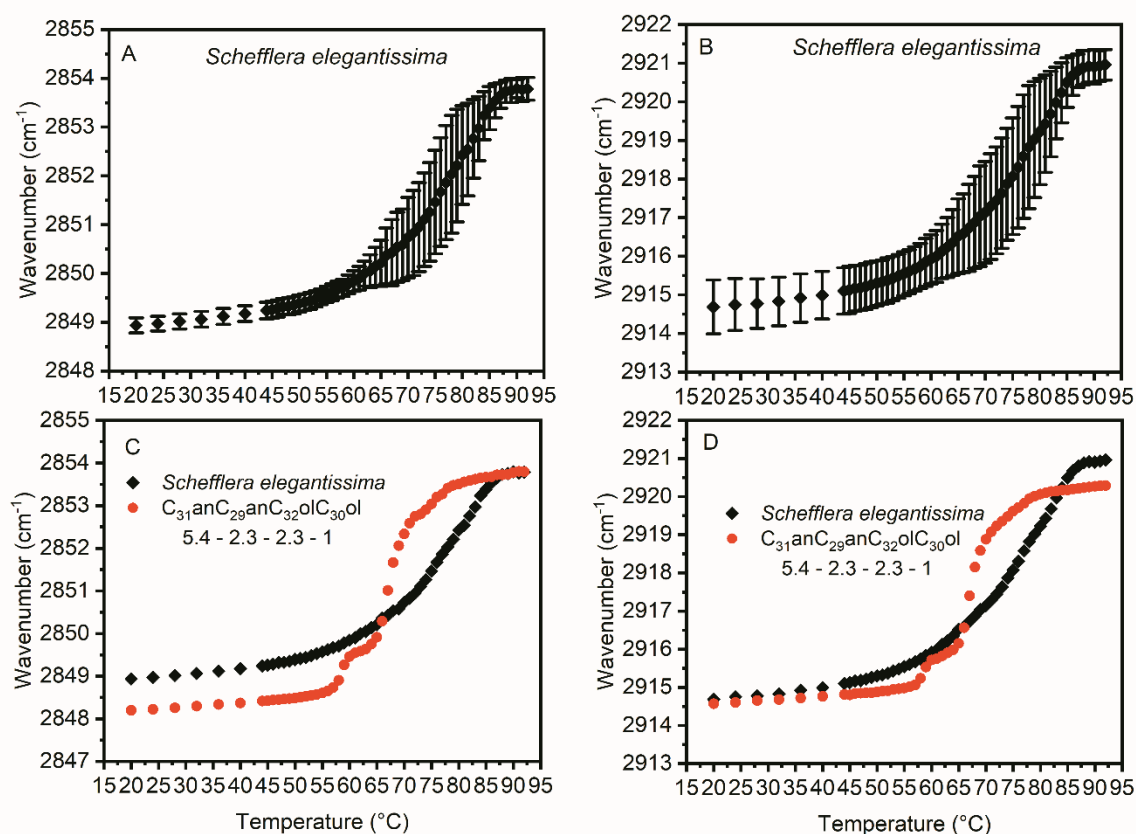
Figure VI.6: Melting behaviour determined from the wavenumber shift of the asymmetric (A, C) and symmetric (B, D) stretching oscillation of carbon-hydrogen bonds of adaxial cuticular wax of *Schefflera elegantissima* (A, B) and a comparison of the plants wax (black diamonds) with the quaternary wax blend (red circles) consisting of hentriacontane (C_{31}an), nonacosane (C_{29}an), dotriacontanol (C_{32}ol) and triacontanol (C_{30}ol) in the ratio 3.5 - 1.5 - 2.7 – 1 (C, D). Data points show the mean and error bars show standard deviation. Error bars were renounced in C and D for clarity purpose. The data with error bars can be found in panels A and C and figure VI.5. (n = 3 - 4)

Comparing the spectra of the artificial blends, which reflected conditions of the adaxial CM wax, with the spectrum of the adaxial CM wax an increasing approach with an increasing number of wax constituents becomes apparent (figure VI.7). However, noticeable differences between the quaternary and the adaxial CM leaf wax are still present (figure VI.6 C, D; figure VI.7)
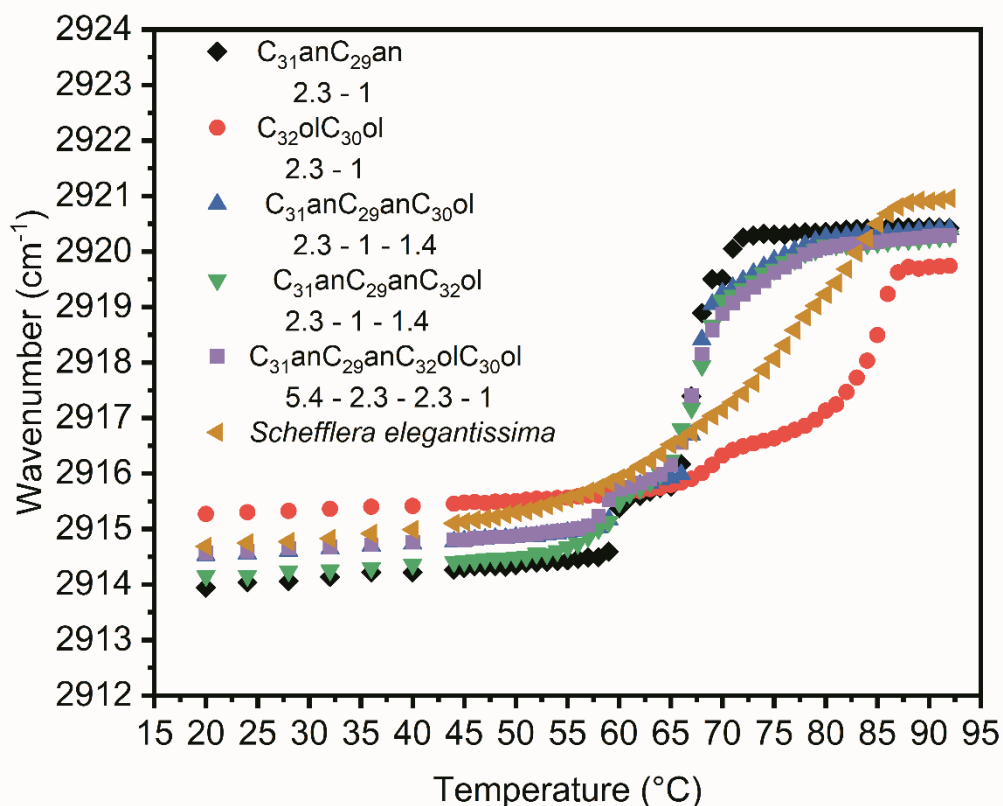
Figure VI.7: Comparison of the melting behaviour of various artificial wax blends and the wax from the adaxial cuticle of *Schefflera elegantissima* (yellow triangle). The Binary alkane blend was made from hentriacontane (C_{31}an) and nonacosane (C_{29}an) with the mole ratio 2.3 – 1 (black diamonds). Ternary mixtures were prepared with C_{31}an and C_{29}an and either triacontanol (C_{30}ol, red circles) or dotriacontanol (C_{32}ol, green triangles) with the mole ratio 2.3 – 1 – 1.4. Quaternary wax mixture C_{31}anC_{29}anC_{32}olC_{30}ol had a ratio of 5.4 – 2-3 – 2.3 – 1 (purple quarters). Data points show the mean. Error bars were renounced for clarity purpose. The data with error bars can be found in figure VI.5 and VI.6. (n = 3 - 4)

The crystallinity of the quaternary wax mixture and *S. elegantissima* adaxial cuticular wax was determined using the split band at 720 cm^{-1} and 730 cm^{-1} and was calculated after Zerbi et al. (1989). The quaternary wax showed a rather constant orthorhombic crystalline fraction until 57 °C (figure VI.8). At 20 °C, the crystallinity was 91 ± 4 % and remained at 91 ± 7 % at 57 °C.

The plant wax crystallinity showed a slow decline. At 20 °C 79 ± 8 % were crystalline, while at 58 °C only 55 ± 13 % had this property. The decline was minor until 48 °C and increased at temperatures above this threshold. Above 58 °C (plant wax) and 57 °C (quaternary wax) no visible peak splitting was seen in the IR spectra.
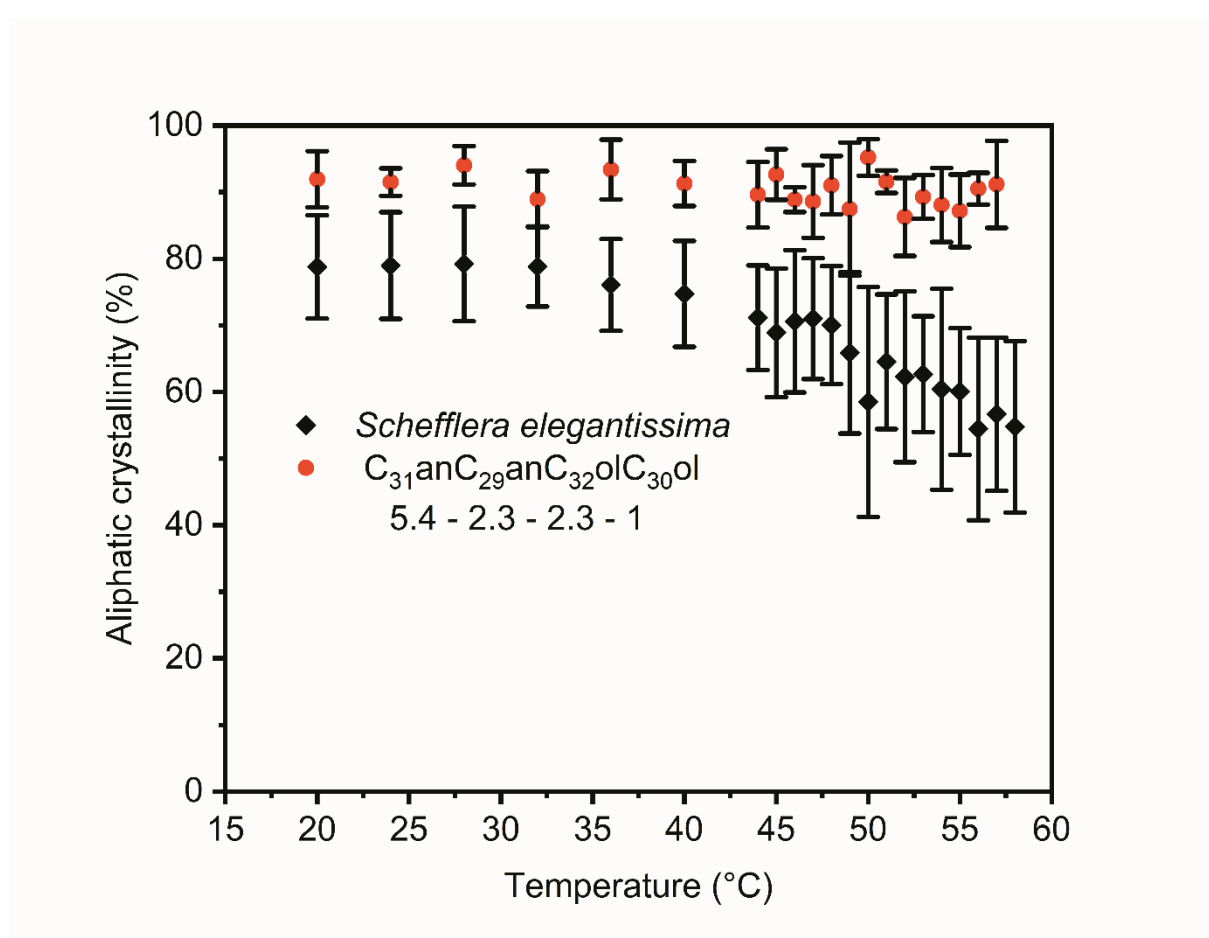
Figure VI.8: Behaviour of aliphatic crystallinity of adaxial cuticular wax of *Schefflera elegantissima* (grey quarters) and a quaternary wax blend (red circles) consisting of hentriacontane (C_{31}an), nonacosane (C_{29}an), dotriacontanol (C_{32}ol) and triacontanol (C_{30}ol) in the ratio 5.4 - 2.3 - 2.3 - 1. (n = 3 - 4)

VI.3.3 Investigation of physical properties of wax mixtures using DSC

Thermograms of commercially available wax compounds showed increased complexity with the growing number of compounds used (figure VI.9). The binary alkane mixture of C_{31}an and C_{29}an (2.3 – 1, figure VI.9 A) showed two separated peaks. The first signal was observed before the wax started to melt, indicating a solid-solid transition at 59.0 °C and one at the melting temperature (66.1 °C). Both showed endothermal processes. The binary alcohol mixture of C_{32}ol and C_{30}ol (2.3 – 1, figure VI.9 B) showed similar results with a solid-solid transition peak at 67.7 °C and the melting peak at 83.7 °C. However, the peaks were strongly broadened. Additionally, thermograms of both blends strongly resembled the thermograms of the pure wax compound (supplement figure 2). Going from a binary blend to a ternary one, the addition of C_{30}ol to the binary alkane blend (figure VI.9 C) increased the numbers of signals found. There was one separated peak at 57.8 °C and three connected peaks at 65.5 °C, 69.3 °C and 75.3°C, respectively, with the highest temperature signifying the melting of the sample. Compared to the melting temperature of the alcohol blend, a shift to lower temperatures was found. The thermogram of the ternary mixture C_{31}anC_{29}anC_{32}ol (2.3 – 1 – 1.4, figure VI.9 D) showed similar signals upon temperature increase as the blend C_{31}anC_{29}anC_{30}ol (2.3 – 1 – 1.4). The thermograms showed one peak at 57.6 °C, 65.8 °C and 70.4 °C each and the melting peak at 75.1 °C. In this blend, no separated peak was found. In the thermogram of the quaternary blend consisting of C31anC29anC32olC30ol (5.4 - 2.3 - 2.3 - 1, figure VI.9 E), three connected peaks were found. One peak at 57.8°C, one at 66.1°C and the final melting peak at 74.2 °C.

Preparation and characterization of physical properties of an artificial wax mixture mimicking *S. elegantissima* adaxial leaf wax.


Figure VI.9: Thermograms of artificial wax blends made from hentriacontane (C_{31}an) and nonacosane (C_{29}an, A), dotriacontanol (C_{32}ol) and triacontanol (C_{30}ol, B), C_{31}anC_{29}anC_{30}ol (C), C_{31}anC_{29}anC_{32}ol (D) and C_{31}anC_{29}anC_{32}olC_{30}ol (E). The substance ratio is normalized depicted in brackets. Total Heat of fusion (HoF) was calculated to energy emission or uptake with temperature change. Negative values signify uptake. (n = 1)

The thermogram of whole leaf wax of *Schefflera elegantissima* (figure VI.10) showed three broad signals with peaks at 62.3 °C, 71.0 °C and 74.9 °C. A comparison of the leaf wax and the quaternary wax blend shows good comparability between the two samples.
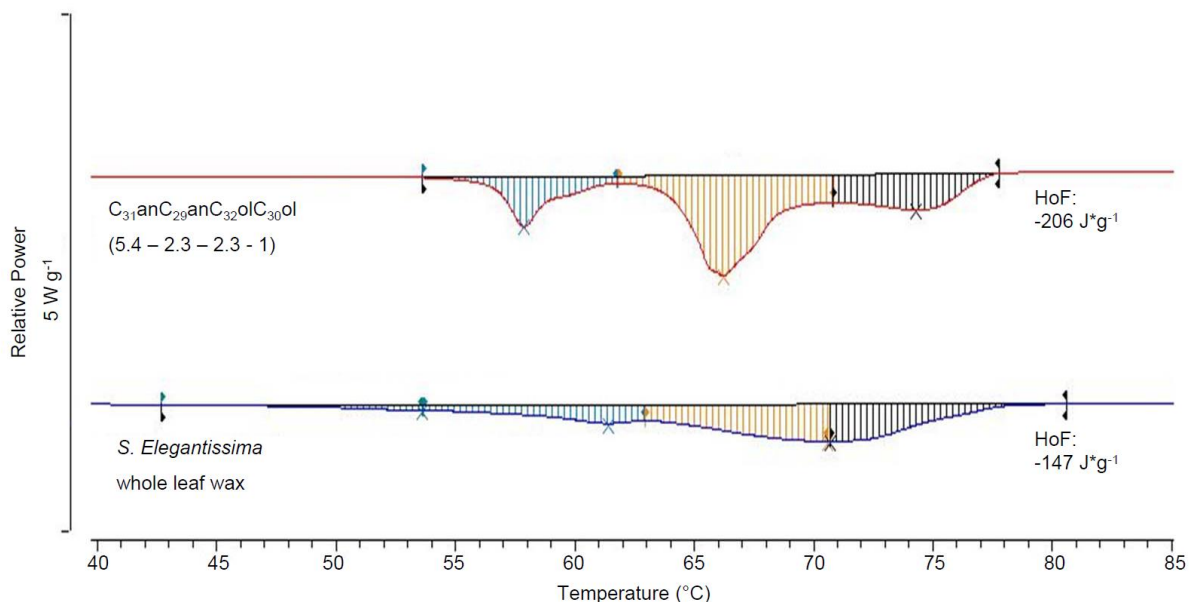
Figure VI.10: Comparison of the thermogram of a quaternary wax blend C31anC29anC32olC30ol (5.4 - 2.3 - 2.3 - 1) and whole leaf wax of *Schefflera elegantissima*. Total Heat of fusion (HoF) was calculated to energy emission or uptake with temperature change. Negative values signify uptake. (n = 1)

The phase diagrams of binary blends made of C_{31}an and C_{29}an showed one transition before melting of the sample throughout all mixtures. Except for varying temperatures, the similar behaviour of the blends and their pure compounds were found (figure VI.11 A). Similar results were found for binary blends of the alcohols C_{32}ol and C_{30}ol. Only for pure C_{30}ol, no signal 1 was found (figure VI.11 B).
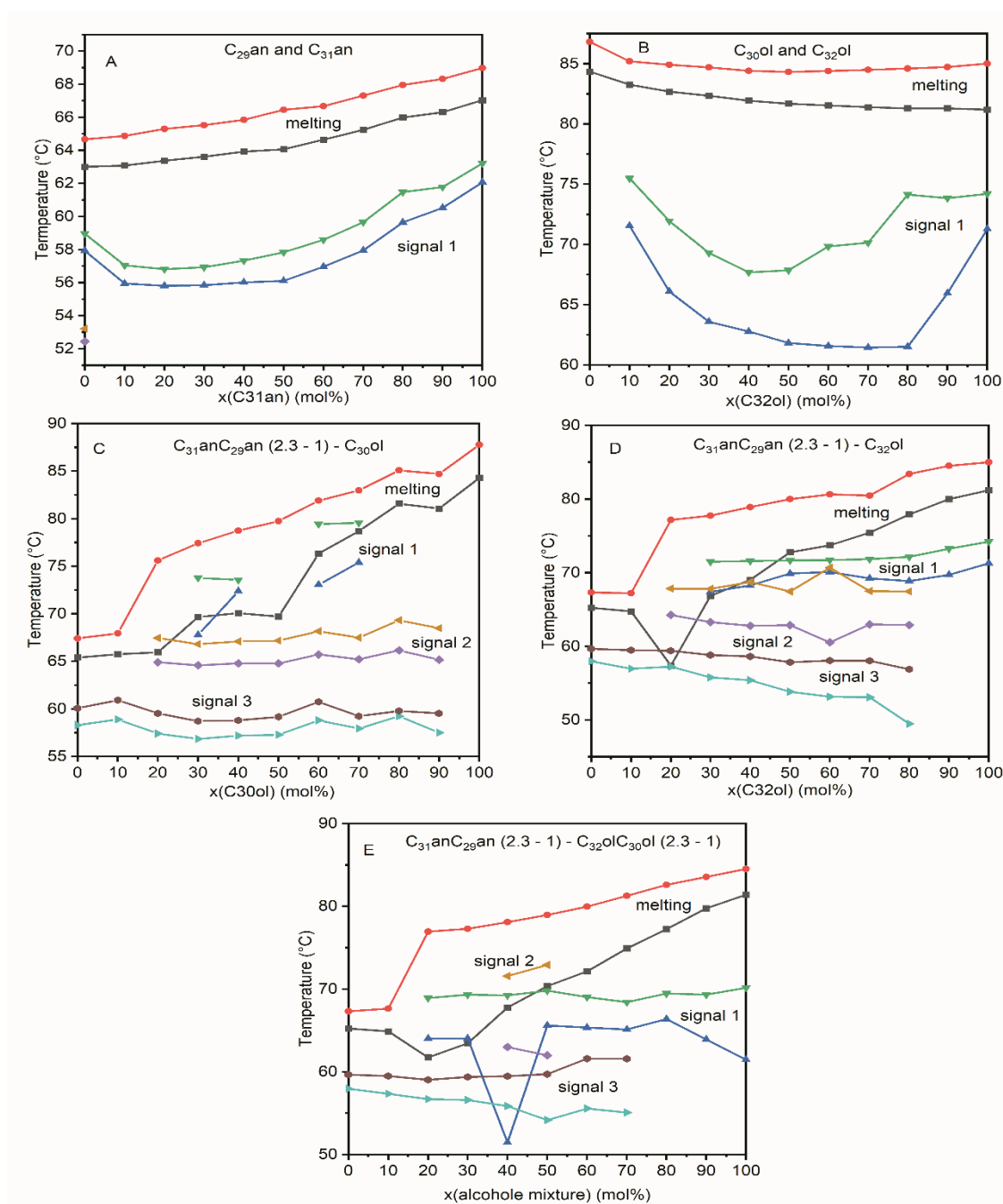
Figure VI.11: Phase diagrams of various wax blends containing hentriacontane (C$_{31}$an) and nonacosane (C$_{29}$an), dotriacontanol (C$_{32}$ol) and triacontanol (C$_{30}$ol). The binary blends were made of the alkanes (A) or the alcohols (B), respectively. For ternary blends, the composition of the alkanes was kept constant (C$_{31}$anC$_{29}$an 2.3 – 1) and either C$_{30}$ol (C) or C$_{32}$ol (D) was added. For the quaternary mixtures, the ratio between the alkanes C$_{31}$an and C$_{29}$an and between the alcohols C$_{32}$ol and C$_{30}$ol was kept constant (2.3 – 1) and the mixtures were mixed in varying ratios. The signals at the highest temperature, after which the samples were liquefied, are marked as melting. Further occurring signals (onset and endset of the peak) are named with decreasing temperature signal 1 (green and dark blue marks), signal 2 (yellow and purple marks) and signal 3 (brown and light blue marks). (n = 1)

The ternary mixtures consisting of two alkanes with constant ratio and one alcohol showed three signals before melting in the investigated temperature range. In the blend with C_{30}ol (figure VI.11 C), signal 1 only occurred at 30 mol% and 40 mol% as well as 60 mol% and 70 mol% of the alcohol. Signal 2 was found at 20 - 90 mol% alcohol, and signal 3 was only missing in the pure alcohol.

In the ternary mixture with C_{32}ol (figure VI.11 D) signal 1 was found at 30 - 100 mol% alcohol. The signal 2 was found at 20 - 80 mol% C_{32}ol and signal 3 was only missing at 90 mol% and the pure alcohol.

The quaternary wax blend, made of a binary alkane mixture with constant ratio (C_{31}anC_{29}an, 2.3 -1, figure VI.11 E) and the binary alcohol mixture with constant ratio (C_{32}olC_{30}ol, 2.3 – 1) showed three signals before melting. Signal 1 at 20 – 100 mol% of the alcohol mixture. Signal 2 was found at 40 mol% and 50 mol%, and signal 3 was found at 0 – 70 mol% of the alcohol mixture.

VI.3.4 Investigation of the crystal structure of wax blends using XRD methods

The investigation of crystallinity was conducted using XRD methods. For the measurement, the molten samples from DSC investigations were used. Binary alkane blends showed a high number of signals in the area below 20 °, indicating a highly ordered crystal structure. Between diffraction angles 20 ° to 25 ° two signals (21.6 ° and 23.9 ° for alkanes and 21.7 ° and 24.5 ° for alcohols) were found for all blends. The pure alcohols showed an additional peak at 23.0 °. Above 25 °, no signals were seen (figure VI.12 A). Binary alcohol blends showed if at all, only a few and a small number of peaks outside the range of 20 ° and 25 °. Within this range, up to four peaks, depending on the composition were found (figure VI.12 B).
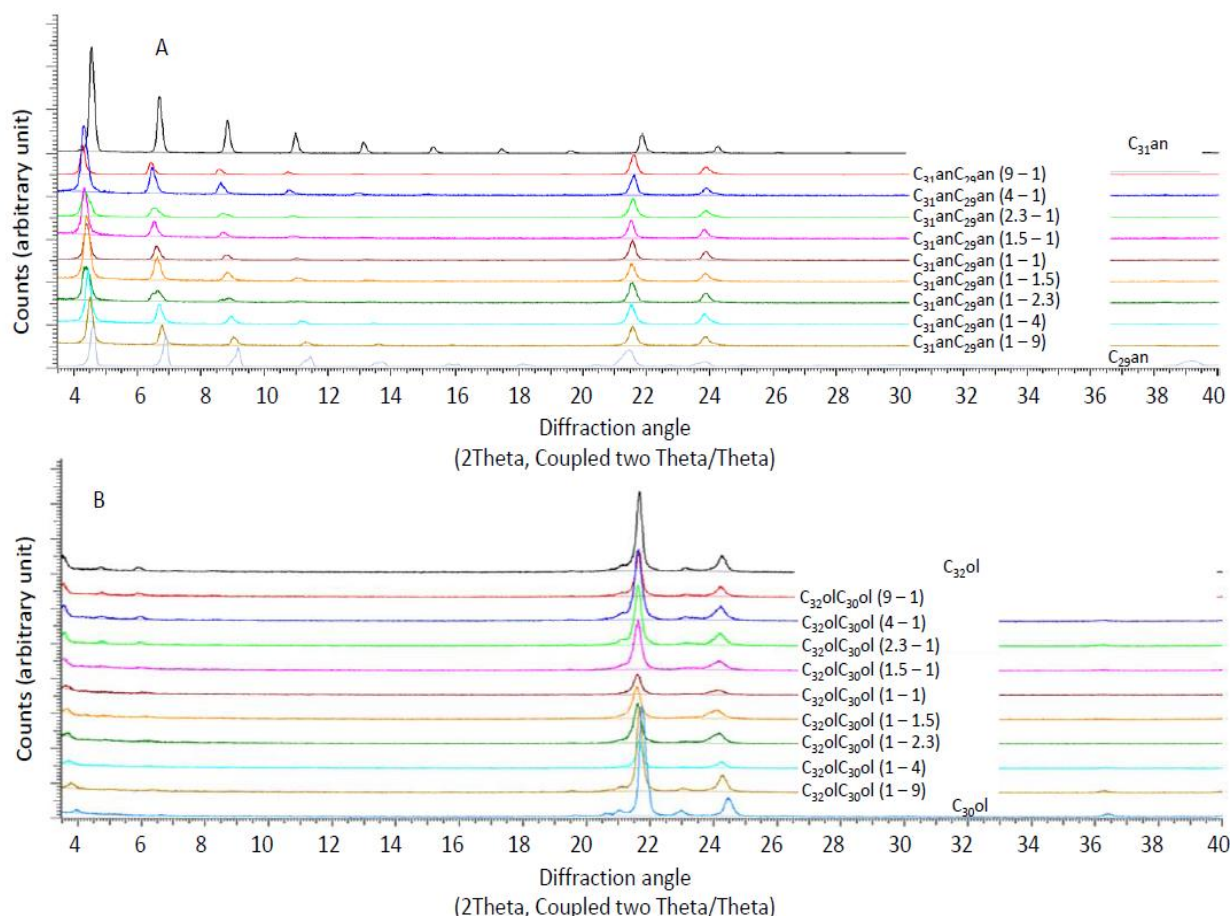
Figure VI.12: Series of diffraction pattern of binary artificial wax blends made from hentriacontane (C_{31}an) and nonacosane (C_{29}an, A), dotriacontanol (C_{32}ol) and triacontanol (C_{30}ol, B). The substance ratio is normalized depicted in brackets.

The ternary mixtures both showed a small number of peaks below 20 °. In the range between 20 ° and 25 ° for the alkane mixture, only two peaks (21.6 ° and 23.9 °) were found. With increasing alcohol content, the peak at 23.9 °gradually decreased, finally vanished and a new peak emerged at 24.5 °. This was first found for an alcohol composition of $C_{31}anC_{29}anC_{30}ol$ of 2.3 -1 -1.4 (figure VI.13 A) and for $C_{31}anC_{29}anC_{30}ol$ of 2.3 -1 - 7.8 (figure VI.13 B)
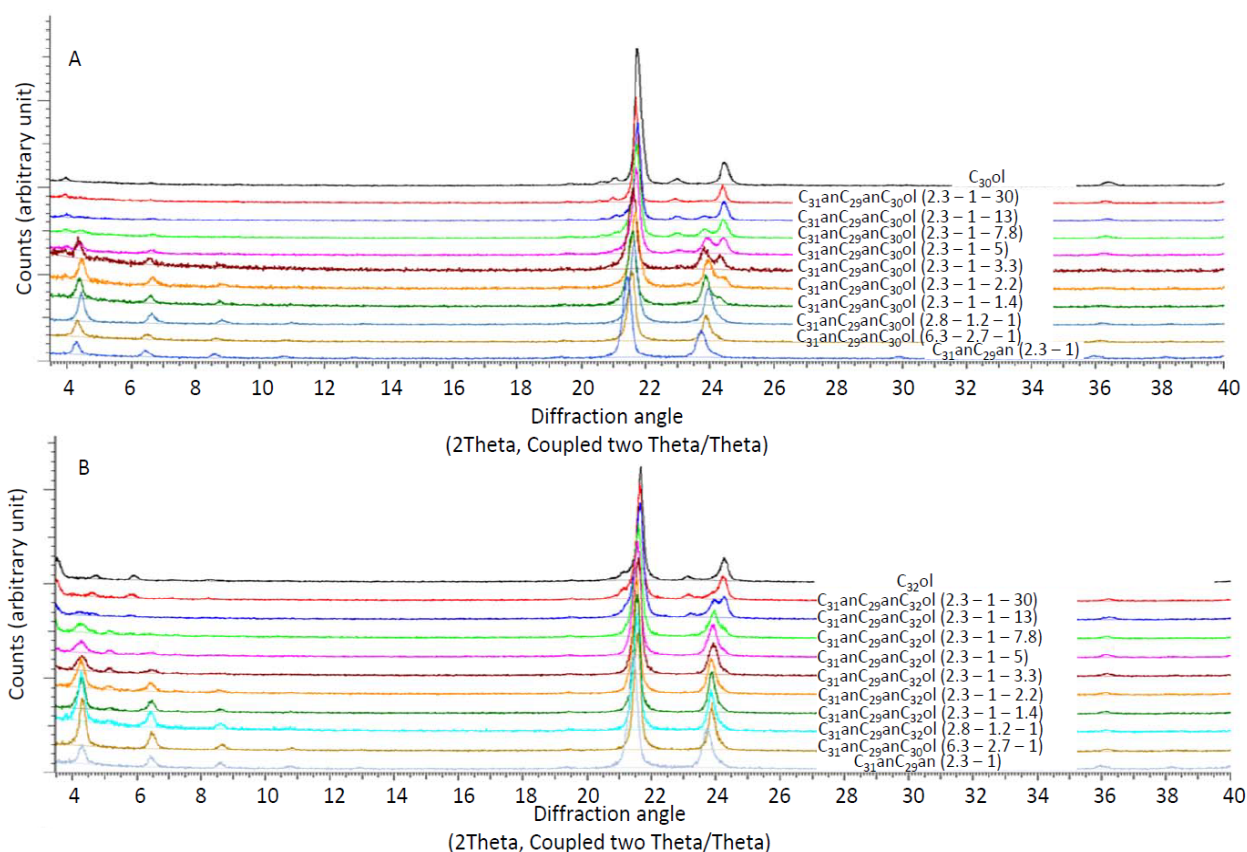
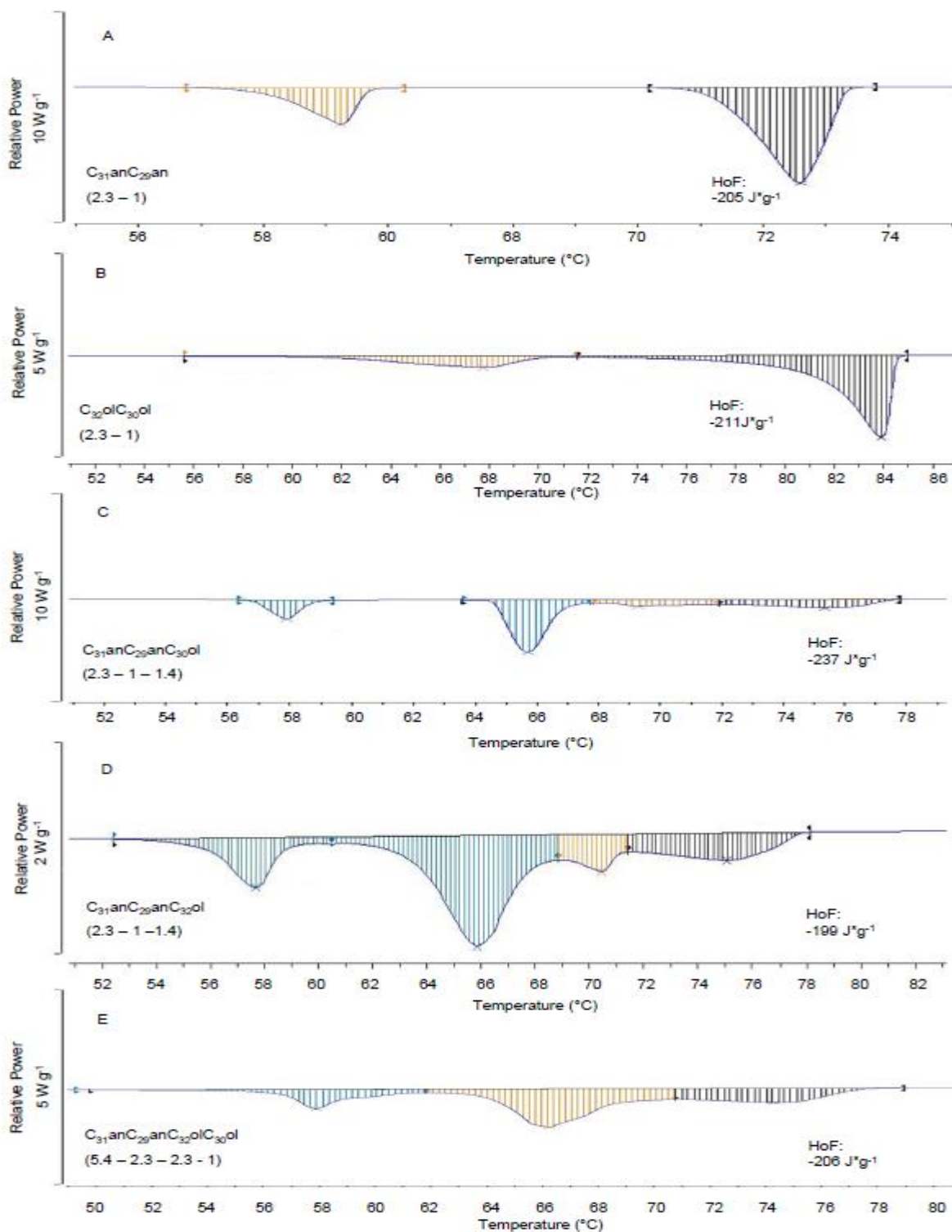Figure VI.13: Series of diffraction pattern of ternary artificial wax blends made from hentriacontane ($C_{31}an$) and nonacosane ($C_{29}an$,), dotriacontanol ($C_{32}ol$) and triacontanol ($C_{30}ol$, B). The ratio of the alkanes was kept constant to each other ($C_{31}anC_{29}an$ 2.3 - 1) and either $C_{30}ol$ (A) or $C_{32}ol$ (B) was added. The substance ratio is normalized depicted in brackets.

With increasing alcohol content, the quaternary mixtures showed a decreasing number and intensity of the peaks below an angle of 20 °. In the range between 20 ° and 25 °, all diffractograms except for the pure alcohols showed two peaks (21.6°° and 23.9 °). The pure alcohol mixture showed three peaks in this range (21.7 °, 23.1 ° and 24.3 °, figure VI.14).
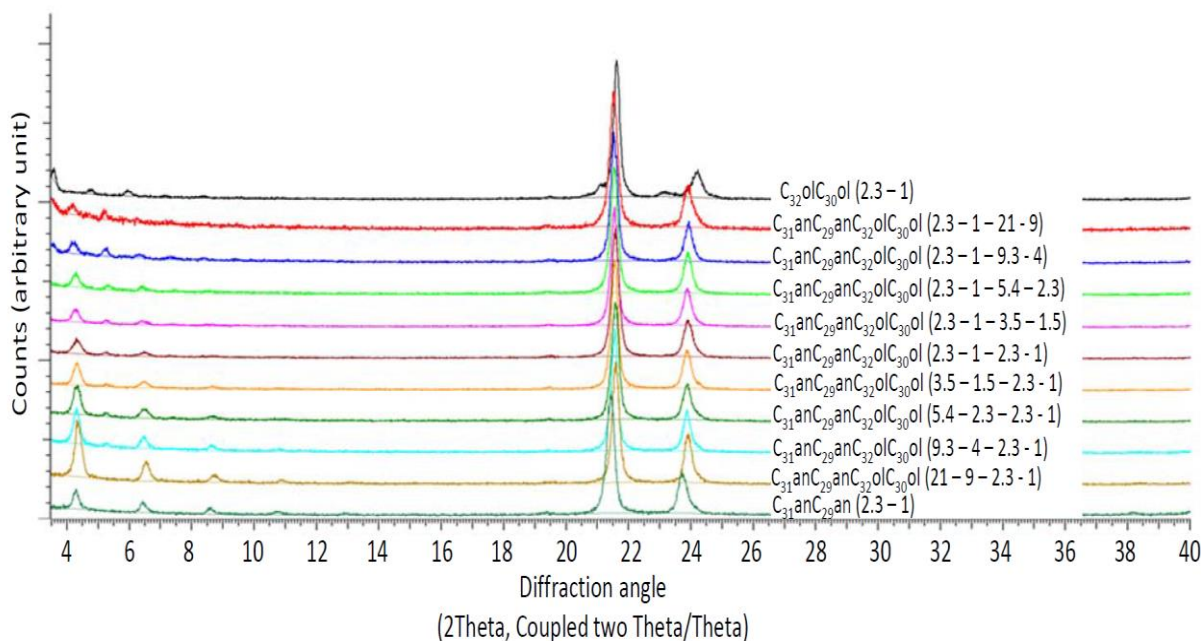
Figure VI.14: Series of diffraction pattern of quaternary artificial wax blends made from hentriacontane (C_{31}an) and nonacosane (C_{29}an,), dotriacontanol (C_{32}ol) and triacontanol (C_{30}ol, B). The ratio of the alkanes and alcohols were kept constant to each other (C_{31}anC_{29}an, C_{32}olC_{30}ol 2.3 - 1). The substance ratio is normalized depicted in brackets.

Comparing the wax blends with ratios similar to those found in the adaxial CM wax, from all mixtures (figure VI.15) the binary alkane mixture (figure VI.15 A) showed the most and the most intense signals below a diffraction angle of 18 °. The binary alcohol mixture (figure VI.15 B) showed almost no signals in this area. Two intensive peaks were found between 20 ° and 25 °. The first peak was found throughout all mixtures at 21.6 °. For the mixtures with alkanes, the second intensive peak was at an angle of 23.9 °. Only in the binary alcohol mixture, the second intensive peak was at 24.5 °, and an additional peak at 23.2 ° Above a diffraction angle of 25 ° only minor peaks can be seen. In comparison to its pure compounds (supplement figure 4 A, B), the binary alkane mixture shows fewer and less intensive peaks below 18 °. The diffractogram of the binary alcohol blend strongly resembled those of the pure compounds (supplement figure 4 C, D). Both ternary and the quaternary blend showed similar diffraction patterns with few low-intensity peaks below 20 °, high-intensity peaks at 21.6 ° and 23.9 ° and only minor peaks above a diffraction angle of 25 °. Although alcohols are present, the peak at 23.2 ° seen in the pure compounds and the binary alcohol mixture was not found.

Preparation and characterization of physical properties of an artificial wax mixture mimicking *S. elegantissima* adaxial leaf wax.
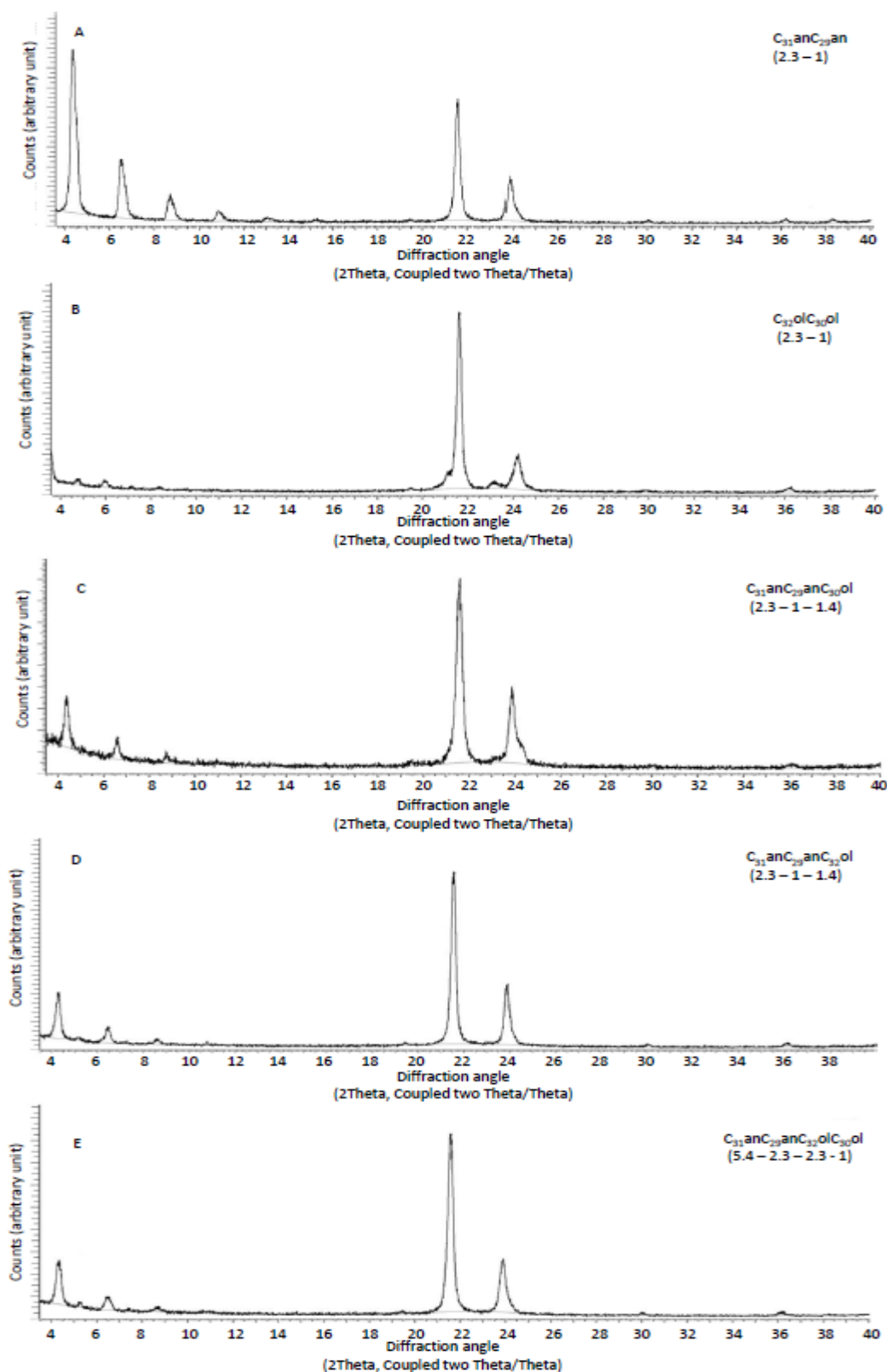
Figure VI.15: Diffraction pattern of artificial wax blends made from hentriacontane (C_{31}an) and nonacosane (C_{29}an, A), dotriacontanol (C_{32}ol) and triacontanol (C_{30}ol, B), C_{31}anC_{29}anC_{30}ol (C), C_{31}anC_{29}anC_{32}ol (D) and C_{31}anC_{29}anC_{32}olC_{30}ol (E). The substance ratio is normalized depicted in brackets.

A comparison of diffractograms of the whole leaf wax and the wax from adaxial CMs revealed remarkable differences. While both share two intensive peaks ant 21.5 ° and 23.9 °, the diffractogram of the whole leaf wax showed additional peaks below 19 ° and above 25 °, while no additional signals were found in the wax from adaxial CMs (figure VI.16).
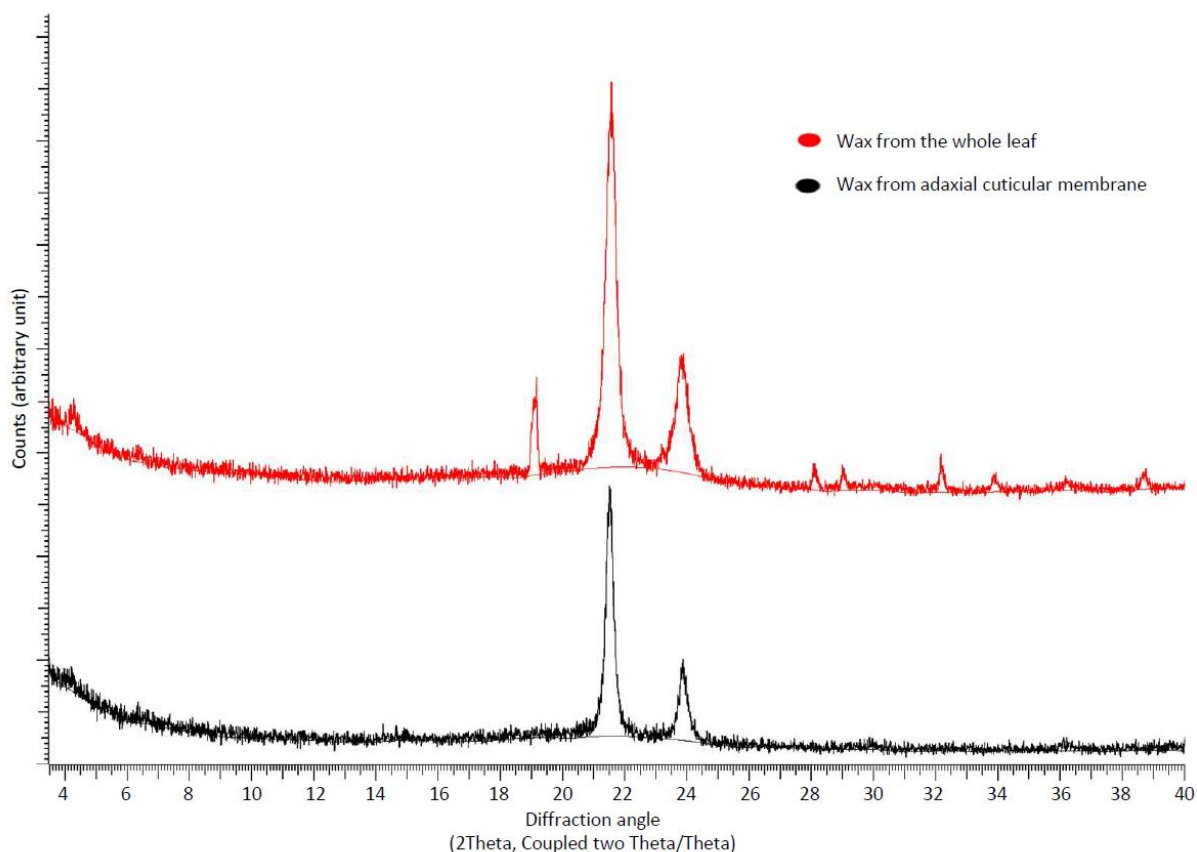
Figure VI.16: Diffraction pattern of whole leaf wax (red) and wax from the isolated adaxial leaf cuticle of *Schefflera elegantissima* (black).

The diffractogram wax from isolated adaxial leaf cuticles of *S. elegantissima* showed only two intensive peaks at a diffraction angle of 21.6 ° and 23.9 ° (figure VI.16). A comparison of the diffraction patterns of this plant wax and the artificial quaternary wax showed good congruence (figure VI.17).
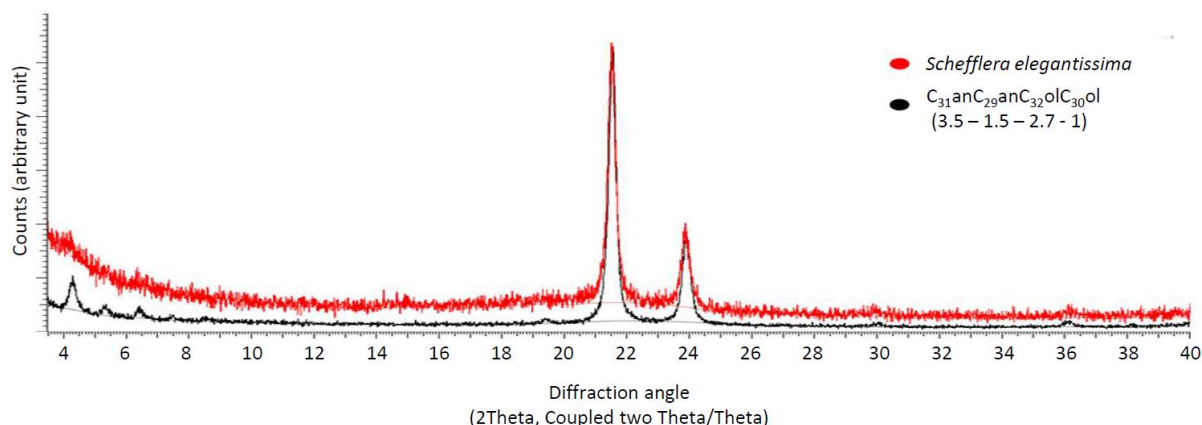
Figure VI.17: Comparison of the diffraction pattern of wax from the isolated adaxial leaf cuticle of *Schefflera elegantissima* to the artificial quaternary wax consisting of hentriacontane (C$_{31}$an), nonacosane (C$_{29}$an), dotriacontanol (C$_{32}$ol) and triacontanol (C$_{30}$ol). The substance ratio is normalized depicted in brackets.

The hot stage experiment with the binary mixture showed three different diffraction patterns (figure VI.18). Until 62 °C, the signals were like the diffractograms taken at room temperature. They showed one intensive peak at a diffraction angle of 21.6 ° and one at 23.9 ° and only minor peaks below 20 ° and above 25 °. At 63 °C, these peaks declined, and the one at 21.6 ° became a double peak between 63 °C and 66 °C. The signal at a diffraction angle of 23.9 ° started to form a shoulder ant 60 °C. Simultaneously, it began to decrease and vanished completely. At temperatures above 69 °C, no peaks were found (figure VI.18).
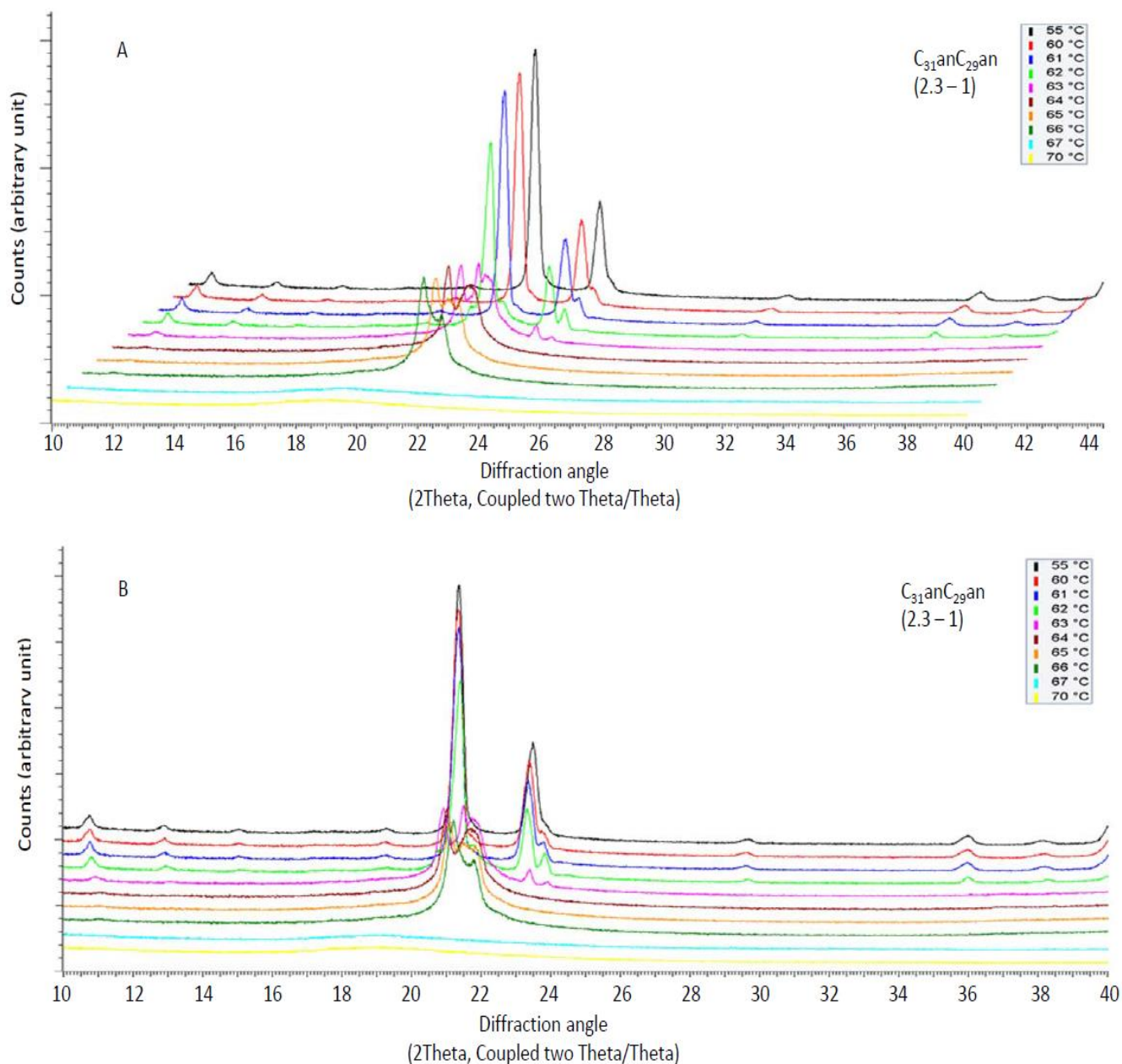
Figure VI.18: Diffraction pattern of the binary alkane blend containing hentriacontane (C$_{31}$an) and nonacosane (C$_{29}$an) at different temperatures. The substance ratio is normalized depicted in brackets. The lowest temperature is at the back and the highest in front. In the diffractograms, an offset on the X and Y axis (A) and only on the Y-axis (B) was given for clarity reasons. The X-axis belongs to the pattern in front with the highest temperature.

The quaternary blend showed different crystalline behaviour upon heating (figure VI.19). Until a temperature of 56 °C, the diffractograms were like those taken at room temperature. They showed two intensive peaks at 21.5 ° and 23.9 ° and only minor signals below 20 ° and above 25 °. Between 58 °C and 62 °C the peak at 21.5 °

declined, resulting in a peak broadened with a shoulder. It stayed constant until 66 °C. At this temperature, a decline set in, and a double peak was formed. The signal vanishes entirely above 77 °C. The signal at 23.9 ° started to decline at 58 °C and disappeared completely at 67 °C. Above 67 °C, a broad signal ranging from diffraction angles of 15 ° to 25 ° can be seen.
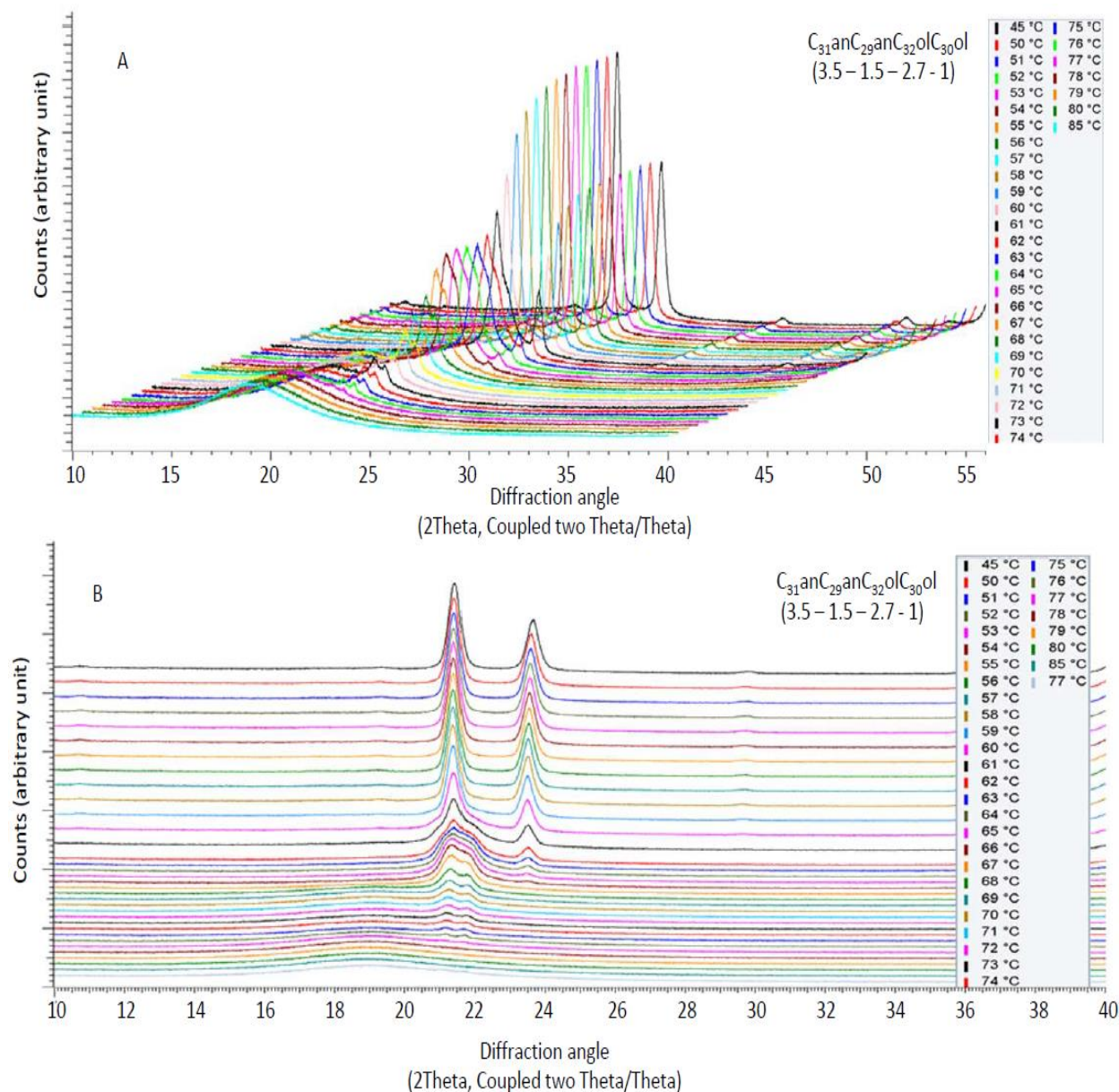
Figure VI.19: Diffraction pattern of the artificial quaternary wax consisting of hentriacontane (C_{31}an), nonacosane (C_{29}an), dotriacontanol (C_{32}ol) and triacontanol (C_{30}ol) at different temperatures. The substance ratio is normalized depicted in brackets. The lowest temperature is at the back and the highest in front. In the diffractograms, an offset on the X and Y axis (A) and only on the Y-axis (B) was given for clarity reasons. The X-axis belongs to the pattern in front with the highest temperature.

The diffractograms of whole leaf wax of *S. elegantissima* (figure VI.20) showed one additional minor double peak at 19.0 °, and several small peaks above a diffraction angle of 25 ° over the whole investigated temperature range. The intensive peaks at 21.5 ° and 23.9 ° stayed constant until 67 °C, then slowly decreased and vanished completely at a temperature of 76°.
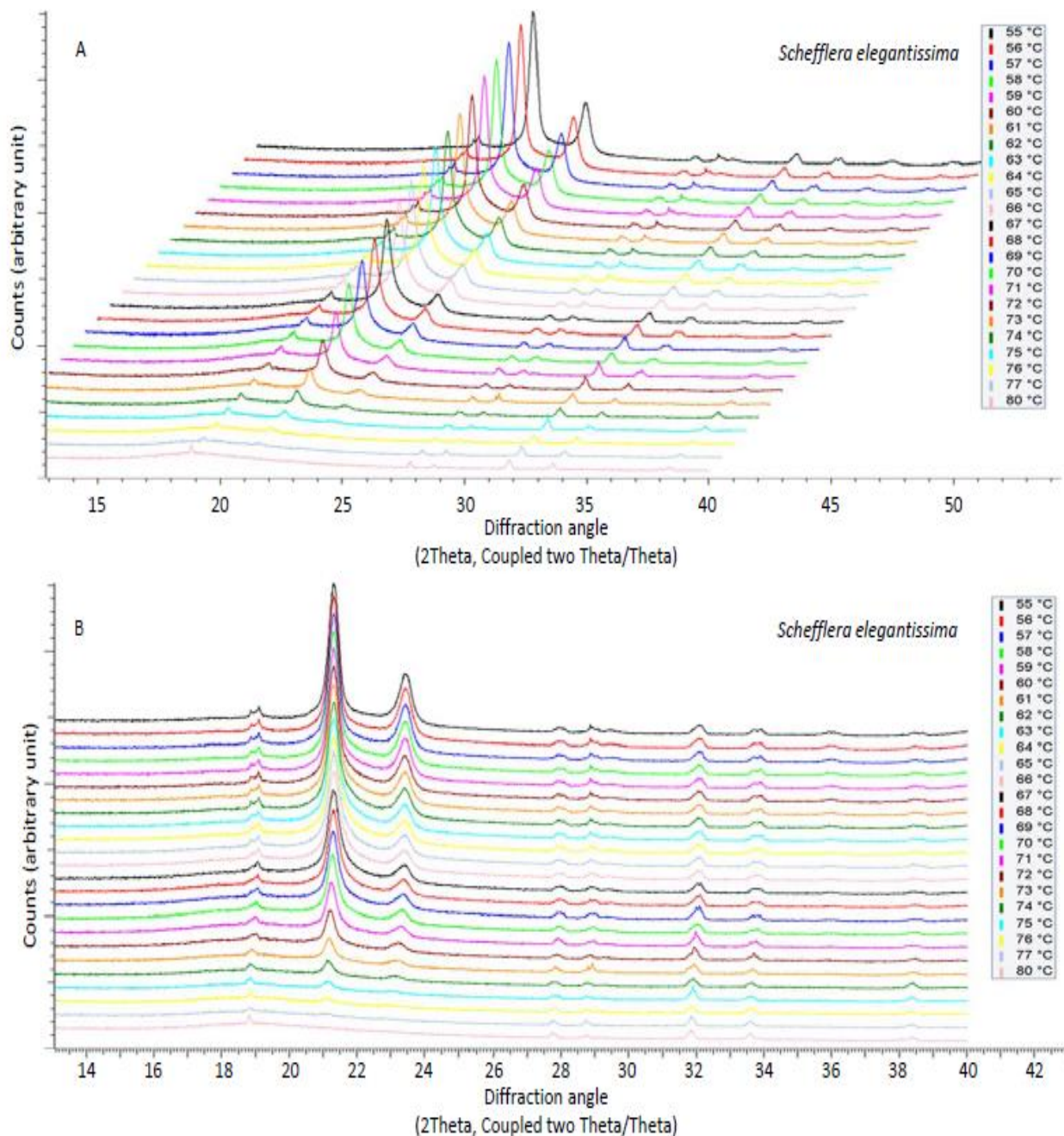
Figure VI.20: Diffraction pattern of whole leaf wax of *Schefflera elegantissima*. The lowest temperature is at the back and the highest in front. In the diffractograms, an offset on the X and Y axis (A) and only on the Y-axis (B) was given for clarity reasons. The X-axis belongs to the pattern in front with the highest temperature.

VI.4 Discussion

This project aimed to create an artificial wax blend from commercially available compounds, which mimics the thermal and crystalline properties of the VLCA fraction of leaf wax of *S. elegantissima* sufficiently. This fraction was shown to constitute the uptake barrier for active ingredients, used in agriculture (Staiger et al. 2019b) and in the first project, its water permeability barrier feature was shown. The investigation of the barriers physical properties was challenging for different reasons. For instance, the accumulation of a pure adaxial cuticular wax sample is extremely time-consuming and material-intensive due to the CM isolation and extraction process. Some techniques to investigate physical properties like DSC or hot stage XRD need rather high amounts of wax to provide reliable results. Moreover, not all plant species are suitable for this research. For example, not all cuticles can be isolated from the leaf. Therefore, a standardized wax blend to investigate the uptake of active ingredients can be beneficial. Another reason to develop such a blend lays within agriculturally used formulations. In agriculture, active ingredients are usually not used alone, but together with adjuvants in a formulation to maximize their effect. Adjuvants influence the behaviour of the mixture on the leaf. Amongst others, they can enhance the uptake into the plant (Burghardt et al. 1998; Schreiber et al. 1996b). Although it is known that some adjuvants act as a wax plasticizer, the mode of action of many adjuvants is still unknown (Burghardt et al. 1998). Therefore, an easily available artificial wax mixture can improve the availability of material-intensive methods like XRD or DSC to investigate effect mechanisms of adjuvants. Another application for agricultural studies could be the development of a fast screening routine to determine diffusion coefficients. To determine this parameter, a method to simulate foliar uptake is used, where CMs are mounted into a chamber and solutes and adjuvants are applied as small droplets to the outer surfaces of the CM (Schönherr and Baur 1994; Arand et al. 2018). With an artificial wax blend, the development of a fast screening method using FTIR methods could complement this procedure.

To develop such a wax mixture, a target plant wax was needed. The wax of adaxial CMs of *S. elegantissima* offered enough advantages to choose it. Since VLCAs have been shown to constitute the uptake barrier for organic substances, the artificial wax should consist only of these compounds (Staiger et al. 2019b). The cuticular wax of *S.*

elegantissima consisted almost completely of VLCAs, and only small amounts of TRPs were found (figure VI.1). A more thorough investigation into the contained substance classes, showed alkanes to be dominant, followed by alcohols, aldehydes and alkyl acids. Benzylic acid esters were found only in meager amounts (figure VI.2). A more detailed view of the chain length distribution revealed four major chain lengths with a carbon number between 29 and 32 (figure VI.3). Chains with 29 and 31 carbons were dominated by alkanes, while the chains with 30 and 32 carbons were dominated by alcohols (table VI.1). Jetter and Riederer (2016) and Zeisler-Diehl et al. (2018) showed for plants with and without epicuticular wax crystals that the water permeation barrier was made up by the intracuticular waxes. Therefore, a target plant without crystalline structures would be beneficial for this investigation. SEM studies revealed the surface to be encrusted but showed no signs of epicuticular wax crystals (figure VI.4), further profiling *S. elegantissima* as target plant. However, the isolation of membranes was time-consuming, and the species was found too late to gain sufficient amounts of pure adaxial CM wax to conduct DSC and hot stage XRD experiments since their schedule couldn´t be changed. Therefore, whole-leaf extracts were prepared to gain enough plant wax for the experiments. However, the comparison of the two sample types shows differences. The whole leaf extracts show a significantly lower total cuticular wax load than extracts of the adaxial CMs (figure VI.1). The whole leaf extracts contained less TRPS (only about 0.1 %), a higher proportion of alkanes (about 90 %). Still, a lower proportion of alcohols (about 2 %) and its chain length distribution was dominated by the carbon chain lengths 31 and 29 (figure VI.3). In comparison, the CM extract contained a slightly higher amount of TRPs (about 6 %), a lower proportion of alkanes (about 54 %), but a higher proportion of alcohols (about 23 %). Its chain length distribution was dominated by the carbon chain lengths 31 and 32, but higher amounts of substances with a chain length of 29 and 30 were found. These differences might be explained by two reasons. The cuticular wax load and composition of adaxial and abaxial leaf sides have been shown to differ (Ringelmann et al. 2009; Tulloch 1973; Buschhaus and Jetter 2011). The wax load found on whole leaf extracts was a bit less than half of the adaxial cuticular wax load. It has been shown, that wax load can change strongly, depending on leaf age (Hauke and Schreiber 1998). Due to a tight schedule, it was not possible to ensure the same age of the harvested leaves compared those

used to obtain CMs. Nevertheless, care was taken to only use mature leaves. Considering this, smaller total wax load and change in the composition of the whole leaf extracts compared to the extracts of isolated adaxial extracts could result from different reasons, including a smaller abaxial wax load and different composition, enriched on alkanes and deprived of alcohols (figure IV.2). Considering the obtained whole leaf wax composition, this could indicate lower overall wax amount with a higher fraction of alkanes, less oxygen-containing VLCAs and less TRPs in the abaxial wax of *S.* elegantissima leaves. To resolve the composition question of the abaxial side of the leaf wax analysis were intended. However, from the isolation used to produce the adaxial CM wax for this experiments, no abaxial CMs were kept and due to the time demanding process was the isolation of new CMs not finished. Therefore, it was not possible to conduct a wax analysis on pure abaxial wax samples. Another process influencing the results of experiments with cuticular wax is the extraction method. In terms of this work, dispersing whole leaves in TCM contained the possibility to solve impurities from within the leave. Therefore, the minimisation of possible impurities in the wax sample was prioritised. Although the extraction was done very carefully, TCM could still penetrate through possibly opened stomata, unseen cracks in the cuticle or through the cuticle itself and solve substance from within the leaf, influencing the result of the experiments. These impurities became visible in a preliminary experiment. After the DSC measurement of a whole leaf wax sample with an added adjuvant, two fractions were visible. One white waxy fraction and a dark green one. This separation was also seen in samples without adjuvants, but only to such a minor degree that a separation from the green substances was hardly possible. These two fractions were separated, and an XRD measurement was conducted separately. A comparison of the XRD diffractogram exhibited that peaks additional to those indicating the orthorhombic crystal structure (peaks at 21.5 ° and 23.9 °) could be assigned to the dark green material, thus indicating this material as impurities from the leaf inside (supplement figure 1). In a subsequent measurement of adaxial CM wax confirmed this indication since only the peaks indicating the orthorhombic crystal structure were found (figure VI.16). Despite the found impurities, this leaf dipping method was shown to deliver better results compared to other methods, making it a solid choice to obtain larger wax amounts sufficiently (Stammitti et al. 1996). Staiger (2019a) analysed whole leaf wax

from *S. elegantissima* and found some consent trends. She showed the adaxial CM and whole leaf wax to consist mostly of VLCAs, dominated by alkanes. She found a higher proportion of oxygen-containing VLCAs, mostly alcohols, in the adaxial CM wax. In addition, her whole leaf extracts exhibited C_{29}an and C_{31}an to be the dominant VLCA species. In her CM wax, she found C_{29}an, C_{31}an, C_{30}ol and C_{32}ol as the dominant VLCA species. Furthermore, the total wax load was higher in the CM wax than in the whole leaf wax, and only minor amounts of TRPs were found (Staiger 2019a). The total wax loads of whole leaf extracts were in a similar range. Nonetheless, some differences could also be found. The composition differed slightly for minor compounds, and C_{32}ol was not as abundant as in the presented data. The biggest distinction lied in the total wax amount of the adaxial CM wax. Staiger (2019a) found a total cuticular wax load of 6.8 µg cm^{-2} (6.8 – 6.9 µg cm^{-2}). To put these differences in perspective, an analysis of plants from which leaves were sampled had to be considered. It has been shown that environmental stresses can alter the cuticular wax composition (Tulloch 1973; Baker 1974; Geyer and Schönherr 1990; Riederer and Schneider 1990). In this work, the leaves were sampled from an older plant, grown for several years in the botanical garden next to different plants in the same pot and was more prone to be exposed to environmental stresses. The plants Staiger (2019a) used were newly from a plant dealer obtained, young and were grown in a pot each in a publicly non-accessible greenhouse, thus making them less prone to environmental stress. Considering the differences in the growing conditions and the age gap of the sampled plants, the found distinctions in this work and the work of Staiger (2019a) were not unexpected. Despite differences within the composition of the adaxial CM and whole leaf waxes, both, the whole leaf wax and the adaxial CM wax were dominated by alkanes (C_{31}an and C_{29}an). Although the whole leaf wax showed a higher ratio of C_{31}an and C_{29}an, the thermogram showed differences to its artificial counterparts (figure VI.9 A, figure VI.10, figure VI.11 A). The differences in the diffractograms of whole leaf wax and adaxial CM wax were presumably explainable by impurities due to the extraction method (figure VI.16, supplement figure 1). Therefore, it was assumed, that the whole leaf wax could be used in DSC and hot stage XRD experiments as a valid proxy to the adaxial CM wax. However, a repetition of the experiments with pure adaxial CM wax deemed desirable.The results of the analysis

of the adaxial CM wax depicted a simple plant wax as a good target wax for this project (figure VI.1, figure VI.2, figure VI.3). There were more plant species available like *H. helix* or *Z. zamiifolia* also had cuticular waxes, majorly made from VLCAs (figure VI.1). However, they showed more distinct features regarding their chain length distribution or wax composition and also had a smaller wax load (figure V.1; figure V.3; figure VI.1, figure VI.3 supplement table 1, supplement table 3). For these reasons, they were discarded as possible target waxes for this project.

FTIR experiments were conducted using pure wax from adaxial CMs. Merk et al. (1997) investigated the melting behaviour of *Hedera helix* L. and *Juglans regia* L. using FTIR spectroscopy. They monitored the peak wavenumber of the asymmetric and the symmetric stretching modes and found a shift with rising temperature. This shift was caused by an increase in the number of gauche conformers, indicating a disorder enhancement of alkyl chains (Merk et al. 1997; Blume 1996). This shift was also present in *S. elegantissima* (figure VI.6) Both stretching oscillation showed a gradually magnifying increase in wavenumber between 20 °C and 88 °C. For paraffin waxes a transition from the orthorhombic to a hexagonal phase before melting was reported (Edwards 1957; Flaherty 1971). This transition was not observed. The spectra showed a double peak at 720 cm^{-1} and 1470 cm^{-1}, both indicative for the orthorhombic lattice (Chapman 1955; Bernays et al. 1976). Both showed similar behaviour upon heating. However, for evaluation purpose, the former was used since water absorbance bands could interfere with the double peak at the higher wavenumbers (Merk et al. 1997). The degree of crystallinity was calculated after a method of Zerbi et al. (1989). Below a temperature of 40 °C, around 80 % of the wax was crystalline (figure VI.8). At higher temperatures, the crystallinity dropped slowly. Above 58 °C, the indicative double peak vanished. This could be the result of an interplay of decreasing intensity of the 730 cm^{-1} band and increased bandwidths. Both were shown on leaves of *H. helix* by Merk et al. (1997). They also found the 730 cm^{-1} band in *H. helix* leaves to disappear before the melting process according to shift in wavenumber of symmetric and asymmetric oscillation was finished. These findings fit together with the beginning of the melting of the binary alkane, the ternary and the quaternary mixtures as seen from the asymmetric and symmetric oscillation. However, orthorhombic crystallinity vanished at lower temperatures than the melting behaviour would suggest. This could be a hint at

a transition into another crystal lattice before melting. The reason could be the high number of compounds and the chain length distribution of the plant wax. This transition could be broadened in a way, in which no sharp shift with a subsequent steady wavenumber level but an accelerating increase before the melting shift could be observed (figure VI.6). In the thermogram of the whole leaf wax, an endothermic transition consisting of three strongly overlaying signals were found. The peak at the highest Temperature (figure VI.10) goes well with the melting, determined by FTIR (figure VI.6), leaving two peaks at lower temperatures. These peaks indicate phase transitions, probably from the orthorhombic too the hexagonal lattice, before melting (Basson and Reynhardt 1991; Reynhardt and Riederer 1994). For the XRD measurements at room temperature wax from adaxial CMs were used. In the diffractogram only two peaks, one at an angle of 21.5 ° and one at 23.9 ° were found (figure VI.17). While investigating Fischer-Tropsch waxes, Reynhardt (1986) showed these signals to indicate the orthorhombic crystal lattice. Wax from different plant species were shown to also have fractions with this lattice (Reynhardt and Riederer 1991, 1994). Taking the results from the FTIR experiments into account, the orthorhombic crystal lattice of the *S. elegantissima* adaxial CM wax becomes apparent. The hot stage XRD experiments were conducted using the wax of the whole leaf, since the necessary sample amount was quite high. A comparison to the XRD at room temperature, which was made using wax from adaxial CMs, revealed additional peaks below a diffraction angle of 20 ° and above 25° over the whole temperature range in the whole leaf wax (figure VI.20). These peaks even persist at temperatures above the melting temperature obtained using FTIR (figure VI.20) and DSC (figure VI.10). As discussed above, these peaks occurred due to extracted impurities from within the leave and therefore could be neglected for the analysis of the wax. Reynhardt and Riederer (1994) and Merk et al. (1997) showed cuticular waxes to do the transition from orthorhombic to a hexagonal crystal lattice. The DSC indicates solid-solid transitions within the whole leaf wax before melting. This wasn´t seen in the hot stage XRD. Therefore, any possible signal for a hexagonal lattice, in the form of peak splitting of the peak at 21.5 ° and a fast decrease of the peak at 23.9 °, could be overlain by signals from impurities. Another explanation could be an influence of the impurities on the wax crystal lattice, which inhibited the formation of a hexagonal phase. However,

the loss of these signals corresponded well with the melting temperatures seen in FTIR and DSC. A repeating of the DSC and hot stage XRD experiments deem highly interesting in future when enough amount of a purer sample could be obtained.

Alkanes constitute the major compound class of *S. elegantissima* wax. Since alkanes were the simplest VLCAs in this plant wax mixture, a binary blend ($C_{31}anC_{29}an$) with the most abundant alkanes posed a good starting point for the development of an artificial wax. For binary alkane mixtures, a solid-solid transition was found below the melting temperature (figure VI.11 A). At ambient temperature odd-numbered paraffin waxes and binary alkane blends were shown to have the orthorhombic lattice and to turn into a hexagonal one before melting (Basson and Reynhardt 1991; Edwards 1957). This aligned well with signal 1 of the plotted phase diagrams (figure VI.11 A). This finding was underlined by results from FTIR and XRD experiments. At lower temperatures, the FTIR spectra (supplement figure 5) of alkane blends ($C_{31}anC_{29}an$ 2.3 - 1) showed a double peak at 720 cm^{-1} and 1470 cm^{-1} both indicative for the orthorhombic lattice (Chapman 1955; Bernays et al. 1976). The peaks at 21.6 ° and 23.9 ° in the diffractograms confirmed this assignment (figure VI.12 A). Above 59 °C, a small wavenumber shift of the asymmetric and symmetric bands was found and the hot stage XRD showed a peak splitting for the signal at 21.6 ° and the vanishing of the peak at 23.9 °. Both were indicative for the hexagonal crystal lattice (Basson and Reynhardt 1991; Merk et al. 1997). The change from an orthorhombic to a hexagonal crystal structure was also seen in the hot stage XRD experiment (figure VI.18). Tashiro et al. (1996) investigated the transition from an orthorhombic to a hexagonal crystal structure in polyethene. Their descriptions were very similar to the presented results, undergirding their validity (Tashiro et al. 1996). A comparison of the binary alkane mixture ($C_{31}anC_{29}an$ 2.3 - 1) and the leaf wax showed major differences between them in all used methods. In FTIR and hot stage XRD experiments, solid-solid transitions were found in the artificial blend, whereas the leaf wax showed none explicitly. The thermogram of the alkane blend showed two separated peaks, while the one of the leaf wax showed three overlapping signals. Despite all differences, these two compounds constitute more than half of all wax compounds and since alkanes were the simplest VLCAs this mixture posed a good starting point for the development of an artificial wax blend with similar properties than *S. elegantissima* leaf wax.

The second biggest compound class in the leaf wax were alcohols, with the most abundant compounds C_{32}ol and C_{30}ol. With the exception of pure C_{30}ol, all alcohol wax samples showed a solid-solid transition below their melting temperature (figure VI.11 B). For C_{30}ol, the transition was only visible during the cooling process (supplement figure 3). At room temperature, XRD measurements (figure VI.1, figure VI.12 B) indicated monoclinic crystal lattice for pure alcohols and investigated alcohol waxes and blends (Valoppi et al. 2016). Valoppi et al. (2016) investigated the crystallization behaviour of alcohols in peanut oil and found them to crystallize in monoclinic form above a content threshold of 30 %. Therefore, it can be presumed for the blends of two alcohols with only the minor difference of two methylene groups to crystallize in this form too. Upon heating the waxes underwent a transition (figure VI.11 B signal 1) from a monoclinic to a hexagonal structure (Tasumi et al. 1964; Cholakova and Denkov 2019). Although existing in significant amounts in the plant wax, thermogram, diffractogram and FTIR spectra of the C_{32}olC_{30}ol wax blend (ratio 2.3 - 1) differed strongly from those of the plant wax mixture.

To approach the composition of *S. elegantissima* adaxial CM wax, C_{30}ol or C_{32}ol were added to the binary alkane blend (C_{31}anC_{29}an 2.3 - 1) to form ternary wax blends. The alkane mixture was chosen to closely reflect the alkane composition of the leaf wax (figure VI.3; table VI.1). The introduction of an alcohol increased the complexity of the phase diagram tremendously. With one signal indicating the melting of the sample, in thermograms of binary wax mixtures usually two signals were found. By contrast ternary mixtures showed up to 4 signals. The melting (figure VI.11 C, D) signified the point where the whole sample became liquid. In the mixture with C_{32}ol, signal 1 was found continuously above an alcohol concentration of 30 mol%. This indicated a connection of this solid-solid transition to this fraction of the wax. For the pure alcohol it was assigned to the transition from the monoclinic to the hexagonal crystal structure (Valoppi et al. 2016; Tasumi et al. 1964; Cholakova and Denkov 2019). Valoppi et al. (2016) showed alcohols in peanut oil to form a monoclinic crystals structure above a fraction threshold of 30 %. Therefore, it was plausible to assign signal 1 to this transition as well. In the blends with C_{30}ol, signal 1 was found in mixtures with an alcohol content of 30, 40, 60 and 70 mol%. However, for 50 mol%, 80 mol%, 90 mol% and the pure C_{30}ol in the cooling an additional peak was found in a similar temperature

range than signal 1 (supplement figure 3). Tasumi et al. (1964) found for alcohols with 28 and 32 carbons no solid-solid transition while heating the sample, but while cooling them down. They were also assigned to the transition from a monoclinic to a hexagonal crystal lattice (Tasumi et al. 1964). Therefore, a similar case can be assumed here. Due to the behaviour of signal 1 with varying alcohol content, an exclusive or at least major impact of the alcohol fraction could be assumed. Signal 3 was not found for high concentrations (above 80 mol% C_{32}ol) or pure alcohols (C_{30}ol, C_{32}ol). In the binary alkane mixture (C_{31}anC_{29}an 2.3 - 1) this signal was assigned to the transition of an orthorhombic to a hexagonal crystal lattice. Judging from the location and progression this could also be the case here. It could also suggest an exclusive or at least major impact of the alkane fraction of the wax. The according XRD measurements showed the formation of new peaks with increasing alcohol content, indicated the coexistence of two different crystalline structures (figure VI.13). In contrast to signal 1 and 3, which could be related to a separate alkane or alcohol phase, signal 2 was found over a broad range of alkane-alcohol mixtures, but not in the pure alkanes or alcohols. Thus, prompting an interaction of the two fractions. The phase diagram received from DSC data and the XRD diffractogram hinted at a system with three phases. One phase dominated by alkanes (figure VI.11 C, D signal 3), one dominated by alcohols (figure VI.11 C, D signal 1) and one mixed phase (figure VI.11 C, D signal 2). XRD measurements showed diffractions for two different crystal structures (figure VI.13), undergirding this theory. In the FTIR spectra of C_{31}anC_{29}anC_{30}ol (2.3 - 1 - 1.4) three separable wavenumber shifts were found, fitting well with the transitions found in the phase diagram further strengthening this assumption. Multicomponent alkane mixtures have been shown to seize an orthorhombic crystal structure (Dirand et al. 1998; Dirand et al. 2002). Signal 2 already occurred at high alkane concentrations and showed rather small changes with increasing alcohol content. This behaviour prompted this intermixed phase to also have an orthorhombic structure, explaining only two observed structures in the diffractograms. Overall, the ternary wax mixture showed more similarity to the plant wax than the binary blends. The FTIR wavenumber shifts (figure VI.5 C, D) were broader compared to the behaviour of the binary mixtures and the behaviour showed more resemblance to the plant wax. The thermograms started to show overlapping peaks, like the target wax. However, more transitions were found.

At high alcohol contents, the diffractograms indicated the formation of a system with two distinct phases with different crystal structures. However, in blends with lower alcohol content, they showed only signals for the orthorhombic lattice, like the *S. elegantissima* wax. The transition from a binary system consisting of alkanes to a ternary system consisting of two alkanes and one alcohol implicated a gain in complexity in the blends structure, most visible in their phase diagrams (figure VI.11 C, D). Nonetheless, this step allowed the assignment of different signals thermo- and diffractograms to different wax fractions. It proved to be a valuable first step towards the preparation of an artificial wax blend with similar properties than the *S. elegantissima* wax.

At room temperature, the plant wax took the orthorhombic crystal lattice and upon heating DSC indicated solid-solid transitions before melting, hinting at a change in the crystal lattice. However, this was not confirmed by hot stage XRD. In contrast to the ternary mixtures, which mostly appeared to consist of two separate phases, the plant wax appeared to form only one phase (figure VI.13, figure VI.20). However, the signals were strongly broadened, presumably due to the chain length distribution and the presence of various compound classes.

The investigation of quaternary system usually involves a high number of measurements to cover a broad range of compositions. To simplify this procedure, the ratio $C_{31}an$ $C_{29}an$ and $C_{32}ol$ $C_{30}ol$ was kept constant (2.3 - 1), to display the ratios within the plant wax and only the ratio of the mixtures was changed. The phase diagram showed some similarities to those of the ternary blends (figure VI.11 E). Besides the melting signal up to three signals were found. Signal 1 appeared above an alcohol content of 20 mol%. Like the ternary blends, a connection to the alcoholic wax fraction could be assumed. However, the diffractograms didn´t show signs of a monoclinic phase, only for an orthorhombic crystal lattice (figure VI.14). The phase diagram of the binary alcohol mixture showed continuous miscibility of the two alcohols and the phase diagrams of the ternary mixtures indicated an at least partial separation into an alkane and alcohol phase. Throughout all quaternary mixtures, the fraction of the $C_{30}ol$ was always below 30 mol%. Therefore, it would seize the orthorhombic crystal structure (Valoppi et al. 2016). Since it formed a solid solution with $C_{32}ol$, together with the present orthorhombic alkane fraction, this could induce the alcohol fraction to seize the

orthorhombic and not monoclinic crystal structure. For signal 3, as described for the ternary blends, a connection to the alkane fraction could be prompted (figure VI.11 E). Since diffractograms showed orthorhombic crystallinity throughout all compositions, signal 1 and 3 depicted a transition from the orthorhombic to the hexagonal crystal lattice (Tasumi et al. 1964; Cholakova and Denkov 2019; Basson and Reynhardt 1991; Edwards 1957). For comparison with the *S. elegantissima* plant wax, the blend with a similar composition was chosen ($C_{31}an C_{29}an C_{32}ol C_{30}ol$ 5.4 - 2.3 - 2.3 - 1, translating to 30 mol% of alcohol mixture in figure VI.11 E). A direct comparison of the thermograms showed good comparability (figure VI.10). They both showed three overlapping peaks in a similar temperature range. However, the plant wax thermogram seemed to have less distinct signals than the artificial wax mixture. This might have occurred due to the difference in wax composition. The artificial wax covered with the four major compounds roughly two thirds of the composition of the plant wax, thus ignoring minor constituents making up the last third. Therefore, differences to some degree were to be expected. Another difference was the HoF. Since the whole leaf extract was used for these experiments, it had to be assumed, that the wax was contaminated with substance from within the leaf. This could change the uptake capability of the wax, leading to the difference in HoF. Despite these minor and explainable differences, the thermogram hinted this artificial wax blend to be a good proxy to the plant wax. A more thorough look into the thermograms of artificial wax blends revealed the first signal of the quaternary wax blend to match nicely with the solid-solid transition of the binary alkane mixture (figure VI.21). The second peak overlaps strongly with the melting of the alkane mixture and the phase transition of the alcohol blend (figure VI.21). This was also indicated by the phase diagram. In the diagram the signal 1, which indicated the phase transition of the alcohol fraction overlapped with the melting interval (figure VI.11). This could be due to the formation of a separated alcohol and alkane phase. While the alcohol phase was still solid, the alkane phase already liquefied. The third peak, after which the quaternary mixture was completely liquefied, did not match to the melting of the alcohol fraction and occurred at lower temperatures. An explanation therefore could be the already molten alkanes. They could act like a solvent and dissolved the alcohols, leading to the early liquefaction.
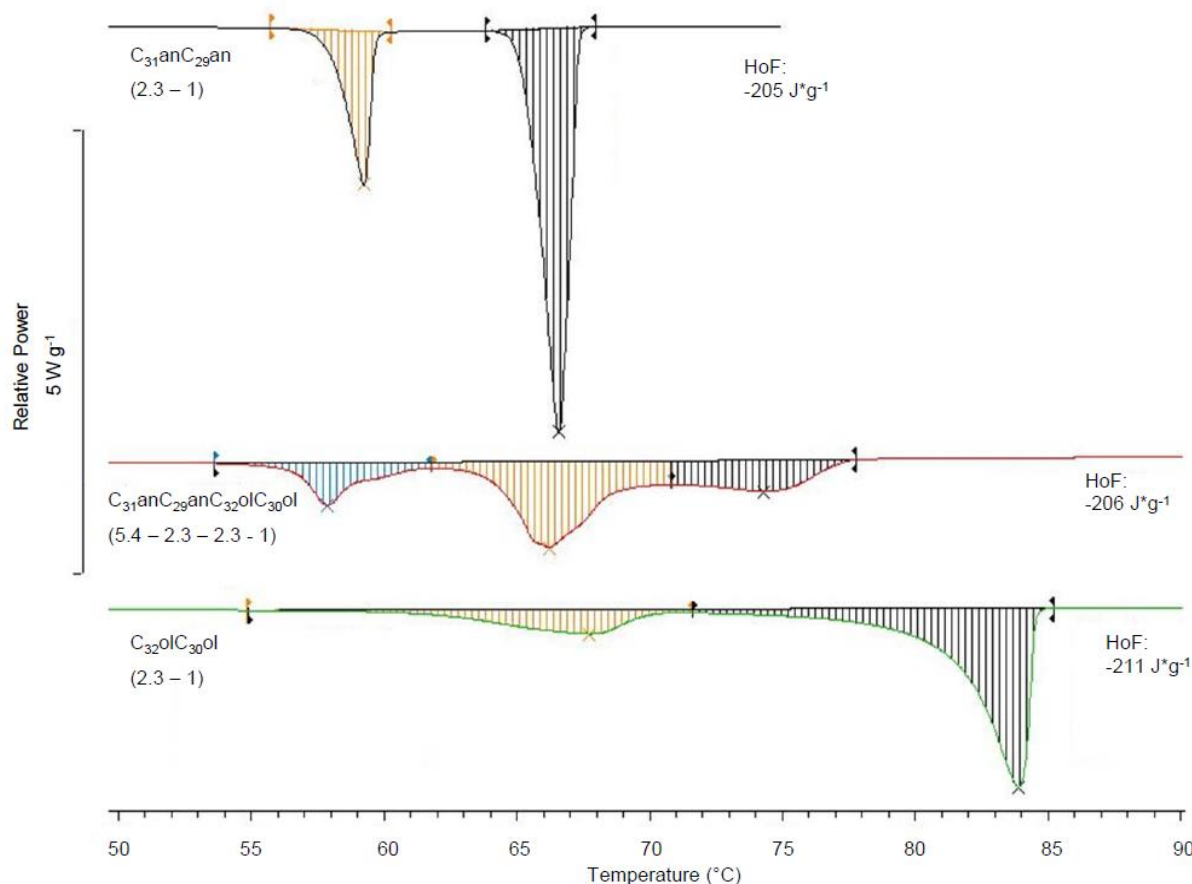
Figure VI.21: Comparison of the binary alkane mixture made of hentriacontane (C$_{31}$an) and nonacosane (C$_{29}$an; 2.3 - 1; top), binary alcohol mixture made of dotriacontanol (C$_{32}$ol) and triacontanol (C$_{30}$ol); 2.3 -1; bottom) and quaternary mixture C$_{31}$anC$_{29}$anC$_{32}$olC$_{30}$ol (3.5 - 1.5 - 2.7 - 1; middle). The substance ratio is normalized depicted in brackets. Total Heat of fusion (HoF) was calculated to energy emission or uptake with temperature change. Negative values signify uptake. (n = 1)

The hot stage XRD experiments undergirded this thesis. When the orthorhombic system of an alkane mixture changed into a hexagonal lattice, the peak at 21.5 ° decreased and split into two, while the peak at 23.9 ° vanished (figure VI.19). The same happened for the alcohol blends from a monoclinic into a hexagonal system, however at a higher temperature. The presumably separated alkane and alcohol phase of the quaternary wax underwent this transition at different temperatures. This resulted in a broad peak with a shoulder at a diffraction angle of 21.5 °, where the signal was indicating a presumably orthorhombic lattice of the alcohol fraction overlaid with the signals for the hexagonal crystal structure of the alkanes. Since the alcohols were not in a hexagonal lattice yet, did the peak at 23.9 ° vanish at higher temperatures. An indicator of the orthorhombic lattice was the peak at 23.9 °, which vanished above

68 °C, a temperature, where the alcohols were shown to undergo the transition to the hexagonal lattice (figure VI.11). In the hot stage diffractogram of the binary alkane mixture, it vanished instantly after the transition at 63 °C (figure VI.18). In the hot stage diffractogram of the quaternary blend, a split peak above 69 °C was visible at 21.5 °, indicating only the presence of a hexagonal phase. At this point the alkanes were molten and the only crystalline structure left was the alcohol phase, which turned hexagonal at similar a temperature as the alkane phase melted. The fast decrease in crystallinity below the melting temperature of the alcohol phase indicated the dissolution of the alcohols in the alkanes (figure VI.19). At room temperature, diffractograms of the plant adaxial CM wax and the quaternary wax both only showed peaks for the orthorhombic crystal structure (figure VI.17 B). The direct comparison showed no differences in the area between 20 ° and 25 ° and only minor differences in the diffraction angle range below 18 °. This indicated a slightly more ordered structure for the artificial mixture than for the plant wax. However, considering compositional differences of the compared waxes, they could be explained by the broader chain length distribution and higher constituent number of the leaf wax. A comparison of the hot stage experiments revealed some differences. While the artificial mixture showed a complex behaviour of transitions before liquefaction, the plant wax kept its orthorhombic structure throughout the complete temperature range (figure VI.20). As explained in the method section, only the impure leaf wax was available in sufficient amounts to perform hot stage experiments, and it proved challenging to estimate to what degree the measurement was influenced by the impurities from within the leaf. Nonetheless, the hot stage experiments helped to gain valuable insight into the behaviour of waxes upon changing temperature. The FTIR spectrum of this blend showed differences to the spectrum of the adaxial CMs leaf wax (figure VI.6 C, D). They are probably explainable by a compositional difference of the artificial and plant wax. However, it indicated a change in the crystalline structure in the leaf wax at 59 °C. A reason for the poor visibility of this transition could lay within the wax composition. Looking at the spectra of the binary and ternary mixtures, the introduction of one compound with a functional group into a binary alkane blend had strong influences on its spectrum. The wavenumber shift, indicating the melting of the sample was strongly broadened, and the transition before melting was not as sharply

zoned, as before. This behaviour was also seen for the quaternary mixture. The plant wax, however, did not only consist of four compounds but roughly 40 or more compounds. Furthermore, were more than one functional group and more than four different chain lengths present in the plant wax. These differences could lead to a more pronounced effect than observed here and visible lack of solid-solid transition in the FTIR spectrum. A comparison of the spectra of the quaternary wax (C_{31}anC_{29}anC_{32}olC_{30}ol 5.4 - 2.3 - 2.3 - 1) and the adaxial CM wax could indicate such a transition in the latter. With an increasing number of constituents, the artificial wax blends showed increasing similarity in the behaviour of their FTIR spectra compared to the spectra of the adaxial CM wax. However, further experiments to improve the validity of this wax as a leaf wax proxy, like a rerun of the hot stage XRD and the DSC experiments with pure wax of adaxial CMs are necessary.

Summarizing the results, the quaternary wax mixture appeared as a good proxy for the *S. elegantissima* adaxial CM wax considering their differences in wax composition. At room temperature, it was shown to have similar properties than the plant wax by XRD measurements, and its behaviour upon heating is very similar in FTIR and DSC measurements. Therefore, this blend could be a starting point for further experiments to improve the understanding of the function of cuticular waxes and their compounds. It has been shown, that various factors, like the developmental stage of the leaf or environmental factors like rain or radiation, affect cuticular wax composition (Jetter and Schäffer 2001; Baker and Hunt 1986; Baker 1974; Gordon et al. 1998). Therefore, a standardized artificial wax blend is beneficial for different investigations. It enables experiments to have a common starting point, increasing their comparability compared to experiments conducted with plant wax. A possible experiment could be the addition of different substance classes like aldehydes, alkyl acids or esters to study of their impact on the waxes. Artificial wax poses the possibility to investigate the mode of action of agricultural used adjuvants more effectively. Experimental setups to investigate foliar uptake of substances or the influence of adjuvants on them are often time-consuming. Furthermore, the choice of a plant species can affect the results. A standardized wax mixture facilitates the possibility to develop a fast and comparable screening method using techniques like FTIR.

VII. Summarizing discussion

An outstanding feature of the cuticle is the reduction of uncontrolled water loss from various plant organs, like leaves or petals, to protect the plant from desiccation. The barrier function is mainly established by cuticular waxes. These waxes can be removed using organic solvents, leading to a significant increase in cuticular water permeability (Schönherr 1976; Schönherr and Lendzian 1981). Nonetheless, the relation of wax constituents and the buildup of this barrier feature were unknown (Kerstiens 2006). Grncarevic and Radler (1967) investigated the influence of different wax fractions onto the water permeability of a plastic membrane. The membrane was coated with grape plant wax or fractions of it. They found aliphatic compounds to have a stronger barrier effect towards transpiration than TRPs (Grncarevic and Radler 1967). However, the reduction of water loss in this artificial system was mostly of minor magnitude (by roughly 50 %) compared to the effect of waxes on cuticles of up to two orders of magnitude and more (Schönherr 1976; Schönherr and Lendzian 1981). Vogg et al. (2004) investigated the influence of cuticular waxes on the transpiration barrier of tomato fruits. In their study, a mutant with a roughly halved amount of intracuticular VLCAs was used. Samples of the mutant showed a fourfold increase in permeability (Vogg et al. 2004). More recent research also indicated intracuticular waxes to constitute the transport limiting barrier of plant cuticles (Jetter and Riederer 2016; Zeisler and Schreiber 2016; Zeisler-Diehl et al. 2018). Jetter and Riederer (2016) further proposed VLCAs to be responsible for the barrier properties. Many clues were found so far for this proposal. However, no direct experimental proof was shown. Therefore, a selective method for the removal of TRPs was developed, and the effect on water permeability of treated and native CMs was measured. In addition, a variety of plant species with varying wax compositions were investigated with this method.

The developed method for selective extraction of TRPS in CMs showed reliable results. To demonstrate this, plant species with varying wax compositions, ranging from waxes with small wax loads and small amounts of TRPs to waxes with high loads majorly consisting of TRPs. The extraction sequence consisted of two steps. The first MeOH extract removed present TRPs reliably and mostly completely and removed only a small fraction of VLCAs with shorter chain lengths (figure V.1, figure V.2). A subsequent TCM extract removed the remaining aliphatic compounds. In a comparison of a combination of these extracts to a conventional extraction method, good

comparability was found (figure V.1). In most cases, no or only minor differences were found after MeOh treatment of CMs. After TCM treatment no surface wax was found on almost all plant species. Only on *H. helix* minor wax remnants were seen (figure V.5, figure V.6, figure V.7, figure V.8). For the measurement of cuticular transpiration, however, these remnants were neglectable. Vogg et al. (2004), Jetter and Riederer (2016), Zeisler and Schreiber (2016) and Zeisler-Diehl et al. (2018) found intracuticular waxes to constitute the major contribution to the transport limiting barrier. The measurement of water transpiration of CMs, Ms and MXs showed a consistent trend. As known to literature, transpiration level of MXs was strongly elevated for all plant species (Schönherr 1976; Schönherr and Lendzian 1981). However, after extraction of TRPs using MeOH, water permeance of most plant species showed no significant increase compared to the value of their corresponding CMs. Even for plant species with a high ratio of TRPs (up to 97 %) only a minor increase in transpiration was found. This increase might be due to cracks or openings within the barrier, which result from an integrity weakening in consequence of removing major proportions of the intracuticular wax. Another reason lay within the small amounts of VLCAs, which were extracted. Though they had shorter chain lengths as indicated by the ACL, their removal could have opened pathways for water to diffuse through. Together with the work of Jetter and Riederer (2016), Zeisler and Schreiber (2016), Zeisler-Diehl et al. (2018) and this study it is arguable to allocated the water permeability barrier (at least mostly) within the VLCA fraction of the intracuticular wax. It could be shown by a combination of stripping methods and the selective extraction of TRPs with MeOH. From an evolutionary view, the localization in the mechanically stable region of the barrier is reasonable. Epicuticular waxes are prone to erosion due to biotic and abiotic interactions (Baker and Hunt 1986; Hadley and Smith 1989; Lindow and Brandl 2003). Therefore, to keep the barrier up continuously, the embedding in intracuticular waxes is essential. In various investigations, attempts were made to correlate cuticular wax load or composition (epicuticular, intracuticular and total) with their water permeance barrier properties. But no or only poor correlations were found (Svenningsson 1988; Riederer and Schneider 1990; Larsson and Svenningsson 1986; Jetter and Riederer 2016). This aligned well with the results, found in this study. While cuticles from species like *N. oleander* or *V. minor* contained a high amount of cuticular wax, their water transpiration values were still about one order of magnitude higher than for plant

species like *H. helix* or *Z. zamiifolia*, which had a very low cuticular wax load (supplement table 2; figure V.1; figure V.4). Therefore, it a connection of the water barrier properties and the physical properties of VLCAs appears exceedingly plausible (Merk et al. 1997). For the analysis of physical properties of wax, a variety of techniques like FTIR, DSC or (hot stage) XRD are viable. However, for DSC or hot stage XRD experiments, high amounts of wax are necessary. To gather those is a highly time and material consuming process. Therefore, since the VLCA fraction is shown to constitute the transpiration barrier, an artificial wax mixture depicting the VLCAs of a plant cuticular wax could be beneficial for further studies. It could allow the continued development of an artificial membrane based on the structure of plant cuticles. Thus, helping to decipher the buildup of the transpiration barrier further. Furthermore, this artificial wax could lead to the development of new techniques to investigate the influence of adjuvants or active ingredients, used in agriculture, onto cuticular wax. Formulations, mixtures made of various substances are used in agriculture to apply active ingredients crops and other plants. Considering the work of Staiger (2019a), it is safe to assume the barrier properties against active ingredient uptake and water loss in the VLCA fraction. A standardized artificial wax mixture could be used as a basis for fast screening methods to analyze adjuvant effects on cuticular wax to produce formulations specifically tailored to a purpose. Riederer and Schneider (1990) proposed the crystalline structure of VLCAs to constitute the transpiration barrier. They assumed the presence from impermeable crystalline zones, formed by the alignment of mid-chain regions of VLCAs and permeable amorphous zones, formed by the end-chain methylene and functional groups. The calculation of the aliphatic crystallinity of adaxial CM wax of *S. elegantissima* exhibited a high crystallinity value (roughly 80 %) for the wax of this plant species. XRD experiments revealed an orthorhombic crystal structure of the crystalline zones. Hot stage XRD and FTIR experiments both hint at a solid solution, where no separation of the wax constituents takes place (figure VI.10, figure VI.20). However, the comparison of the plant wax data with the data of the artificial quaternary wax blend as well as the DSC thermogram of the whole leaf wax could hint at a system with separate phases, as presumed for the ternary and quaternary wax blends (discussed below, figure V.10). To answer the question of the structure of the plant wax, more experiments to investigate the influence of wax constituents on the physical properties have to be conducted. Therefore, a

standardized initial point was developed, based on the composition of the adaxial CM wax of *S. elegantissima* leaves. This plant species was used due to beneficial wax properties (figure VI.1, figure VI.2, figure VI.3) To keep the complexity of the blend at bay, the constituents were restricted to the four most abundant compounds. With this, not only the amount and compound class were considered, but also their chain length. Therefore, C_{31}an, C_{29}an, C_{32}ol and C_{30}ol were used.

The phase diagrams of binary alkane and alcohol mixtures each showed one solid-solid transition before melting, also visible through a small wavenumber shift in the FTIR spectra (figure VI.5 A, B, figure VI.11 A, B). The according diffractograms (figure VI12) at room temperature showed the alkane mixture to have the orthorhombic and the alcohol blends to have the monoclinic crystal structure (Valoppi et al. 2016; Craig et al. 1998). The hot stage diffractograms (figure VI.18) of the binary alkane blend C_{31}anC_{29}an (2.3 - 1) displayed the transition to a hexagonal crystal lattice before melting (Tashiro et al. 1996). The transition from a monoclinic to a hexagonal lattice was described for alcohols (Tasumi et al. 1964; Cholakova and Denkov 2019). To produce the ternary blends, the ratio of the two alkanes (C_{31}anC_{29}an) was kept constant (2.3 - 1), and either C_{30}ol or C_{32}ol was added. For the quaternary mixture, the ratios between C_{31}anC_{29}an and C_{32}ol C_{30}ol (2.3 – 1) was kept constant, and the ratio between alkane and alcohol fraction wax changed. The transitions described for binary mixtures were also found in the ternary and quaternary wax blends. Therefore, signal 1 and 3 in their phase diagrams could be assigned to separate wax fractions (figure VI.11 C, D, E). This system of two separate phases, one alkane and one alcohol phase, was confirmed by the XRD at room temperature of the ternary wax blends, where peaks for two different crystal lattices became visible in mixtures with alkanes and alcohols, but not for the pure alkane blend or the pure alcohol (figure VI.13). With increasing alcohol content in ternary mixtures, the intensity of the signal indicating orthorhombic crystallinity (23.9 °) decreased and the one indicating a monoclinic lattice (24.3 °) increased (figure VI.13). Another indicator for this system was found in the FTIR spectra of the ternary mixture C_{31}anC_{29}anC_{30}ol (2.3 – 1 – 1.4) and the quaternary mixture C_{31}anC_{29}anC_{32}olC_{30}ol (5.4 – 2.3 – 2.3 – 1). Here were three wavenumber shifts visible in similar areas as the signals were found in the corresponding thermogram. In the phase diagram, for some of the mixtures, an additional signal (signal 2) was found (figure v.11 C, D, E). It indicated a mixed-phase between the alcohols and the alkanes

(figure VII.1). Flaherty (1971) and Edwards (1957) showed paraffin waxes to have the orthorhombic crystal structure. Therefore, it can also be assumed for signal 2.
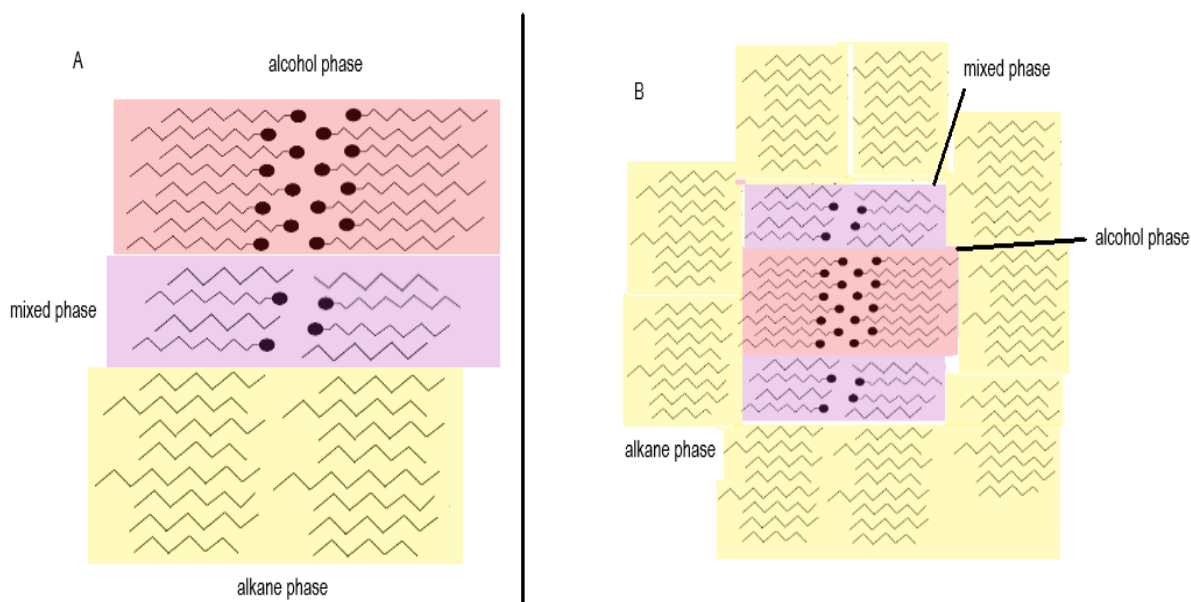
Figure VII.1: Schematic of two possible wax structures of the ternary and quaternary wax blends. The chains indicate methylene groups and circles indicate functional groups. A Separation into two distinct phases with one mixed phase in between. B Alcohol "Islands" surrounded by a crystalline alkane phase and a mixed-phase in between.

However, from these techniques, it was not possible to distinguish between the two structures (figure VII.1). To do this, a technique like the atomic force microscopy could be suitable. Further investigations into the crystalline structure of these waxes are highly interesting since it influences the brittleness of waxes (Sun et al. 2014). During the experiments with the ternary and the quaternary wax blends, an increasing brittleness with increasing alcohol content was noticed. Therefore, the elucidation of the wax structure could become very important to understand the function of cuticular waxes.

A comparison of the thermogram of the quaternary mixture ($C_{31}anC_{29}anC_{32}olC_{30}ol$, 5.4 - 2.3 - 2.3 - 1) with the thermograms of the binary wax mixtures (2.3 -1) undergirded the assumptions from the phase diagrams regarding the solid-solid transitions (figure VI.21). The temperature range of signal 3 was similar to the change from an orthorhombic lattice to a hexagonal one in the binary alkane blend. Signal 1 overlapped strongly with the melting of the alkane blend, and the transition of the alcohol fraction from a monoclinic to a hexagonal lattice. However, the melting signal of the alcohol blend had higher temperatures and didn´t match with the melting signal of the

quaternary blend. Therefore, it was assumed, that the already molten alkanes acted as a solvent towards the alcohols, accelerating the liquefaction of the sample. The assumption was undergirded by the hot stage diffractograms of this wax. At temperatures, where the alkanes where presumably molten a signal indicating a crystalline phase with a hexagonal lattice was still found. Furthermore, a broad halo indicating an amorphous phase was seen (figure VI.19). For the wax blends, depicting the conditions within the plant wax, an increasing congruence of the artificial blend with the plant wax was noticed. The thermogram of this mixture was very similar to the plant wax one. Three strongly overlapping peaks were visible in both, and the temperature range was also resembling (figure VI.10). Furthermore, the XRD diffractograms at room temperature (wax from adaxial CMs was used) showed both few peaks, besides those indicating orthorhombic crystal structure (figure VI.17 B). Compared to the other investigated artificial blends, the IR spectra of the quaternary mixture and the plant wax converged. A comparison of both hinted at the presence of a hexagonal phase in the plant wax, which was not visible from the pure plant wax (figure VI.6 C, D; figure VI.7). However, although it represented around 70 % of the total adaxial CM wax of *S. elegantissima* leaves, even the quaternary mixture ($C_{31}anC_{29}anC_{32}olC_{30}ol$, 5.4 - 2.3 - 2.3 - 1) still showed differences compared to the plant wax. The shifts in the wavenumber diagrams crossed at higher temperatures, and the quaternary wax showed two distinct shifts in wavenumber, while the plant wax showed a smooth, accelerating increase. This might be due to the complexity of the leaf wax composition of the two samples. As seen from the transition from a binary to ternary and to quaternary system, an increased number of constituents could lead to a broadening of the wavenumber shifts. The plant wax contains roughly ten times more compounds than the quaternary wax, leading to the observed melting behaviour. Though showing some differences to the plant wax, it can be assumed from the present results, that the quaternary wax blend can form a good standardized initial point for further research. Various attempts have been made to find a correlation between the transpiration properties of the cuticle and characteristics of the according cuticular waxes, but so far no or only very weak correlations were discovered (Svenningsson 1988; Riederer and Schneider 1990; Larsson and Svenningsson 1986; Jetter and Riederer 2016; Huang et al. 2017). Riederer and Schneider (1990) and Riederer and Schreiber (1995) proposed crystalline features, like size and shape of crystallites to define the transport

limiting barrier. The presented data does not allow to conclude a connection of the crystal structure or the influence of individual wax constituents to the transpiration barrier. Cuticular waxes are highly complex mixtures of numerous compound classes. Price and Anderson (1985) showed that the uptake enhancing effects of formulations found for a certain plant species does not necessarily transfer to another. Therefore, it could be doubted that insights on the barrier properties were transferable to other plant species. However, the data verified the location of the barrier properties within the VLCAs, giving the possibility to concentrate efforts of further investigations on the transpiration barrier on the features of this wax fraction. Furthermore, the results support the layered structure of cuticular waxes supposed by Jetter and Riederer (2016). In preliminary experiments (results not shown) TRPs were not extractable from whole leaves, but from isolated cuticles, indicating a localization at the inside of the cuticle (figure V.5). Nonetheless, this work could give hints for further experiments, for example, a combination of DSC, FTIR and XRD experiments with transpiration measurements. Another project could be the utilization of the artificial wax mixture, mimicking *S. elegantissima* CM wax, to investigate changes in physical properties due to added constituents or to produce an artificial membrane and investigate the influence of different components on the barrier properties.

So far, the connection between VLCAs and water permeability barrier was only assumed and has not been confirmed directly by experimental evidence (Vogg et al. 2004; Jetter and Riederer 2016). This evidence was now provided by this study, improving the insight into the chemistry-function relationship of plant cuticles. The knowledge about the structure of the permeability barrier does not only have value for fundamental research. It also provides the foundation for basic approaches in experiments, dealing with more application-oriented issues. Together with Staiger et al. (2019b) the permeability barrier for uptake and release of substances through the cuticle could now be dedicated to the VLCA fraction of its waxes. In agriculture, active ingredients are commonly applied in aqueous mixtures by foliar spray application and diffuse through the cuticle to the inside plant tissue (Kirkwood 1999; Schreiber et al. 1996a). To improve the uptake adjuvants are used. The investigation of the impact of these substances on the foliar uptake of active ingredients is very time-consuming. Experiments to simulate foliar penetration use CMs mounted on single or double chambers (Staiger et al. 2019b; Arand et al. 2018). To obtain CMs, plants have to be

cultivated and nurtured, and the CM has to be isolated. The latter alone can take several weeks up to a few months, depending on the plant species. This procedure has to be repeated for every plant species. Price and Anderson (1985) showed the assumption of high uptake of one formulation into a particular species would lead to similar behaviour in another species as invalid. They also indicated the requisiteness of formulations to be specifically tailored to their application and plant species (Price and Anderson 1985). Since it is now clear, that only aliphatic compounds are responsible for the barrier function, an artificial wax mixture could be developed to accelerate investigations to tailor formulations application-specific.

Besides their transport limiting properties, cuticular waxes were described to fulfil a plethora of tasks. Epicuticular waxes were shown to play a role in the interaction with insects, the self-cleaning of the surface or for protection against ultraviolet radiation (Müller and Riederer 2005; Bernays et al. 1976; Scholz et al. 2010; Koch and Ensikat 2008; Barthlott and Neinhuis 1997; Jansen et al. 1998). Intracuticular waxes were found to serve as supporting nanofillers, increasing toughness, rigidity and stiffness, improving mechanical strength (Khanal et al. 2013; Tsubaki et al. 2013; Petracek and Bukovac 1995). The almost exclusively intracuticular TRPs play a major part to fulfil these tasks and were proposed to form a nanocomposite with the cutin matrix (Buschhaus et al. 2007; Jetter and Riederer 2016; Tsubaki et al. 2013). TRPs usually have high melting points (Starratt 1966). TRPs could be important to restrict temperature influence on the permeability barrier of desert plants. In a study on *Rhazya stricta* TRPs were shown to restrict the water permeance increase due to elevated temperatures. To enable this, intracuticular TRPs were proposed to restrict thermal expansion of the cutin polymer, thus preventing thermal damage to the barrier (Schuster et al. 2016). Therefore, it can be suggested, that even though TRPs do not contribute to the transport limiting barrier itself, in some plant species, they can contribute to its preservation.

For further investigations, the preparation of pure plant wax and the conductance of FTIR, hot stage XRD and DSC experiments could give further information about the similarity of the quaternary wax, and the wax from adaxial CMs of *S. elegantissima*. In addition, this artificial wax could be used in various experiments as a standardized initial point. Experiments to investigate the effect of different constituents of cuticular waxes could be conducted, by adding them to this wax. Another potential use was the

development of a fast screening method to investigate the effects of agricultural used adjuvants on waxes.

VIII. Publication bibliography

Abbate, S; Gussoni, M; Zerbi, G 1979: Infrared and Raman intensities of polyethylene and perdeuteropolyethylene: Factor group splittings. *The Journal of chemical physics.* **70**, 3577–3585.

Abe, I; Rohmer, M; Prestwich, GD 1993: Enzymatic cyclization of squalene and oxidosqualene to sterols and triterpenes. *Chemical Reviews.* **93**, 2189–2206.

Aggarwal, P 2001: Phase transition of apple cuticles. A DSC study. *Thermochimica Acta.* **367**, 9–13.

Arand, K; Asmus, E; Popp, C; Schneider, D; Riederer, M 2018: The Mode of Action of Adjuvants—Relevance of Physicochemical Properties for Effects on the Foliar Application, Cuticular Permeability, and Greenhouse Performance of Pinoxaden. *Journal of agricultural and food chemistry.* **66**, 5770–5777.

Baker, EA 1974: The influence of environment on leaf wax development in Brassica Oleracea var. Gemmifera. *New Phytologist.* **73**, 955–966.

Baker, EA; Hunt, GM 1986: Erosion of waxes from leaf surfaces by simulated rain. *New Phytologist.* **102**, 161–173.

Baker, EA; Procopiou, J 1975: The cuticles of Citrus species. Composition of the intracuticular lipids of leaves and fruits. *Journal of the Science of Food and Agriculture.* **26**, 1347–1352.

Bargel, H; Koch, K; Cerman, Z; Neinhuis, C 2006: Structure–function relationships of the plant cuticle and cuticular waxes—a smart material? *Functional Plant Biology.* **33**, 893–910.

Barthlott, W; Mail, M; Bhushan, B; Koch, K 2003: Plant Surfaces: Structures and Functions for Biomimetic Innovations. *Nano-Micro Letters.* **9**, 23.

Barthlott, W; Neinhuis, C 1997: Purity of the sacred lotus, or escape from contamination in biological surfaces. *Planta.* **202**, 1–8.

Barton, FE; Himmelsbach, DS; Duckworth, JH; Smith, MJ 1992: Two-dimensional vibration spectroscopy: correlation of mid-and near-infrared regions. *Applied spectroscopy.* **46**, 420–429.

Baskar, K; Duraipandiyan, V; Ignacimuthu, S 2014: Bioefficacy of the triterpenoid friedelin against Helicoverpa armigera (Hub.) and Spodoptera litura (Fab.)(Lepidoptera: Noctuidae). *Pest Management Science.* **70**, 1877–1883.

Basson, I; Reynhardt, EC 1991: Identification of defect chain motions in the low temperature orthorhombic phase of binary mixtures of n-alkanes by means of nuclear magnetic resonance spin-lattice relaxation time measurements. *The Journal of chemical physics.* **95**, 1215–1222.

Bateman, RM; Crane, PR; DiMichele, WA; Kenrick, PR; Rowe, NP; Speck, T; Stein, WE 1998: Early evolution of land plants: phylogeny, physiology, and ecology of the primary terrestrial radiation. *Annual Review of Ecology and Systematics.* **29**, 263–292.

Bernays, EA; Blaney, WM; Chapman, RF; Cook, AG 1976: The ability of Locusta migratoria L. to perceive plant surface waxes. **16**, 35–40.

Birkholz, M 2006: Thin film analysis by X-ray scattering. Weinheim: John Wiley & Sons.

Blume, A 1996: Properties of lipid vesicles: FT-IR spectroscopy and fluorescence probe studies. *Current opinion in colloid & interface science.* **1**, 64–77.

Brycki, B; Kowalczyk, I; Kozirog, A 2011: Synthesis, molecular structure, spectral properties and antifungal activity of polymethylene-α, ω-bis (N, N-dimethyl-N-dodecyloammonium bromides). *Molecules.* **16**, 319–335.

Buchholz, A 2006: Characterization of the diffusion of non-electrolytes across plant cuticles: properties of the lipophilic pathway. *Journal of Experimental Botany.* **57**, 2501–2513.

Burghardt, M; Riederer, M 2003: Ecophysiological relevance of cuticular transpiration of deciduous and evergreen plants in relation to stomatal closure and leaf water potential. *Journal of Experimental Botany.* **54**, 1941–1949.

Burghardt, M; Riederer, M 2008: Cuticular transpiration. *Biology of the plant cuticle.* **23**, 292–309.

Burghardt, M; Schreiber, L; Riederer, M 1998: Enhancement of the diffusion of active ingredients in barley leaf cuticular wax by monodisperse alcohol ethoxylates. *Journal of agricultural and food chemistry.* **46**, 1593–1602.

Buschhaus, C; Herz, H; Jetter, R 2007: Chemical composition of the epicuticular and intracuticular wax layers on adaxial sides of Rosa canina leaves. *Annals of botany.* **100**, 1557–1564.

Buschhaus, C; Jetter, R 2011: Composition differences between epicuticular and intracuticular wax substructures: How do plants seal their epidermal surfaces? *Journal of Experimental Botany.* **62**, 841–853.

Chapman, D 1955: Infra-red spectra and the polymorphism of glycerides. *Nature.* **176**, 216–217.

Cheng, YT; Rodak, DE; Wong, CA; Hayden, CA 2006: Effects of micro-and nano-structures on the self-cleaning behaviour of lotus leaves. *Nanotechnology.* **17**, 1359–1362.

Chibnall, AC; Piper, SH; Pollard, A; Smith, JAB; Williams, EF 1931: The wax constituents of the apple cuticle. *Biochemical Journal.* **25**, 2095–2110.

Chibnall, AC; Piper, SH; Pollard, A; Williams, EF; Sahai, PN 1934: The constitution of the primary alcohols, fatty acids and paraffins present in plant and insect waxes. *Biochemical Journal.* **28**, 2189–2208.

Cholakova, D; Denkov, N 2019: Rotator phases in alkane systems: In bulk, surface layers and micro/nano-confinements. *Advances in colloid and interface science.* **269**, 7–42.

Chung, FH; Scott, RW 1973: A new approach to the determination of crystallinity of polymers by X-ray diffraction. *Journal of Applied Crystallography.* **6**, 225–230.

Craig, SR; Hastie, GP; Roberts, KJ; Gerson, AR; Sherwood, JN; Tack, RD 1998: Investigation into the structures of binary-, tertiary- and quinternary-mixtures ofn-alkanes and real diesel waxes using high-resolution synchrotron X-ray powder diffraction. *Journal of Materials Chemistry.* **8**, 859–869.

Croteau, R; Fagerson, IS 1971: The chemical composition of the cuticular wax of cranberry. *Phytochemistry.* **10**, 3239–3245.

Cussler, EL; Hughes, SE; Ward, WJ; Aris, R 1988: Barrier membranes. *Journal of Membrane Science.* **38**, 161–174.

Dirand, M; Bouroukba, M; Chevallier, V; Petitjean, D; Behar, E; Ruffier-Meray, V 2002: Normal alkanes, multialkane synthetic model mixtures, and real petroleum waxes: crystallographic structures, thermodynamic properties, and crystallization. *Journal of Chemical & Engineering Data.* **47**, 115–143.

Dirand, M; Chevallier, V; Provost, E; Bouroukba, M; Petitjean, D 1998: Multicomponent paraffin waxes and petroleum solid deposits: structural and thermodynamic state. *Fuel.* **77**, 1253–1260.

Domínguez, E; Heredia-Guerrero, JA; Heredia, A 2011: The biophysical design of plant cuticles: an overview. *New Phytologist.* **189**, 938–949.

Dubis, EN; Dubis, AT; Morzycki, JW 1999: Comparative analysis of plant cuticular waxes using HATR FT-IR reflection technique. *Journal of Molecular structure.* **511-512**, 173–179.

Dubis, EN; Dubis, AT; Popławski, J 2001: Determination of the aromatic compounds in plant cuticular waxes using FT-IR spectroscopy. *Journal of Molecular structure.* **596**, 83–88.

Edwards, RT 1957: Crystal habit of paraffin wax. *Industrial & Engineering Chemistry.* **49**, 750–757.

Eglinton, G; Hamilton, RJ 1967: Leaf Epicuticular Waxes. *Science.* **156**, 1322–1335.

Ensikat, HJ; Boese, M; Mader, W; Barthlott, W; Koch, K 2006: Crystallinity of plant epicuticular waxes: electron and X-ray diffraction studies. *Chemistry and Physics of Lipids.* **144**, 45–59.

Eschenmoser, A; Ruzicka, L; Jeger, O; Arigoni, D 1955: Zur kenntnis der triterpene. 190. Mitteilung. Eine stereochemische interpretation der biogenetischen isoprenregel bei den triterpenen. *Helvetica Chimica Acta.* **38**, 1890–1904.

Fagerström, A; Kocherbitov, V; Westbye, P; Bergström, K; Arnebrant, T; Engblom, J 2014: Surfactant softening of plant leaf cuticle model wax–A Differential

Scanning Calorimetry (DSC) and Quartz Crystal Microbalance with Dissipation (QCM-D) study. *Journal of colloid and interface science.* **426**, 22–30.

Fagerström, A; Kocherbitov, V; Westbye, P; Bergström, K; Mamontova, V; Engblom, J 2013: Characterization of a plant leaf cuticle model wax, phase behaviour of model wax–water systems. *Thermochimica Acta.* **571**, 42–52.

Farber, C; Li, J; Hager, E; Chemelewski, R; Mullet, J; Rogachev, AY; Kurouski, D 2019: Complementarity of Raman and Infrared Spectroscopy for Structural Characterization of Plant Epicuticular Waxes. *ACS Omega.* **4**, 3700–3707.

Fich, EA; Segerson, NA; Rose, JKC 2016: The Plant Polyester Cutin: Biosynthesis, Structure, and Biological Roles. *Annual review of plant biology.* **67**, 207–233.

Fischmeister, I 1975: Infrared absorption spectroscopy of normal and substituted long-chain fatty acids and esters in the solid state. *Progress in the Chemistry of Fats and other Lipids.* **14**, 91–162.

Flaherty, B 1971: Characterisation of waxes by differential scanning calorimetry. *Journal of Applied Chemistry and Biotechnology.* **21**, 144–148.

Geyer, U; Schönherr, J 1990: The effect of the environment on the permeability and composition of Citrus leaf cuticles. *Planta.* **180**, 147–153.

Gimzewski, E; Audley, G 1993: Monitoring wax crystallisation in diesel using differential scanning calorimetry (DSC) and microcalorimetry. *Thermochimica Acta.* **214**, 149–155.

Gordon, DC; Percy, KE; Riding, RT 1998: Effects of UV-B radiation on epicuticular wax production and chemical composition of four Picea species. *New Phytologist.* **138**, 441–449.

Grncarevic, M; Radler, F 1967: The effect of wax components on cuticular transpiration-model experiments. *Planta.* **75**, 23–27.

Guhling, O; Kinzler, C; Dreyer, M; Bringmann, G; Jetter, R 2005: Surface composition of myrmecophilic plants: cuticular wax and glandular trichomes on leaves of Macaranga tanarius. *Journal of Chemical Ecology.* **31**, 2323–2341.

Gülz, P-G; Markstädter, C; Riederer, M 1993: Isomeric alkyl esters in Quercus robur leaf cuticular wax. *Phytochemistry.* **35**, 79–81.

Günzler, H; Gremlich, H-U 2012: IR-Spektroskopie: Eine Einführung. 4th ed. Weinheim: John Wiley & Sons.

Haas, K; Rentschler, I 1984: Discrimination between epicuticular and intracuticular wax in blackberry leaves: ultrastructural and chemical evidence. *Plant Science Letters.* **36**, 143–147.

Hadley, JL; Smith, WK 1989: Wind erosion of leaf surface wax in alpine timberline conifers. *Arctic and Alpine Research.* **21**, 392–398.

Hamburger, M; Dudan, G; Nair, AR; Jayaprakasam, R; Hostettmann, K 1989: An antifungal triterpenoid from Mollugo pentaphylla. *Phytochemistry.* **28**, 1767–1768.

Hastie, GP; Roberts, KJ 1994: Investigation of inter-and intra-molecular packing in the solid state for crystals of normal alkanes and homologous mixtures using FT-IR spectroscopy. *Journal of materials science.* **29**, 1915–1919.

Hauke, V; Schreiber, L 1998: Ontogenetic and seasonal development of wax composition and cuticular transpiration of ivy (Hedera helix L.) sun and shade leaves. *Planta.* **207**, 67–75.

Heredia-Guerrero, JA; Benítez, JJ; Domínguez, E; Bayer, IS; Cingolani, R; Athanassiou, A; Heredia, A 2016: Infrared spectroscopy as a tool to study plant cuticles. *Spectroscopy Europe.* **28**, 10–13.

Hoerr, CW; Harwood, HJ; Ralston, AW 1944: Solubilities of high molecular weight normal aliphatic primary alcohols. *The Journal of Organic Chemistry.* **9**, 267–280.

Höhne, G; Hemminger, WF; Flammersheim, H-J 2013: Differential scanning calorimetry. 2nd ed. Berlin Heidelberg: Springer Science & Business Media.

Holmes, MG; Keiller 2002: Effects of pubescence and waxes on the reflectance of leaves in the ultraviolet and photosynthetic wavebands: a comparison of a range of species. *Plant, Cell & Environment.* **25**, 85–93.

Horrocks, RL 1964: Wax and the water vapour permeability of apple cuticle. *Nature.* **203**, 547.

Huang, H; Burghardt, M; Schuster, A; Leide, J; Lara, I; Riederer, M 2017: Chemical composition and water permeability of fruit and leaf cuticles of Olea europaea L. *Journal of agricultural and food chemistry.* **65**, 8790–8797.

Jansen, MAK; Gaba, V; Greenberg, BM 1998: Higher plants and UV-B radiation. Balancing damage, repair and acclimation. *Trends in Plant Science.* **3**, 131–135.

Jeffree, CE 2006: The fine structure of the plant cuticle. *Biology of the plant cuticle.* **23**, 11–125.

Jetter, R; Kunst, L; Samuels, AL 2008: Composition of plant cuticular waxes. *Biology of the plant cuticle.* **23**, 145–181.

Jetter, R; Riederer, M 2016: Localization of the transpiration barrier in the epi-and intracuticular waxes of eight plant species. Water transport resistances are associated with fatty acyl rather than alicyclic components. *Plant Physiology.* **170**, 921–934.

Jetter, R; Schäffer, S 2001: Chemical composition of the Prunus laurocerasus leaf surface. Dynamic changes of the epicuticular wax film during leaf development. *Plant Physiology.* **126**, 1725–1737.

Jetter, R; Schäffer, S; Riederer, M 2000: Leaf cuticular waxes are arranged in chemically and mechanically distinct layers: evidence from Prunus laurocerasus L. *Plant, Cell & Environment.* **23**, 619–628.

Jin, I; Ko, Y; Kim, Y; Han, S 1997: Solubilization of oleanolic acid and ursolic acid by cosolvency. *Archives of pharmacal research.* **20**, 269–274.

Kenrick, P; Crane, PR 1997: The origin and early evolution of plants on land. *Nature.* **389**, 33–39.

Kerstiens, G 2006: Water transport in plant cuticles: an update. *Journal of Experimental Botany.* **57**, 2493–2499.

Khanal, BP; Grimm, E; Finger, S; Blume, A; Knoche, M 2013: Intracuticular wax fixes and restricts strain in leaf and fruit cuticles. *New Phytologist.* **200**, 134–143.

Kim, S-H; Rich, A 1968: Single crystals of transfer RNA: an X-ray diffraction study. *Science.* **162**, 1381–1384.

Kirkwood, RC 1999: Recent developments in our understanding of the plant cuticle as a barrier to the foliar uptake of pesticides. *Pesticide Science.* **55**, 69–77.

Kirsch, T; Kaffarnik, F; Riederer, M; Schreiber, L 1997: Cuticular permeability of the three tree species Prunus laurocerasus L., Ginkgo biloba L. and Juglans regia L.:

comparative investigation of the transport properties of intact leaves, isolated cuticles and reconstituted cuticular waxes. *Journal of Experimental Botany.* **48**, 1035–1045.

Kiser, R; Johnson, G; Shetlar, M 1961: Solubilities of various hydrocarbons in methanol. *Journal of Chemical & Engineering Data.* **6**, 338–341.

Koch, K; Ensikat, H-J 2008: The hydrophobic coatings of plant surfaces: Epicuticular wax crystals and their morphologies, crystallinity and molecular self-assembly. *Micron.* **39**, 759–772.

Krauss, P; Markstädter, C; Riederer, M 1997: Attenuation of UV radiation by plant cuticles from woody species. *Plant, Cell & Environment.* **20**, 1079–1085.

Kunst, L; Jetter, R; Samuels, AL 2008: Biosynthesis and transport of plant cuticular waxes. *Annual Plant Reviews.* **23**, 182–215.

Kunst, L; Samuels, AL 2003: Biosynthesis and secretion of plant cuticular wax. *Progress in Lipid Research.* **42**, 51–80.

Larsson, S; Svenningsson, M 1986: Cuticular transpiration and epicuticular lipids of primary leaves of barley (Hordeum vulgare). *Physiologia Plantarum.* **68**, 13–19.

Lendzian, KJ; Nakajima, A; Ziegler, H 1986: Isolation of cuticular membranes from various conifer needles. *Trees.* **1**, 47–53.

Leopold, CS; Lippold, BC 1995: An attempt to clarify the mechanism of the penetration enhancing effects of lipophilic vehicles with differential scanning calorimetry (DSC). *Journal of pharmacy and pharmacology.* **47**, 276–281.

Lindow, SE; Brandl, MT 2003: Microbiology of the phyllosphere. *Appl. Environ. Microbiol.* **69**, 1875–1883.

Littlejohn, GR; Mansfield, JC; Parker, D; Lind, R; Perfect, S; Seymour, M et al. 2015: In vivo chemical and structural analysis of plant cuticular waxes using stimulated Raman scattering microscopy. *Plant Physiology.* **168**, 18–28.

Mahato, S; Nandy, A; Roy, G 1992: Triterpenoids. *Phytochemistry.* **31**, 2199–2249.

Maréchal, Y; Chamel, A 1996: Water in a Biomembrane by Infrared Spectrometry. *The Journal of Physical Chemistry.* **100**, 8551–8555.

Markstädter, C; Federle, W; Jetter, R; Riederer, M; Hölldobler, B 2000: Chemical composition of the slippery epicuticular wax blooms on Macaranga (Euphorbiaceae) ant-plants. *Chemoecology.* **10**, 33–40.

Marsen, H 1961: Infrarotspektroskopische Untersuchungen zur Temperaturabhängigkeit der Kristallinität von Kohlenwasserstoff-Wachsen. *Fette, Seifen, Anstrichmittel.* **63**, 42–48.

Merk, S; Blume, A; Riederer, M 1997: Phase behaviour and crystallinity of plant cuticular waxes studied by Fourier transform infrared spectroscopy. *Planta.* **204**, 44–53.

Müller, C; Riederer, M 2005: Plant Surface Properties in Chemical Ecology. *Journal of Chemical Ecology.* **31**, 2621–2651.

Naidoo, G; Chirkoot, D 2004: The effects of coal dust on photosynthetic performance of the mangrove, Avicennia marina in Richards Bay, South Africa. *Environmental Pollution.* **127**, 359–366.

Neinhuis, C; Barthlott, W 1997: Characterization and distribution of water-repellent, self-cleaning plant surfaces. *Annals of botany.* **79**, 667–677.

Orgell, WH 1955: The Isolation of Plant Cuticle with Pectic Enzymes. *Plant Physiology.* **30**, 78–80.

Perkins, MC; Roberts, CJ; Briggs, D; Davies, MC; Friedmann, A; Hart, C; Bell, G 2005: Macro and microthermal analysis of plant wax/surfactant interactions. Plasticizing effects of two alcohol ethoxylated surfactants on an isolated cuticular wax and leaf model. *Applied surface science.* **243**, 158–165.

Petracek, PD; Bukovac, MJ 1995: Rheological properties of enzymatically isolated tomato fruit cuticle. *Plant Physiology.* **109**, 675–679.

Pope, CG 1997: X-ray diffraction and the Bragg equation. *Journal of chemical education.* **74**, 129–131.

Price, CE; Anderson, NH 1985: Uptake of chemicals from foliar deposits. Effects of plant species and molecular structure. *Pest Management Science.* **16**, 369–377.

Radler, F; Horn, DHS 1965: The composition of grape cuticle wax. *Australian Journal of Chemistry.* **18**, 1059–1069.

Reynhardt, EC 1985: NMR investigation of Fischer-Tropsch waxes. II. Hard wax. *Journal of Physics D: applied physics.* **18**, 1185–1197.

Reynhardt, EC 1986: Temperature dependence of the cell parameters of Fischer-Tropsch waxes: hard wax and oxidised hard wax. *Journal of Physics D: applied physics.* **19**, 1925–1938.

Reynhardt, EC 1997: The role of hydrogen bonding in the cuticular wax of Hordeum vulgare L. *European Biophysics Journal.* **26**, 195–201.

Reynhardt, EC; Riederer, M 1991: Structure and molecular dynamics of the cuticular wax from leaves of Citrus aurantium L. *Journal of Physics D: applied physics.* **24**, 478–486.

Reynhardt, EC; Riederer, M 1994: Structures and molecular dynamics of plant waxes. *European Biophysics Journal.* **23**, 59–70.

Riedel, M; Eichner, A; Jetter, R 2003: Slippery surfaces of carnivorous plants: composition of epicuticular wax crystals in Nepenthes alata Blanco pitchers. *Planta.* **218**, 87–97.

Riederer, M; Schneider, G 1989: Comparative study of the composition of waxes extracted from isolated leaf cuticles and from whole leaves of Citrus: Evidence for selective extraction. *Physiologia Plantarum.* **77**, 373–384.

Riederer, M; Schneider, G 1990: The effect of the environment on the permeability and composition of Citrus leaf cuticles. II. Composition of soluble cuticular lipids and correlation with transport properties. *Planta.* **180**, 154–165.

Riederer, M; Schreiber, L 1995: Waxes: the transport barriers of plant cuticles. In: Hamilton RJ, ed. Waxes: chemistry, molecular biology and functions, Vol 6. Dundee: The Oily Press, 131–156.

Riederer, M; Schreiber, L 2001: Protecting against water loss: analysis of the barrier properties of plant cuticles. *Journal of Experimental Botany.* **52**, 2023–2032.

Ringelmann, A; Riedel, M; Riederer, M; Hildebrandt, U 2009: Two sides of a leaf blade: Blumeria graminis needs chemical cues in cuticular waxes of Lolium perenne for germination and differentiation. *Planta.* **230**, 95–105.

Saitoh, I; Ikeda, K; Takagishi, Y 1995: Effect of benzyl alcohol on rat skin as a solvent of liquid droplet dispersion ointment. *Biological and Pharmaceutical Bulletin.* **18**, 321–325.

Samuels, L; Kunst, L; Jetter, R 2008: Sealing plant surfaces. Cuticular wax formation by epidermal cells. *Annual review of plant biology.* **59**, 683–707.

Scholz, I; Bückins, M; Dolge, L; Erlinghagen, T; Weth, A; Hischen, F et al. 2010: Slippery surfaces of pitcher plants: Nepenthes wax crystals minimize insect attachment via microscopic surface roughness. *Journal of Experimental Biology.* **213**, 1115–1125.

Schönherr, J 1976: Water permeability of isolated cuticular membranes. The effect of cuticular waxes on diffusion of water. *Planta.* **131**, 159–164.

Schönherr, J; Baur, P 1994: Modelling penetration of plant cuticles by crop protection agents and effects of adjuvants on their rates of penetration. *Pesticide Science.* **42**, 185–208.

Schönherr, J; Lendzian, K 1981: A simple and inexpensive method of measuring water permeability of isolated plant cuticular membranes. *Zeitschrift für Pflanzenphysiologie.* **102**, 321–327.

Schönherr, J; Riederer, M 1986: Plant cuticles sorb lipophilic compounds during enzymatic isolation. *Plant, Cell & Environment.* **9**, 459–466.

Schreiber, L 2001: Effect of temperature on cuticular transpiration of isolated cuticular membranes and leaf discs. *Journal of Experimental Botany.* **52**, 1893–1900.

Schreiber, L 2010: Transport barriers made of cutin, suberin and associated waxes. *Trends in Plant Science.* **15**, 546–553.

Schreiber, L; Kirsch, T; Riederer, M 1996a: Transport properties of cuticular waxes: ecophysiological relevance for cuticular transpiraton. Oxford: BIOS Scientific Publischers LtD.

Schreiber, L; Riederer, M 1996: Ecophysiology of cuticular transpiration. Comparative investigation of cuticular water permeability of plant species from different habitats. *Oecologia.* **107**, 426–432.

Schreiber, L; Riederer, M; Schorn, K 1996b: Mobilities of organic compounds in reconstituted cuticular wax of barley leaves: effects of monodisperse alcohol ethoxylates on diffusion of pentachlorophenol and tetracosanoic acid. *Pesticide Science.* **48**, 117–124.

Schreiber, L; Schorn, K; Heimburg, T 1997: 2H NMR study of cuticular wax isolated from Hordeum vulgare L. leaves. Identification of amorphous and crystalline wax phases. *European Biophysics Journal.* **26**, 371–380.

Schuster, A-C; Burghardt, M; Alfarhan, A; Bueno, A; Hedrich, R; Leide, J et al. 2016: Effectiveness of cuticular transpiration barriers in a desert plant at controlling water loss at high temperatures. *AoB Plants.* **8**, plw027.

Sitte, P; Rennier, R 1963: Untersuchungen an cuticularen Zellwandschichten. *Planta.* **60**, 19–40.

Smith III, AB; Strongin, RM; Brard, L; Furst, GT; Romanow, WJ; Owens, KG; King, RC 1993: 1, 2-Methanobuckminsterfullerene (C61H2), the parent fullerene cyclopropane: synthesis and structure. *Journal of the American Chemical Society.* **115**, 5829–5830.

Staiger, S 2019a: Chemical and physical nature of the barrier against active ingredient penetration into leaves: effects of adjuvants on the cuticular diffusion barrier; Chemische und physikalische Beschaffenheit der Barriere gegenüber Wirkstoffen: Adjuvantieneffekte auf die kutikuläre Diffusionsbarriere. Dissertation. University Würzburg, Würzbrug. Botany II.

Staiger, S; Seufert, P; Arand, K; Burghardt, M; Popp, C; Riederer, M 2019b: The permeation barrier of plant cuticles: uptake of active ingredients is limited by very long-chain aliphatic rather than cyclic wax compounds. *Pest Management Science.* **75**, 3405–3412.

Stammitti, L; Derridj, S; Garrec, JP 1996: Leaf epicuticular lipids of Prunus laurocerasus: importance of extraction methods. *Phytochemistry.* **43**, 45–48.

Starratt, AN 1966: Triterpenoid constituents of Euphorbia cyparissias. *Phytochemistry.* **5**, 1341–1344.

Sümmchen, P; Markstädter, C; Wienhaus, O 1995: Composition of the epicuticular wax esters of Picea abies (L.) Karst. *Zeitschrift für Naturforschung C.* **50**, 11–14.

Sun, G; Zhang, J; Li, H 2014: Structural behaviors of waxy crude oil emulsion gels. *Energy & Fuels.* **28**, 3718–3729.

Svenningsson, M 1988: Epi-and intracuticular lipids and cuticular transpiration rates of primary leaves of eight barley (Hordeum vulgare) cultivars. *Physiologia Plantarum.* **73**, 512–517.

Tashiro, K; Sasaki, S; Kobayashi, M 1996: Structural investigation of orthorhombic-to-hexagonal phase transition in polyethylene crystal: the experimental confirmation of the conformationally disordered structure by X-ray diffraction and infrared/Raman spectroscopic measurements. *Macromolecules.* **29**, 7460–7469.

Tasumi, M; Shimanouchi, T; Watanabe, A; Goto, R 1964: Infrared spectra of normal higher alcohols—I. *Spectrochimica Acta.* **20**, 629–666.

Thimmappa, R; Geisler, K; Louveau, T; O'Maille, P; Osbourn, A 2014: Triterpene biosynthesis in plants. *Annual review of plant biology.* **65**, 225–257.

Thompson, JR; Mueller, PW; Flückiger, W; Rutter, AJ 1984: The effect of dust on photosynthesis and its significance for roadside plants. *Environmental Pollution Series A, Ecological and Biological.* **34**, 171–190.

Tsubaki, S; Sugimura, K; Teramoto, Y; Yonemori, K; Azuma, J-i 2013: Cuticular membrane of Fuyu persimmon fruit is strengthened by triterpenoid nano-fillers. *PLoS One.* **8**, e75275.

Tulloch, AP 1973: Composition of leaf surface waxes of Triticum species: variation with age and tissue. *Phytochemistry.* **12**, 2225–2232.

Valoppi, F; Calligaris, S; Marangoni, AG 2016: Phase transition and polymorphic behavior of binary systems containing fatty alcohols and peanut oil. *Crystal Growth & Design.* **16**, 4209–4215.

van Maarseveen, C; Jetter, R 2009: Composition of the epicuticular and intracuticular wax layers on Kalanchoe daigremontiana (Hamet et Perr. de la Bathie) leaves. *Phytochemistry.* **70**, 899–906.

Vogg, G; Fischer, S; Leide, J; Emmanuel, E; Jetter, R; Levy, AA; Riederer, M 2004: Tomato fruit cuticular waxes and their effects on transpiration barrier

properties. Functional characterization of a mutant deficient in a very-long-chain fatty acid β-ketoacyl-CoA synthase. *Journal of Experimental Botany.* **55**, 1401–1410.

Waters, ER 2003: Molecular adaptation and the origin of land plants. *Plant Molecular Evolution.* **29**, 456–463.

Wissemann, V; Riedel, M; Riederer, M 2007: Matroclinal inheritance of cuticular waxes in reciprocal hybrids of Rosa species, sect. Caninae (Rosaceae). *Plant Systematics and Evolution.* **263**, 181–190.

Wollrab, V 1969: Secondary alcohols and paraffins in the plant waxes of the family Rosaceae. *Phytochemistry.* **8**, 623–627.

Xu, R; Fazio, GC; Matsuda, SPT 2004: On the origins of triterpenoid skeletal diversity. *Phytochemistry.* **65**, 261–291.

Yeats, T; Rose, J 2013: The Formation and Function of Plant Cuticles. *Plant Physiology.* **163**, 5–20.

Zeisler, V; Schreiber, L 2016: Epicuticular wax on cherry laurel (Prunus laurocerasus) leaves does not constitute the cuticular transpiration barrier. *Planta.* **243**, 65–81.

Zeisler-Diehl, V; Müller Y.; **Schreiber, L** 2018: Epicuticular wax on leaf cuticles does not establish the transpiration barrier, which is essentially formed by intracuticular wax. *Journal of Plant Physiology.* **227**, 66–74.

Zerbi, G; Gallino, G; Del Fanti, N; Baini, L 1989: Structural depth profiling in polyethylene films by multiple internal reflection infra-red spectroscopy. *Polymer.* **30**, 2324–2327.

IX. Appendix

Supplement Table 1: Detailed depiction of chain length distribution of eight investigated plants. One full extract (FE) sample consisted of five cuticular membranes (CM) dispersed in chloroform (TCM) overnight. Samples of methanol (MeOH) extracts were prepared by extracting five CMs overnight. Subsequent TCM extracts were prepared by dispersing the MeOH extracted membranes with TCM overnight (n = 4 - 8)

Plant species	Compound class	Chain length	Coverage MeOH extract ($\mu g\ cm^{-2}$)	Coverage TCM extract ($\mu g\ cm^{-2}$)	Coverage FE ($\mu g\ cm^{-2}$)
Camellia sinensis	Alkanes				
		25	0.03 ± 0.01	0.02 ± 0.01	0.03 ± 0.01
		26	0.01 ± 0.01	0.02 ± 0.01	0.02 ± 0.00
		27	0.05 ± 0.01	0.09 ± 0.01	0.08 ± 0.01
		28	0.01 ± 0.02	0.04 ± 0.01	0.01 ± 0.02
		29	0.18 ± 0.03	0.63 ± 0.03	0.60 ± 0.10
		30	0.01 ± 0.02	0.02 ± 0.01	0.01 ± 0.01
		31	0.03 ± 0.03	0.17 ± 0.01	0.17 ± 0.03
		32	0.04 ± 0.05	0.03 ± 0.01	0.01 ± 0.02
		33		0.05 ± 0.02	
		34		0.04 ± 0.02	
		35		0.04 ± 0.03	
		36		0.03 ± 0.02	
		37		0.02 ± 0.02	
		38		0.02 ± 0.02	
		39		0.02 ± 0.02	
		40		0.01 ± 0.01	
		Total	0.36 ± 0.08	1.24 ± 0.16	0.93 ± 0.14
	Alcohols				
		24	0.01 ± 0.00	0.01 ± 0.01	traces
		25			
		26	0.06 ± 0.01	0.03 ± 0.01	0.07 ± 0.02
		27	0.02 ± 0.00	traces	0.01 ± 0.01

	28	0.29± 0.03	0.15 ± 0.02	0.17 ± 0.05
	29	0.06± 0.09	0.04 ± 0.02	0.02 ± 0.03
	30	0.15± 0.15	0.18 ± 0.03	0.65 ± 0.32
	31		0.02 ± 0.00	0.10 ± 0.10
	32		0.11 ± 0.02	0.52 ± 0.19
	34		traces	
	Total	0.59 ± 0.10	0.55 ± 0.09	1.54 ± 0.31
Aldehydes				
	26	traces	traces	
	28	0.03 ± 0.02	0.07 ± 0.08	
	30		0.10 ± 0.10	
	31		traces	
	32		0.08 ± 0.10	
	45			traces
	Total	0.04 ± 0.03	0.42 ± 0.18	0.02 ± 0.04
Alkyl acids				
	24	0.02 ± 0.02	traces	0.02 ± 0.03
	26	0.06 ± 0.06	traces	0.03 ± 0.04
	27			traces
	28	0.09 ± 0.08	0.02 ± 0.03	0.06 ± 0.10
	30	0.09 ± 0.09	traces	0.02 ± 0.04
	32			traces
	Total	0.25 ± 0.25	0.05 ± 0.08	0.30 ± 0.24
Alkyl ester				
	22	traces		
	23	traces	traces	
	Total	traces	traces	
Coumaric acid ester				
	24	traces		
	26	0.01 ± 0.01	0.04 ± 0.03	0.04 ± 0.04
	28	0.04 ± 0.02	0.03 ± 0.02	0.06 ± 0.11
	30	0.02 ± 0.02	0.04 ± 0.02	0.07 ± 0.12

		32	0.02 ± 0.02	0.06 ± 0.04	
		Total	0.09 ± 0.06	0.17 ± 0.10	0.17 ± 0.25
	Total VLCAs		1.34 ± 0.25	2.36 ± 0.26	2.96 ± 0.34
	TRPs				
		Canophyllal			0.23 ± 0.40
		Camposterol		0.01 ± 0.02	
		Epifridelinol			0.10 ± 0.18
		Erythrodiol	0.04 ± 0.07		
		Fridelin	2.20 ± 0.09		2.42 ± 0.59
		Lupenon			0.01 ± 0.02
		Lupeol	0.04 ± 0.05		
		Stigmasterol	0.06 ± 0.10	0.01 ± 0.02	
		Stigmasterol 5, 24 dien		0.01 ± 0.02	
		α-Amyrin	0.01 ± 0.02		0.46 ± 0.16
		β-Amyrin	0.06 ± 0.10		0.02 ± 0.04
		β-Sitosterol	0.07 ± 0.12	0.08 ± 0.07	
		Ursolic acid		0.05 ± 0.09	0.09 ± 0.16
		Unspecified	7.25 ± 0.68	0.05 ± 0.06	6.38 ± 0.86
	Total TRPs		9.74 ± 0.97	0.22 ± 0.18	9.72 ± 0.79
	Not identified		0.63 ± 0.29	0.41 ± 0.18	0.76 ± 0.26
	Total wax		11.7 ± 1.10	3.05 ± 0.16	13.4 ± 1.19
Ficus elastica	Alkanes				
		25	0.06 ± 0.02	0.10 ± 0.07	0.05 ± 0.04
		26		traces	
		27	traces	0.21 ± 0.8	0.31 ± 0.02
		28		traces	0.05 ± 0.04
		29	traces	0.21 ± 0.15	0.22 ± 0.07
		30		0.05 ± 0.02	0.04 ± 0.05
		31		0.45 ± 0.28	0.48 ± 0.14
		32		0.06 ± 0.04	0.18 ± 0.24
		33		0.29 ± 0.21	
		34			
		Total	0.06 ± 0.03	1.40 ± 0.75	1.33 ± 0.42

Alcohols				
	24		0.02 ± 0.01	0.02 ± 0.02
	26		0.05 ± 0.02	0.08 ± 0.04
	27		traces	
	28		0.10 ± 0.08	0.22 ± 0.05
	29		0.03 ± 0.02	
	30	0.24 ± 0.27	0.14 ± 0.14	
	31		0.10 ± 0.05	0.44 ± 0.33
	32		0.21 ± 0.14	0.32 ± 0.26
	33		0.08 ± 0.06	0.13 ± 0.11
	34		0.15 ± 0.10	0.22 ± 0.10
	Total	0.24 ± 0.27	0.89 ± 0.59	1.42 ± 0.54
Aldehydes				
	28		0.05 ± 0.06	0.05 ± 0.05
	29			0.27 ± 0.39
	30		0.22 ± 0.21	
	31		traces	0.02 ± 0.06
	32		0.89 ± 0.51	1.32 ± 0.60
	33		0.09 ± 0.07	
	34		0.36 ± 0.17	1.13 ± 0.76
	Total		1.63 ± 0.83	2.53 ± 1.27
Carbon acids				
	20	traces		0.02 ± 0.03
	21			
	22	traces		0.01 ± 0.01
	24	0.03 ± 0.03	0.04 ± 0.02	0.10 ± 0.04
	25			traces
	26	0.03 ± 0.03	0.07 ± 0.05	0.19 ± 0.08
	27		traces	
	28	0.14 ± 0.14	0.13 ± 0.09	0.51 ± 0.27
	29		0.05 ± 0.05	0.43 ± 0.34
	30		0.21 ± 0.20	0.37 ± 0.27
	31		traces	0.22 ± 0.18

		32	0.10 ± 0.25	0.41 ± 0.47	0.90 ± 0.63
		33		traces	
		34		0.18 ± 0.28	0.38 ± 0.34
		Total	0.22 ± 0.10	1.20 ± 1.15	3.13 ± 1.69
	Alkyl ester				
		24			
		25			0.03 ± 0.08
		26		0.05 ± 0.11	
		27		traces	
		28		0.05 ± 0.10	
		29		0.28 ± 0.44	
		31		0.12 ± 0.28	
		33			0.19 ± 0.30
		36		0.04 ± 0.09	
	Unidentified chain length				0.45 ± 0.19
		Total		0.62 ± 0.18	0.92 ± 0.66
	Total VLCAs		0.55 ± 0.32	5.74 ± 2.44	9.32 ± 3.38
	TRPs				
		α-Amyrin	0.20 ± 0.20		0.13 ± 0.17
		β-Amyrin	0.75 ± 0.75		0.47 ± 0.62
		δ-Amyrin	0.09 ± 0.09		0.11 ± 0.19
		Fridelin	14.1 ± 1.12	0.04 ± 0.10	15.3 ± 0.09
		Fridelinol	3.31 ± 0.87		3.49 ± 0.95
		Lanosterol	8.85 ± 3.69		8.04 ± 1.97
		Lupeol	5.93 ± 1.37		6.57 ± 0.69
		β-Sitosterol		0.04 ± 0.05	
		Taraxerol	0.22 ± 0.22		0.02 ± 0.06
		Unspecified	10.4 ± 7.11	0.17 ± 0.17	14.2 ± 8.36
	Total TRPs		44.7 ± 2.88	0.42 ± 0.46	48.3 ± 8.10
	Not identified		0.51 ± 0.119	0.27 ± 0.18	0.76 ± 0.84
	Total wax		45.7 ± 2.91	6.43 ± 2.46	58.4 ± 10.2
Hedera helix	Alkanes				

25	traces	traces	0.06 ± 0.05
26			0.04 ± 0.03
27	traces	0.11 ± 0.03	0.10 ± 0.06
28		0.03 ± 0.04	0.07 ± 0.07
29	0.11 ± 0.06	0.77 ± 0.08	0.84 ± 0.20
30	traces	traces	0.06 ± 0.06
31	0.16 ± 0.17	0.32 ± 0.16	0.28 ± 0.19
32	traces	0.02 ± 0.04	0.04 ± 0.05
33		0.08 ± 0.11	
34			0.03 ± 0.04
35			0.03 ± 0.03
36			traces
Total	0.31 ± 0.27	1.29 ± 0.39	1.57 ± 0.64
Alcohols			
22	0.06 ± 0.01	0.04 ± 0.01	0.08 ± 0.04
23	traces		traces
24	0.11 ± 0.02	0.12 ± 0.02	0.26 ± 0.08
25	traces	traces	0.04 ± 0.01
26	0.18 ± 0.02	0.31 ± 0.08	0.73 ± 0.14
27		traces	0.04 ± 0.01
28	0.14 ± 0.04	0.35 ± 0.12	0.96 ± 0.16
29		0.08 ± 0.03	0.07 ± 0.05
30	0.13 ± 0.01	0.50 ± 0.20	1.57 ± 0.41
31		traces	0.11 ± 0.03
32	0.04 ± 0.01	0.22 ± 0.05	0.57 ± 0.13
33			traces
34		traces	0.05 ± 0.03
Total	0.67 ± 0.10	1.67 ± 0.51	4.50 ± 0.72
Aldehydes			
24			0.05 ± 0.03
25			traces
26		0.09 ± 0.07	0.14 ± 0.04
27			traces

28		0.14 ± 0.11	0.19 ± 0.05
29			0.03 ± 0.03
30		0.28 ± 0.09	0.56 ± 0.19
31			0.03 ± 0.03
32		0.12 ± 0.07	0.22 ± 0.09
35			
Total		0.63 ± 0.30	1.25 ± 0.41
Carbon acids			
20			0.04 ± 0.02
21			traces
22	0.05 ± 0.01	0.05 ± 0.03	0.11 ± 0.05
23	0.02 ± 0.00		0.03 ± 0.02
24	0.11 ± 0.02	0.14 ± 0.08	0.32 ± 0.10
25	traces		0.04 ± 0.02
26	0.08 ± 0.01	0.14 ± 0.09	0.29 ± 0.07
27		traces	0.05 ± 0.01
28	0.05 ± 0.02	0.17 ± 0.12	0.29 ± 0.08
29		0.07 ± 0.04	0.13 ± 0.04
30	0.08 ± 0.02	0.37 ± 0.27	0.58 ± 0.21
31		traces	0.06 ± 0.06
32	traces	0.13 ± 0.13	0.21 ± 0.17
Total	0.45 ± 0.10	1.28 ± 0.53	2.16 ± 0.72
Alkyl ester			
23		0.11 ± 0.10	
25		traces	
26		traces	
29			traces
32		0.07 ± 0.12	traces
34			traces
36			traces
37		traces	
38			0.03 ± 0.03
40			0.05 ± 0.05

		42		0.08 ± 0.06	0.09 ± 0.04
		44		0.19 ± 0.12	0.10 ± 0.07
		46		0.16 ± 0.10	0.19 ± 0.08
		48		0.11 ± 0.07	0.13 ± 0.04
		50			0.10 ± 0.03
		52			traces
		55			0.03 ± 0.05
		Unidentified chain length	0.04 ± 0.03	0.36 ± 0.24	0.34 ± 0.24
		Total	0.04 ± 0.03	1.46 ± 0.24	1.16 ± 0.37
	Cumaric acid ester				
		20	0.32 ± 0.04		0.34 ± 0.23
		21	traces		
		22	0.23 ± 0.01	0.04 ± 0.03	0.24 ± 0.12
		23	traces		
		24	0.17 ± 0.03	0.13 ± 0.08	0.26 ± 0.07
		26	0.03 ± 0.02	0.06 ± 0.09	0.09 ± 0.02
		28	traces	0.04 ± 0.04	0.06 ± 0.05
		30		0.11 ± 0.12	0.13 ± 0.07
		32			0.05 ± 0.05
		Total	0.78 ± 0.10	0.44 ± 0.24	1.18 ± 0.37
	Total VLCAs		2.24 ± 0.54	6.77 ± 1.64	11.8 ± 1.17
	TRPs				
		Stigmasterol		traces	
		β-Sitosterol	traces		
		unspecified	0.16 ± 0.04		0.29 ± 0.32
	Total TRPs		0.18 ± 0.06	traces	0.29 ± 0.32
	Not identified		0.56 ± 0.11	0.79 ± 0.21	0.55 ± 0.60
	Total Wax		2.98 ± 0.52	7.58 ± 1.48	12.7 ± 2.01
Ilex *aquifolium*	Alkanes				
		27			0.01 ± 0.03
		28			

		29		0.08 ± 0.02	0.11 ± 0.04
		30			
		31		0.19 ± 0.03	0.22 ± 0.07
		Total		0.27 ± 0.02	0.34 ± 0.13
	Alkyl acids				
		26		0.06 ± 0.02	0.11 ± 0.04
		29	0.49 ± 0.14		0.29 ± 0.07
		32			0.12 ± 0.17
		Total	0.49 ± 0.14	0.06 ± 0.02	0.53 ± 0.14
	Total VLCAs		0.49 ± 0.14	0.35 ± 0.06	0.87 ± 0.12
	TRPs				
		α-Amyrin	8.58 ± 2.44		4.89 ± 3.50
		β-Amyrin	2.01 ± 0.49		3.42 ± 4.29
		δ-Amyrin			1.37 ± 0.79
		Betulinic acid	3.64 ± 0.41		3.02 ± 0.71
		Erythrodiol	0.86 ± 0.12		0.97 ± 0.45
		Hederagenin	0.89 ± 0.13		1.03 ± 0.19
		Lupeol	1.67 ± 0.34		1.64 ± 0.29
		Oleanolic acid	19.1 ± 2.24	0.03 ± 0.05	18.3 ± 1.95
		β-Sitosterol	0.09 ± 0.16		
		Ursolic acid	91.8 ± 9.91	0.19 ± 0.34	87.7 ± 12.7
		Uvaol	4.15 ± 0.73		4.74 ± 1.11
		unspecified	15.5 ± 1.44	0.14 ± 0.20	16.5 ± 2.63
	Total TRPs		148 ± 15.1	0.37 ± 0.35	144 ± 16.3
	Not identified		4.46 ± 1.45	0.03 ± 0.06	4.18 ± 1.33
	Total Wax		153 ± 14.0	0.75 ± 0.38	149 ± 16.2
Nerium oleander	Alkanes				
		29	0.21 ± 0.07	0.27 ± 0.10	0.41 ± 0.11
		30	0.05 ± 0.09	0.09 ± 0.03	0.09 ± 0.07
		31	0.49 ± 0.43	0.78 ± 0.30	1.00 ± 0.25
		32		0.14 ± 0.05	0.19 ± 0.04
		33		0.87 ± 0.37	1.18 ± 0.20

	34		0.08 ± 0.09	
	35	2.30 ± 0.79	0.77 ± 0.25	2.10 ± 1.45
	36		0.16 ± 0.09	
	37	0.40 ± 0.42	0.58 ± 0.17	0.47 ± 0.09
	39			0.10 ± 0.10
	Total	3.45 ± 0.85	3.74 ± 1.33	5.55 ± 1.74
Alcohols				
	29	0.15 ± 0.14	0.11 ± 0.04	0.13 ± 0.04
	30	0.17 ± 0.18	0.03 ± 0.04	0.21 ± 0.14
	31		0.18 ± 0.07	
	34	0.29 ± 0.31	0.19 ± 0.07	0.39 ± 0.32
	36			0.06 ± 0.11
	Total	0.62 ± 0.48	0.52 ± 0.16	0.79 ± 0.28
Alkyl acids				
	30	0.22 ± 0.38		0.07 ± 0.13
	32			0.24 ± 0.41
	34			
	Total	0.22 ± 0.38		0.31 ± 0.39
Alkyl ester				
	Unidentified chain length		0.13 ± 0.23	
	Total		0.13 ± 0.23	
Total VLCAs		4.29 ± 1.37	4.39 ± 1.43	6.65 ± 1.71
TRPs				
	α-Amyrin	0.14 ± 0.10		0.13 ± 0.04
	Betulinic acid	1.67 ± 1.70		0.91 ± 1.57
	Erythrodiol	0.39 ± 0.25		0.70 ± 0.63
	Hederagenin	0.63 ± 0.24		1.18 ± 0.69
	Oleanolic acid	40.6 ± 4.37		42.5 ± 9.59
	Ursolic acid	123 ± 18.1	0.04 ± 0.07	126 ± 43.8
	Uvaol			0.55 ± 0.95
	unspecified	15.6 ± 1.79	0.07 ± 0.07	17.9 ± 0.71
Total TRPs		188 ± 26.4	0.16 ± 0.04	190 ± 52.0

	Not identified			2.18 ± 1.46	0.06 ± 0.09	1.80 ± 0.53
	Total Wax			188 ± 26.4	4.61 ± 1.50	198 ± 53.9
Prunus laurocerasus	Alkanes					
		25	traces	traces	0.03 ± 0.02
		26	traces	traces	0.02 ± 0.00
		27	0.10 ± 0.04	0.13 ± 0.06	0.21 ± 0.02
		28	traces	0.07 ± 0.05	0.12 ± 0.00
		29	0.45 ± 0.11	1.98 ± 0.12	2.49 ± 0.18
		30	traces	0.22 ± 0.03	0.26 ± 0.02
		31	0.26 ± 0.08	2.01 ± 0.10	2.42 ± 0.19
		32	traces	0.11 ± 0.06	0.12 ± 0.12
		33		0.21 ± 0.02	traces
		34		traces	
		Total	0.93 ± 0.34	4.83 ± 0.18	5.70 ± 0.34
	Alcohols				
		22	traces	traces	0.02 ± 0.00
		24	0.07 ± 0.04	0.07 ± 0.04	0.22 ± 0.10
		25	traces	traces	0.03 ± 0.01
		26	0.13 ± 0.05	0.12 ± 0.02	0.26 ± 0.04
		27	0.02 ± 0.01	0.02 ± 0.00	0.04 ± 0.00
		28	0.14 ± 0.06	0.22 ± 0.07	0.26 ± 0.03
		29	0.03 ± 0.02	0.06 ± 0.01	0.11 ± 0.08
		30	0.10 ± 0.04	0.23 ± 0.02	0.24 ± 0.11
		31		0.08 ± 0.02	
		32		0.12 ± 0.13	
		33		0.06 ± 0.01	0.17 ± 0.11
		34		0.09 ± 0.01	0.14 ± 0.13
		35		traces	
		36		traces	
		Total	0.51 ± 0.22	1.07 ± 0.18	1.49 ± 0.31
	Aldehydes				
		23	traces		

28		traces	
29		traces	
30		traces	traces
31			
32		traces	
34		traces	
Total	traces	traces	traces
Alkyl acids			
20	traces		
21	traces		
22	traces		traces
23	traces		
24	0.09 ± 0.05	0.03 ± 0.01	0.09 ± 0.02
25	traces		traces
26	0.05 ± 0.03	0.04 ± 0.01	0.07 ± 0.01
27	traces	traces	0.05 ± 0.01
28	0.17 ± 0.08	0.10 ± 0.03	0.22 ± 0.09
29	0.06 ± 0.04	0.05 ± 0.01	0.17 ± 0.12
30	0.49 ± 0.29	0.37 ± 0.13	0.41 ± 0.22
31		traces	
32	0.10 ± 0.10	0.21 ± 0.08	0.19 ± 0.06
33		traces	
34	traces	traces	0.14 ± 0.11
total	1.07 ± 0.37	0.85 ± 0.27	1.38 ± 0.46
Alkyl ester			
22		traces	traces
23	traces		traces
24			traces
27	traces		
32	traces		traces
33		traces	
34		0.06 ± 0.06	
35		traces	

		36		traces	traces
		37		traces	
		38		traces	
		44		traces	
		46		0.06 ± 0.04	
		47		traces	
		48		0.24 ± 0.02	0.28 ± 0.11
		49		traces	
		50		0.25 ± 0.01	0.23 ± 0.15
				traces	
		52		0.15 ± 0.09	0.26 ± 0.09
		Total	0.08 ± 0.05	0.90 ± 0.14	1.20 ± 0.24
	Total VLCAs		2.58 ± 0.50	7.73 ± 0.49	9.84 ± 1.31
	TRPs				
		Hederagenin	1.46 ± 0.87		1.12 ± 0.10
		Oleanolic acid	7.06 ± 0.50	traces	5.06 ± 0.65
		Ursolic acid	31.9 ± 14.2	traces	30.8 ± 1.90
		Unspecified	6.21 ± 2.46	0.16 ± 0.13	3.49 ± 0.29
	Total TRPs		46.7 ± 12.4	0.25 ± 0.05	47.3 ± 5.84
	Not identified		2.40 ± 1.39	0.71 ± 0.19	1.97 ± 0.75
	Total wax		51.7 ± 13.6	8.69 ± 0.61	59.1 ± 7.77
Vinca minor	Alkanes				
		25	traces	traces	
		26	traces		
		27	traces	traces	0.02 ± 0.01
		28	traces	0.06 ± 0.02	
		29	0.05 ± 0.05	0.07 ± 0.01	0.14 ± 0.14
		30	traces	0.04 ± 0.02	0.02 ± 0.01
		31	0.09 ± 0.11	0.29 ± 0.03	0.56 ± 0.32
		32			0.07 ± 0.01
		33		0.27 ± 0.04	0.34 ± 0.04
		34			
		35			

	Total	0.19 ± 0.24	0.77 ± 0.09	1.16 ± 0.42
Alcohols				
	24		0.04 ± 0.01	0.05 ± 0.00
	25			0.02 ± 0.00
	26	0.02 ± 0.00	0.12 ± 0.02	0.18 ± 0.01
	27		traces	0.05 ± 0.01
	28	0.05 ± 0.01	0.14 ± 0.03	0.23 ± 0.02
	29	0.03 ± 0.02		0.06 ± 0.00
	30		0.08 ± 0.05	0.18 ± 0.06
	31		0.07 ± 0.04	0.07 ± 0.12
	32		0.16 ± 0.01	
	33		0.08 ± 0.05	0.25 ± 0.05
	34		0.10 ± 0.06	0.20 ± 0.08
	Total	0.11 ± 0.02	0.80 ± 0.21	1.29 ± 0.11
Aldehydes				
	31		0.07 ± 0.04	
	32		0.20 ± 0.14	0.10 ± 0.12
	33		0.06 ± 0.03	
	34		0.17 ± 0.15	0.60 ± 0.15
	Total		0.49 ± 0.34	0.70 ± 0.12
Alkyl acids				
	24			0.03 ± 0.01
	26		traces	0.04 ± 0.00
	27			
	28	0.02 ± 0.04	0.07 ± 0.04	0.08 ± 0.01
	29			traces
	30		0.09 ± 0.05	
	31		0.12 ± 0.07	
	32		0.14 ± 0.09	0.17 ± 0.10
	33			
	34			0.13 ± 0.06
	total	0.02 ± 0.04	0.43 ± 0.26	0.46 ± 0.11
Alkyl ester				

	32			0.03 ± 0.01
	Total			0.03 ± 0.01
Total VLCAs		0.22 ± 0.04	1.65 ± 0.93	3.17 ± 0.30
TRPs				
	α-Amyrin	traces		0.04 ± 0.00
	Erythrodiol	0.08 ± 0.01		0.24 ± 0.07
	Oleanolic acid	7.10 ± 0.99		6.88 ± 0.33
	Ursolic acid	32.3 ± 8.80		27.0 ± 2.85
	Uvaol	1.44 ± 0.06		1.63 ± 0.10
	Unspecified	3.58 ± 0.30	0.04 ± 0.06	3.49 ± 0.29
Total TRPs		44.5 ± 40.1	0.04 ± 0.06	39.3 ± 2.75
Not identified		0.26 ± 0.03	0.08 ± 0.06	0.86 ± 0.34
Total wax		45.1 ± 10.4	2.61 ± 0.60	43.8 ± 2.66
Zamioculcas zamiifolia	Alkanes			
	25	traces	0.03 ± 0.01	0.04 ± 0.01
	26	traces	traces	
	27	traces	0.06 ± 0.01	0.06 ± 0.01
	28	traces	traces	
	29	0.04 ± 0.05	0.09 ± 0.03	0.06 ± 0.01
	30	traces	0.02 ± 0.01	
	31	0.08 ± 0.03	0.25 ± 0.14	0.19 ± 0.03
	32		traces	
	Total	0.14 ± 0.08	0.47 ± 0.20	0.34 ± 0.04
	Alcohols			
	24	0.03 ± 0.01	0.03 ± 0.01	0.05 ± 0.01
	25	0.16 ± 0.10	traces	
	26	traces	0.52± 0.18	0.70 ± 0.06
	27		0.03 ± 0.01	0.06 ± 0.01
	28	0.25 ± 0.09	1.50± 0.41	1.76 ± 0.12
	29		0.04 ± 0.01	
	30	0.08 ± 0.02	0.68 ± 0.15	0.72 ± 0.07
	31		traces	

	32	0.09 ± 0.04	0.66 ± 0.15	0.59 ± 0.10
	33		traces	
	34		0.09 ± 0.02	0.05 ± 0.03
	Total	0.62 ± 0.21	3.60 ± 0.61	3.89 ± 0.35
Aldehydes				
	27		0.04 ± 0.01	
	28		0.04 ± 0.01	
	29		0.09 ± 0.06	
	30		traces	
	31		traces	
	32		0.12 ± 0.10	
	total		0.30 ± 0.08	
Alkyl acids				
	20	0.03 ± 0.01	0.01 ± 0.00	0.06 ± 0.01
	24	0.03 ± 0.02	0.03 ± 0.02	0.06 ± 0.01
	25		traces	
	26	0.12 ± 0.06	0.54 ± 0.35	0.69 ± 0.22
	27		0.04 ± 0.01	
	28	0.10 ± 0.07	1.51 ± 0.93	1.10 ± 0.59
	29		0.22 ± 0.29	
	30	0.03 ± 0.02	1.09 ± 0.29	0.30 ± 0.20
	31		0.17 ± 0.12	
	32		0.16 ± 0.08	traces
	Total	0.31 ± 0.16	3.58 ± 1.36	2.25 ± 1.04
Alkyl ester				
	26		traces	
	27		traces	
	33		0.06 ± 0.10	
	34		0.10 ± 0.17	
	42		0.16 ± 0.10	0.24 ± 0.01
	44		0.29 ± 0.18	0.37 ± 0.02
	46		0.11 ± 0.07	0.13 ± 0.01
	48		traces	

	Unidentified chain length		0.04 ± 0.03	traces
	Total		0.75 ± 0.23	0.78 ± 0.03
Total VLCAs		1.07 ± 0.31	8.70 ± 1.51	7.27 ± 0.93
TRPs				
	Camposterol	0.03 ± 0.02		0.04 ± 0.02
	Oleanoic acid			0.07 ± 0.12
	β-Sitosterol	traces		
	Stigmasterol	traces		
	δ-Tocopherol	traces		traces
	Ursolic acid	0.06 ± 0.10		0.04 ± 0.06
	Unspecified			0.07 ± 0.05
Total TRPs		0.12 ± 0.12		0.24 ± 0.23
Not identified		0.06 ± 0.04	0.12 ± 0.01	traces
Total wax		1.26 ± 0.30	8.81 ± 1.93	7.53 ± 0.85

Supplement Table 2: Water permeability (Median; 25th - 75th percentile) and effect on the permeance barrier of adaxial cuticular leaf discs of seven plant species after different treatments in untreated (CM), methanol extracted (M) and dewaxed condition (MX).

|	Permeance		
Plant species	CM (x 10^{-5} m s^{-1})	M (x 10^{-5} m s^{-1})	MX (x 10^{-5} m s^{-1})
Camellia sinensis	4.27; 1.49 - 7.60	1.23; 0.67 - 5.49	24.9; 18.9 - 35.6
Ficus elastica	0.97; 0.301 - 3.01	1.44; 0.15 - 8.23	5.39; 3.59 - 10.6
Hedera helix	0.40; 0.26 - 0.79	0.69; 0.28 - 1.31	76.0; 2.37 - 18.4
Ilex aquifolium	1.31; 0.41 - 3.66	2.03; 1.45 - 5.52	30.9; 26.2 - 38.3
Nerium oleander	2.14; 1.30 - 3.23	9.19; 5.51 - 15.2	41.0; 33.9 - 48.3
Prunus laurocerasus	0.38; 0.28 - 0.55	2.67; 1.83 - 4.53	22.2; 20.0 - 26.6
Vinca minor	1.24; 0.77 - 2.10	6.57; 4.78 - 11.5	50.9; 37.0 - 65.0
Zamioculcas zamiifolia	0.45; 0.14 - 1.22	0.57; 0.14 - 2.07	1.07; 0.52 - 2.85

Supplement Table 3: Detailed depiction of chain length distribution of *Schefflera elegantissima*. Cuticular membranes (CM) were dispersed in chloroform overnight. Whole leaf samples were prepared by dispersing on leaf in chloroform twice for 30 s. (n = 4 - 8)

Compound class	Chain length	Coverage adaxial CM ($\mu g\ cm^{-2}$)	Coverage whole leaf ($\mu g\ cm^{-2}$)
Alkanes			
	27	0.03 ± 0.00	0.08 ± 0.01
	28	traces	0.05 ± 0.01
	29	2.62 ± 0.11	3.06 ± 0.03
	30	0.10 ± 0.00	0.13 ± 0.00
	31	4.88 ± 0.15	7.16 ± 0.08
	32	0.03 ± 0.00	0.11 ± 0.01
	33	0.10 ± 0.01	0.28 ± 0.01
	Total	10.9 ± 0.12	7.78 ± 0.21
Alcohols			
	26	traces	0.01 ± 0.00
	27	traces	
	28	0.08 ± 0.05	0.02 ± 0.00
	29	traces	
	30	0.94 ± 0.02	0.10 ± 0.00
	31	0.10 ± 0.02	
	32	2.68 ± 0.77	0.09 ± 0.11
	33	0.11 ± 0.01	
	34	0.83 ± 0.13	
	Total	4.80 ± 0.88	0.21 ± 0.01
Aldehydes			
	28	traces	0.03 ± 0.01
	29	traces	
	30	0.39 ± 0.18	0.26 ± 0.03
	31	traces	
	32	1.92 ± 0.41	0.19 ± 0.02
	34	0.21 ± 0.13	
	Total	2.60 ± 0.79	0.47 ± 0.06

|			
Alkyl acids			
	20	0.04 ± 0.01	
	22	0.02 ± 0.01	0.02 ± 0.00
	24	0.02 ± 0.01	traces
	26	0.02 ± 0.01	
	28	0.12 ± 0.01	0.03 ± 0.01
	29	0.03 ± 0.02	
	30	0.49 ± 0.10	0.13 ± 0.02
	31	traces	
	32	0.80 ± 0.30	0.03 ± 0.01
	34	traces	
	Total	1.61 ± 0.43	0.22 ± 0.05
Benzylic acid ester			
	28	0.05 ± 0.10	traces
	30	0.05 ± 0.06	traces
	Total	0.21 ± 0.12	0.05 ± 0.01
Total VLCAs		20.1 ± 1.41	8.73 ± 0.25
TRPs			
	Oleanolic acid	traces	
	Ursolic acid	0.42 ± 0.72	
	β-Tocopherol	0.44 ± 0.01	traces
	δ-Tocopherol	0.07 ± 0.00	
	Unspecified	0.38 ± 0.40	
Total TRPs		1.37 ± 0.67	traces
Not identified		2.23 ± 0.60	0.15 ± 0.02
Total wax		23.7 ± 0.59	8.73 ± 0.25
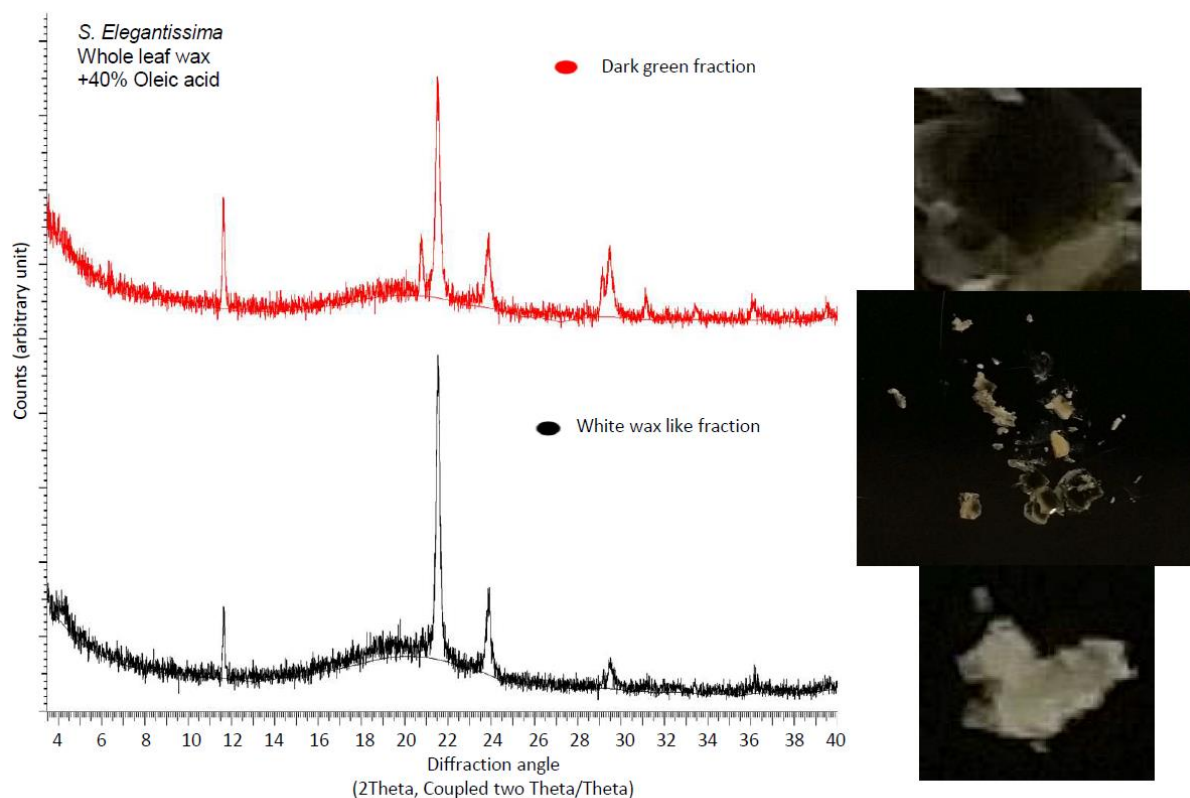
Supplement Figure 1: Diffractograms of the separated dark green fraction and the white wax like fraction after DSC experiments. The separated dark green fraction (red, top) and the white wax like fraction (bottom, black) was obtained from a whole leaf wax sample of *Schefflera elegantissima*, to which 40 % oleic acid was added. The sample was first used for a DSC experiment. Afterwards the splitting of the fractions was possible and the diffractograms were recorded.
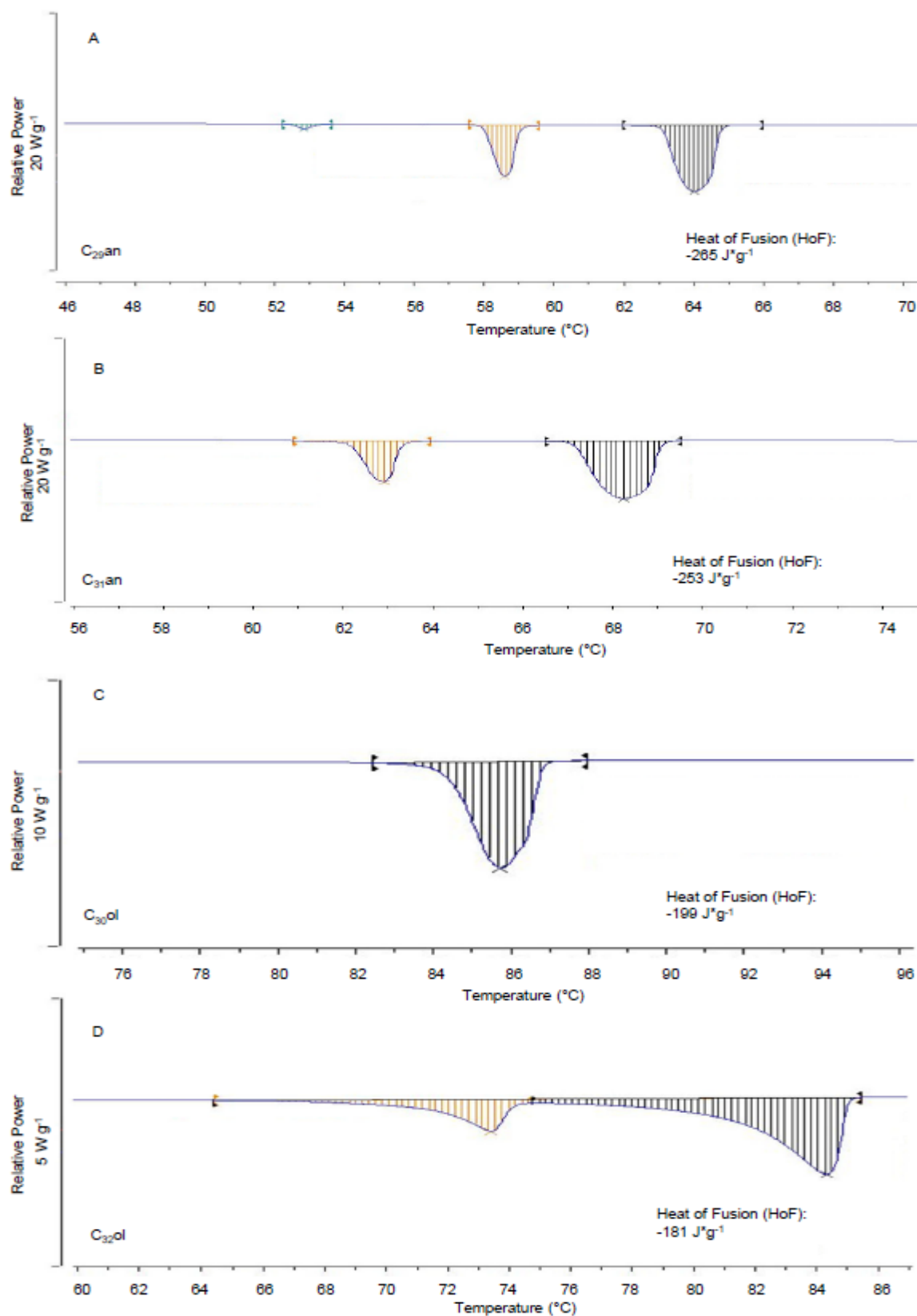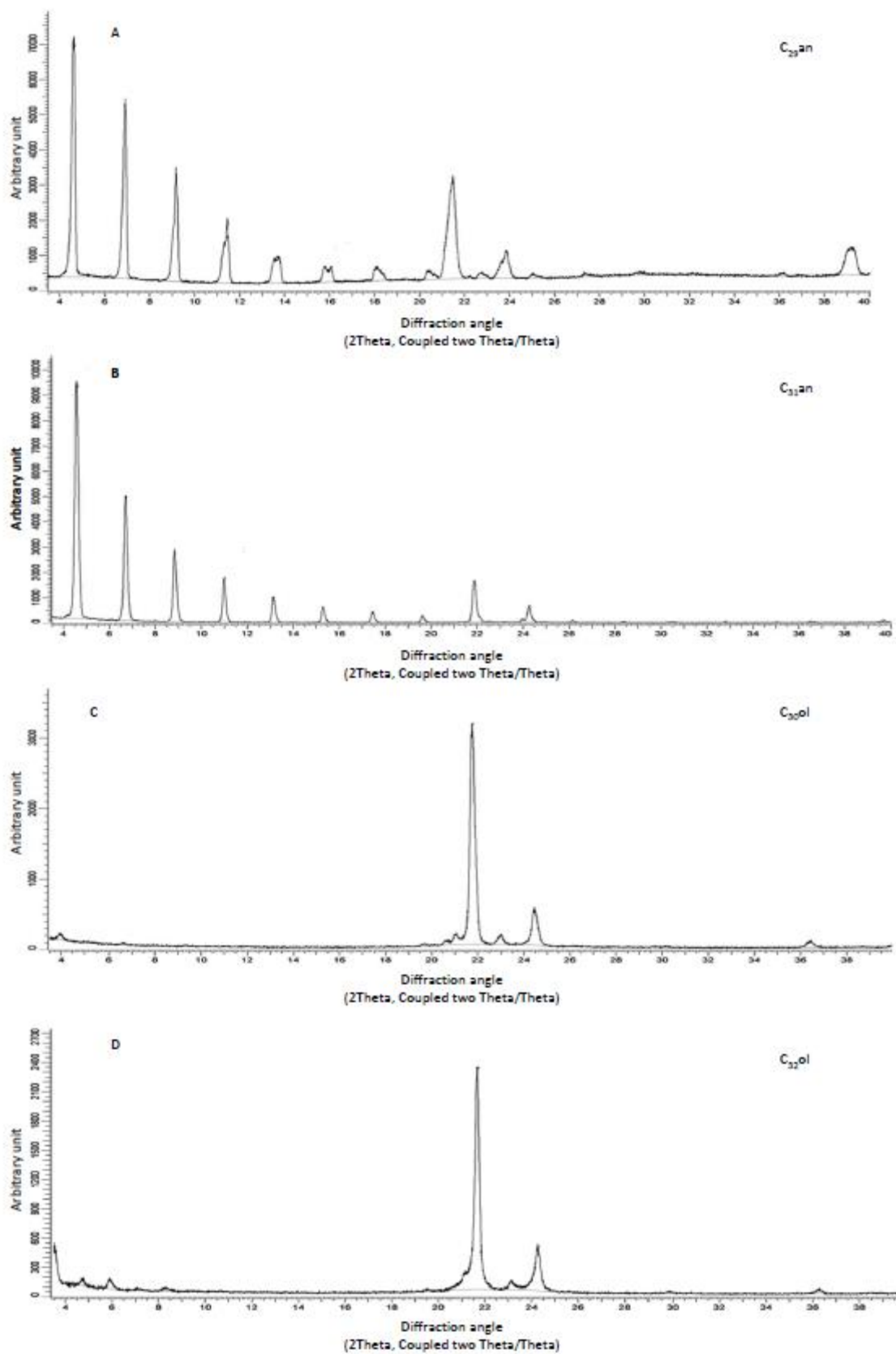
Supplement Figure 2: Thermograms of the pure artificial wax compounds nonacosane (C29an, A), hentriacontane (C31an, B), triacontanol (C30ol, C) and dotriacontanol (C32ol, D). Total Heat of fusion (HoF) was calculated to measure energy emission or uptake with temperature change. Negative values signify uptake.
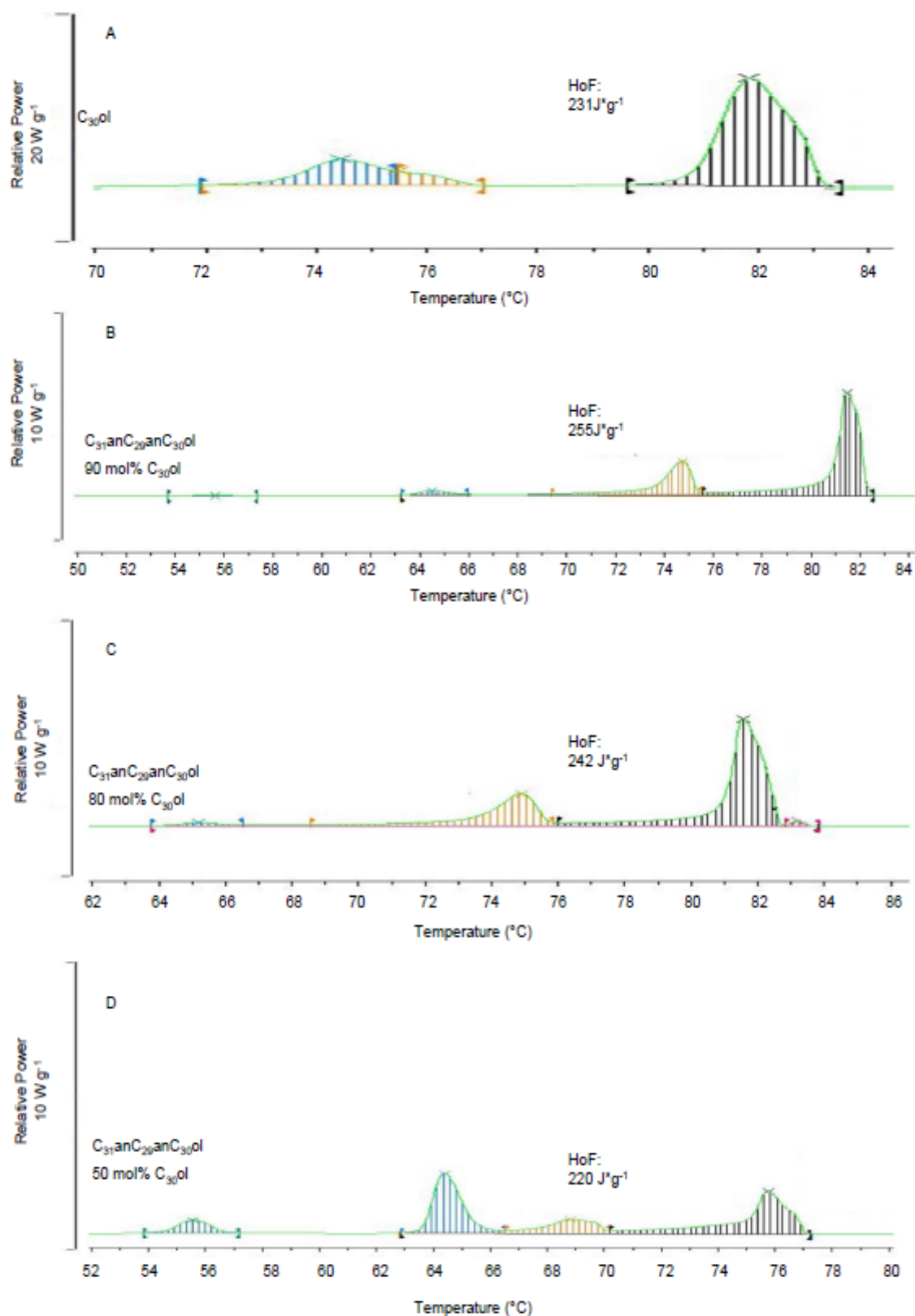
Supplement Figure 3: Thermograms of the artificial waxes consisting of nonacosane (C29an), hentriacontane (C31an) and triacontanol (C30ol). They show the behaviour of pure C30ol (A) and mixtures with 90 mol% (B), 80 mol% (C) and 50 mol% (D) C30ol Total Heat of fusion (HoF) was calculated to measure energy emission or uptake with temperature change. Positive values signify emission.

Supplement Figure 4: Thermograms of the pure artificial wax compounds nonacosan (C29an, A), hentriacontane (C31an, B), triacontanol (C30ol, C) and dotriacontanol (C32ol, D).
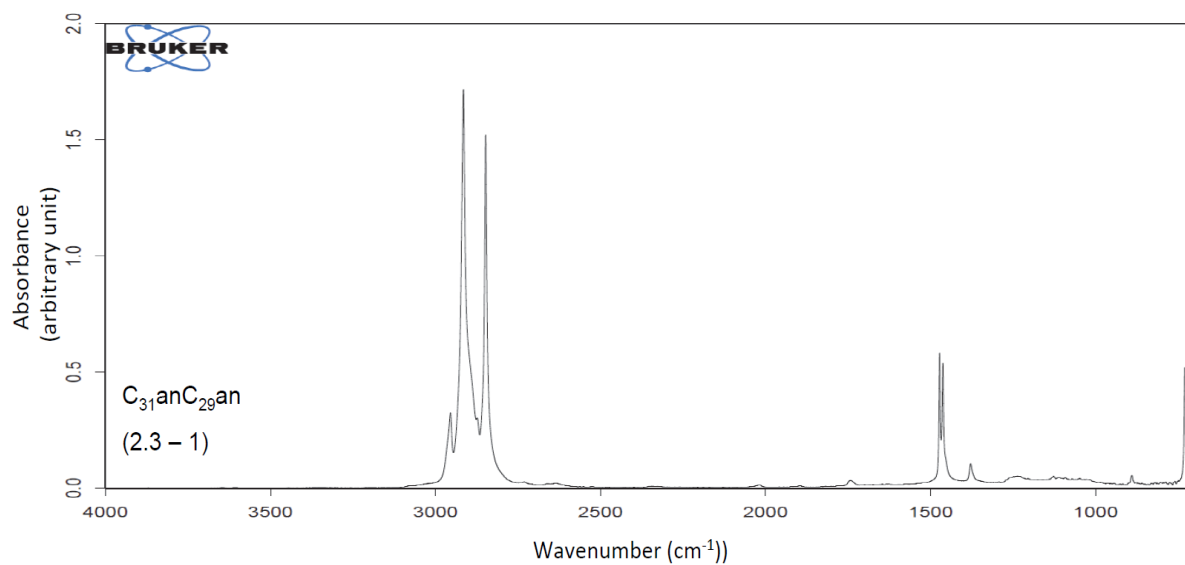
Supplement Figure 5: Fourier transform infrared spectrum of binary wax blend consisting of hentriacontane (C$_{31}$an) and nonacosane (C$_{29}$an) at room temperature

Acknowledgements

Curriculum vitae

Publication list

First-author ship

Staiger S, **Seufert P**, Arand K, Burghardt M, Popp C, Riederer M. (2019). The permeation barrier of plant cuticles: uptake of active ingredients is limited by very long-chain aliphatic rather than cyclic wax compounds, *Pest Management Science* (doi: 10.1002/ps.5589).

Co-author ship

Bueno A, Alfarhan A, Arand K, Burghardt M, Deininger AD, Hedrich H, Leide J, **Seufert P**, Staiger S, Riederer M. (2019). Temperature effects on the cuticular transpiration barrier of two desert plants with water-spender and water-saver life strategies, *Journal of Experimental Botany* (doi.org/10.1093/jxb/erz018).

Affidavit

I hereby confirm that my thesis entitled 'Chemical and physical structure of the barrier against water transpiration of leaves: Contribution of different wax compounds' is the result of my own work. I did not receive any help or support from commercial consultants. All sources and / or materials applied are listed and specified in the thesis. Furthermore, I confirm that this thesis has not yet been submitted as part of another examination process neither in identical nor in similar form.

Würzburg, 04.05.2020

Place, Date   Signature

Eidesstattliche Erklärung

Hiermit erkläre ich an Eides statt, die Dissertation „Chemischer und physikalischer Aufbau der Wassertranspirationsbarriere von Blättern: Beitrag verschiedener Wachskomponenten" eigenständig, d.h. insbesondere selbständig und ohne Hilfe eines kommerziellen Promotionsberaters, angefertigt und keine anderen als die von mir angegebenen Quellen und Hilfsmittel verwendet zu haben. Ich erkläre außerdem, dass die Dissertation weder in gleicher noch in ähnlicher Form bereits in einem anderen Prüfungsverfahren vorgelegen hat.

Würzburg, 04.05.2020

Ort, Datum   Unterschrift